



저작자표시-비영리-변경금지 2.0 대한민국

이용자는 아래의 조건을 따르는 경우에 한하여 자유롭게

- 이 저작물을 복제, 배포, 전송, 전시, 공연 및 방송할 수 있습니다.

다음과 같은 조건을 따라야 합니다:



저작자표시. 귀하는 원저작자를 표시하여야 합니다.



비영리. 귀하는 이 저작물을 영리 목적으로 이용할 수 없습니다.



변경금지. 귀하는 이 저작물을 개작, 변형 또는 가공할 수 없습니다.

- 귀하는, 이 저작물의 재이용이나 배포의 경우, 이 저작물에 적용된 이용허락조건을 명확하게 나타내어야 합니다.
- 저작권자로부터 별도의 허가를 받으면 이러한 조건들은 적용되지 않습니다.

저작권법에 따른 이용자의 권리는 위의 내용에 의하여 영향을 받지 않습니다.

이것은 [이용허락규약\(Legal Code\)](#)을 이해하기 쉽게 요약한 것입니다.

[Disclaimer](#)

공학박사 학위논문

**An Electroencephalogram-based
Noninvasive Critical Care Monitoring
for Emergency Patients**

비침습적 뇌파 신호를 이용한
응급환자의 생체반응 모니터링 기법

2021년 2월

서울대학교 대학원
협동과정 바이오엔지니어링 전공
김 희 진

An Electroencephalogram-based Noninvasive Critical Care Monitoring for Emergency Patients

지도교수 김 희 찬

이 논문을 공학박사 학위논문으로 제출함
2021년 2월

서울대학교 대학원
협동과정 바이오엔지니어링 전공
김 희 진

김희진의 박사 학위논문을 인준함
2021년 2월

위원장	이 정 찬	(인)
부위원장	김 희 찬	(인)
위 원	윤 형 진	(인)
위 원	송 경 준	(인)
위 원	구 윤 서	(인)

Ph. D. Dissertation

**An Electroencephalogram-based
Noninvasive Critical Care Monitoring
for Emergency Patients**

BY

HEEJIN KIM

FEBRUARY 2021

**INTERDISCIPLINARY PROGRAM IN
BIOENGINEERING
THE GRADUATE SCHOOL
SEOUL NATIONAL UNIVERSITY**

An Electroencephalogram-based Noninvasive Critical Care Monitoring for Emergency Patients

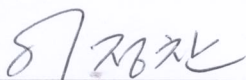
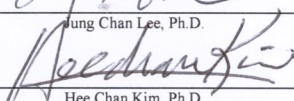
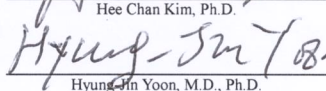
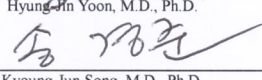
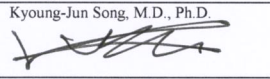
BY
HEEJIN KIM

INTERDISCIPLINARY PROGRAM IN
BIOENGINEERING
THE GRADUATE SCHOOL
SEOUL NATIONAL UNIVERSITY

THIS DISSERTATION IS APPROVED FOR
THE DEGREE OF DOCTOR OF PHILOSOPHY

FEBRUARY 2021

Approved by Thesis Committee:

Professor		Chairman
	<small>Jung Chan Lee, Ph.D.</small>	
Professor		Vice chairman
	<small>Hee Chan Kim, Ph.D.</small>	
Professor		Member
	<small>Hyung-Jin Yoon, M.D., Ph.D.</small>	
Professor		Member
	<small>Kyoung-Jun Song, M.D., Ph.D.</small>	
Professor		Member
	<small>Yunseo Ku, Ph.D.</small>	

Abstract

An Electroencephalogram-based Noninvasive Critical Care Monitoring for Emergency Patients

Heejin Kim

Interdisciplinary Program in Bioengineering

The Graduate School

Seoul National University

Electroencephalogram (EEG) is a recording of the electrical activity of the brain, measured using electrodes attached to the cerebrum cortex or the scalp. As a diagnostic tool for brain disorders, EEG has been widely used for clinical purposes such as epilepsy- and dementia diagnosis. This study develops an EEG-based noninvasive critical care monitoring method for emergency patients.

In the first two studies, ventricular fibrillation swine models were designed to develop EEG-based monitoring methods for evaluating the effectiveness of cardiopulmonary resuscitation (CPR). The CPR guidelines recommend measuring end-tidal carbon dioxide (ETCO₂) via endotracheal intubation to assess systemic circulation. However, accurate insertion of the endotracheal tube might be difficult in an out-of-hospital setting (OOHS). Therefore, an easily measurable EEG, which has been used to predict resuscitated patients' neurologic prognosis, was suggested as a surrogate indicator for CPR feedback. In the first experimental setup, the high- and low quality CPRs were altered 10 times repeatedly, and the EEG parameters were analyzed. Linear regression of an EEG-based brain resuscitation index (EBRI) was used to estimate ETCO₂

levels as a novel feedback indicator of systemic circulation during CPR. A positive correlation was found between the EBRI and the real ETCO₂, which indicates the feasibility of EBRI in OOHSSs. In the second experimental setup, two types of CPR mode were performed: basic life support and advanced cardiovascular life support. EEG signals that were measured between chest compressions and defibrillation shocks were analyzed to monitor the cerebral circulation with respect to the recovery of carotid blood flow (CaBF) during CPR. Significant EEG parameters were identified to represent the CaBF recovery, and machine learning (ML)-based classification models were established to differentiate between the higher ($\geq 30\%$) and lower ($< 30\%$) CaBF recovery. The prediction model based on the support vector machine (SVM) showed the best performance, with an accuracy of 0.853 and an area under the curve (AUC) of 0.909. The proposed models are expected to guide better cerebral resuscitation and enable early recovery of brain function.

In the third study, a swine model of traumatic brain injury (TBI) was designed to develop an EEG-based prediction model of an elevated intracranial pressure (ICP). TBI is defined as the disruption of normal brain function due to physical impact. This can increase ICP, and the resulting hypoperfusion can affect the cerebral electrical activity. Thus, we developed EEG-based prediction models to monitor ICP levels. During the experiments, EEG was measured while the ICP was adjusted with the Foley balloon catheter. Significant EEG parameters were determined to differentiate between the normal (< 25 mmHg) and dangerous (≥ 25 mmHg) ICP levels and ML-based binary classifiers were established to distinguish between these two groups. The multilayer perceptron model showed the best performance with an accuracy of 0.686 and an AUC of 0.754, which were improved to 0.760 and 0.834, respectively, when a noninvasive heart rate was also used as an input. The proposed prediction models are expected to instantly treat an elevated ICP (≥ 25 mmHg) in emergency settings.

This study presents a new EEG-based noninvasive monitoring method of the physiologic parameters of emergency patients, especially in an OOHS, and evaluates the performance of the proposed models. In this study, EEG was analyzed to predict immediate ETCO₂, CaBF, and ICP. The prediction models demonstrate that a noninvasive EEG can yield clinically important predictive outcomes. Eventually, the EEG parameters should be investigated with regard to the long-term neurological and functional outcomes. Further clinical trials are warranted to improve and evaluate the feasibility of the proposed method with respect to the neurological evaluation scores, such as the cerebral performance category and modified Rankin scale.

Keywords: Emergency situation, Electroencephalogram, Cardiopulmonary resuscitation, Traumatic brain injury, Physiologic parameters, Prediction models

Student Number: 2015-30263

Contents

Abstract	i
Contents.....	iv
List of Tables	viii
List of Figures	x
List of Abbreviations.....	xii

Chapter 1 General Introduction 1

1.1 Electroencephalogram.....	1
1.2 Clinical use of spontaneous EEG	5
1.3 EEG and cerebral hemodynamics	7
1.4 EEG use in emergency settings.....	9
1.5 Noninvasive CPR assessment	10
1.6 Noninvasive traumatic brain injury assessment.....	16
1.7 Thesis objectives	21

Chapter 2 EEG-based Brain Resuscitation Index for Monitoring Systemic Circulation During CPR 23

2.1 Introduction	23
2.2 Methods.....	25
2.2.1 Ethical statement	25

2.2.2	Study design and setting.....	25
2.2.3	Experimental animals and housing	27
2.2.4	Surgical preparation and hemodynamic measurements	27
2.2.5	EEG measurement.....	29
2.2.6	Data analysis	32
2.2.7	EBRI calculation	33
2.2.8	Delta-EBRI calculation	34
2.3	Results	36
2.3.1	Hemodynamic parameters.....	36
2.3.2	Changes in EEG parameters.....	37
2.3.3	EBRI calculation	39
2.3.4	Delta-EBRI calculation	41
2.4	Discussion	42
2.4.1	Accomplishment	42
2.4.2	Limitations	45
2.5	Conclusion.....	46

Chapter 3 EEG-based Prediction Model of the Recovery of Carotid Blood Flow for Monitoring Cerebral Circulation During CPR..... 47

3.1	Introduction	47
3.2	Methods	50
3.2.1	Ethical statement	50
3.2.2	Study design and setting.....	50
3.2.3	Experimental animals and housing	52
3.2.4	Surgical preparation and hemodynamic measurements	54
3.2.5	EEG measurement.....	55
3.2.6	Data processing	57

3.2.7	Data analysis	58
3.2.8	Development of machine-learning based prediction model.....	59
3.3	Results	63
3.3.1	Results of CPR process	63
3.3.2	EEG changes with the recovery of CaBF.....	66
3.3.3	Changes in EEG parameters depending on four CaBF groups ..	68
3.3.4	Changes in EEG parameters depending on two CaBF groups..	69
3.3.5	EEG parameters for prediction models	70
3.3.6	Performances of prediction models.....	73
3.4	Discussion	76
3.4.1	Accomplishment	76
3.4.2	Limitations	78
3.5	Conclusion.....	80

Chapter 4 EEG-based Prediction Model of an Increased Intra-Cranial Pressure for TBI patients ... 81

4.1	Introduction	81
4.2	Methods	83
4.2.1	Ethical statement	83
4.2.2	Study design and setting.....	83
4.2.3	Experimental animals and housing	85
4.2.4	Surgical preparation and hemodynamic measurements	86
4.2.5	EEG measurement.....	88
4.2.6	Data processing	90
4.2.7	Data analysis	90
4.2.8	Development of machine-learning based prediction model.....	91
4.3	Results	92
4.3.1	Hemodynamic changes during brain injury phase	92

4.3.2	EEG changes with an increase of ICP.....	93
4.3.3	EEG parameters for prediction models	94
4.3.4	Performances for prediction models	95
4.4	Discussion	100
4.4.1	Accomplishment	100
4.4.2	Limitations	104
4.5	Conclusion.....	104
Chapter 5 Summary and Future works		105
5.1	Thesis summary and contributions.....	105
5.2	Future direction	108
Bibilography.....		113
Abstract in Korean		135

List of Tables

Table 1.1	Noninvasive monitoring methodologies applied during CPR....	15
Table 1.2	Characteristics of noninvasive ICP monitoring methods.	20
Table 2.1	Technical specifications of the EEG device.	31
Table 2.2	Four EEG parameters derived to establish the EBRI model.	33
Table 2.3	Hemodynamic parameters depending on the CPR modes	37
Table 2.4	Correlation coefficients between the actual ETCO ₂ and EBRI .	41
Table 2.5	Performance of the delta-EBRI	42
Table 3.1	Technical specifications of the EEG device	57
Table 3.2	EEG parameters considered in this study	58
Table 3.3	Additional 9 EEG parameters considered for the prediction models	60
Table 3.4	Recovery rates of each hemodynamic parameter throughout the experiments	64
Table 3.5	Pearson correlation coefficients between EEG parameters and the recovery rates of CaBF.....	67
Table 3.6	Multiple comparisons between groups in three EEG parameters	69
Table 3.7	Results of the ROC curve analysis for the three EEG parameters	70
Table 3.8	Results of feature selection process.....	71
Table 3.9	Final 10 EEG parameters for the prediction models; their median, IQRs, and <i>p value</i>	72
Table 3.10	Comparison of EEG parameters from the normal brain and damaged brain	73
Table 3.11	Performance of prediction models for the recovery of CaBF	74
Table 4.1	Technical specifications of the EEG device	89
Table 4.2	Physiological data during baseline and brain injury phase	93
Table 4.3	Multiple comparisons between groups in three EEG parameters	94

Table 4.4	Final 10 EEG parameters for the ICP prediction models; their median, IQRs, and <i>p value</i>	95
Table 4.5	Performance of prediction models for the ICP groups with the EEG parameters alone	97
Table 4.6	Performance of prediction models for the ICP groups with the EEG parameters and the HR data	97

List of Figures

Figure 1.1	Generating mechanism of the EEG	3
Figure 1.2	Basic measurement setup for scalp EEG.....	4
Figure 1.3	Comparison of each frequency band.....	5
Figure 1.4	Cerebral ischemic thresholds	8
Figure 1.5	Hypothetical EEG measurement and analysis during CPR.....	14
Figure 2.1	The complete test protocol with a timeline	26
Figure 2.2	Four-channel EEG device	31
Figure 2.3	Artifact-removal process.....	33
Figure 2.4	Changes in the four EEG parameters throughout the experiments	38
Figure 2.5	Scatter plots between each EEG parameter and ETCO ₂	39
Figure 2.6	Comparison between the actual ETCO ₂ and estimated ETCO ₂ with the EBRI model.....	40
Figure 2.7	Performance of the delta-EBRI with 10 s time interval	42
Figure 3.1	Experimental setup.....	52
Figure 3.2	The entire test protocol.....	53
Figure 3.3	A single-channel portable EEG device used in this study	56
Figure 3.4	The entire development process of the prediction model for the recovery of CaBF	63
Figure 3.5	Comparison of EEG over time between ROSC and non-ROSC cases	66
Figure 3.6	Box plots of the means	68
Figure 3.7	ROC curves for three EEG parameters	70
Figure 3.8	The confusion matrices and the ROC curve of the five prediction models	75
Figure 4.1	The entire test protocol of TBI model with a timeline	85
Figure 4.2	Placement of the EEG device and catheters.....	87
Figure 4.3	An improved single-channel portable EEG device	89
Figure 4.4	Box plots of the means.....	94

Figure 4.5	Confusion matrices and ROC curves of the five prediction models with the EEG parameters alone as an input	98
Figure 4.6	Confusion matrices and ROC curves of the five prediction models with the EEG parameters and the HR data as inputs	99

List of Abbreviations

EEG	Electroencephalogram
CPR	Cardiopulmonary resuscitation
ETCO ₂	End-tidal carbon dioxide
OOHS	Out-of-hospital setting
EBRI	EEG-based brain resuscitation index
CaBF	Carotid blood flow
ML	Machine learning
SVM	Support vector machine
AUC	Area under the curve
TBI	Traumatic brain injury
ICP	Intracranial pressure
ADC	Analogue-to-digital converter
BIS	Bispectral index score
rCBF	Regional cerebral blood flow
CA	Cardiac arrest
ROSC	Return of spontaneous circulation
CNS	Central nervous system
CC	Chest compression
AHA	American Heart Association
QIP	Quantitative infrared pupillometry
TCD	Transcranial Doppler ultrasonography
PLR	Pupillary light response
FV	Flow velocity
rSO ₂	Regional cerebral oxygen saturation
NIRS	Near-infrared spectroscopy
HI	Hypoxia-ischemia
MAP	Mean arterial blood pressure
CBFV	Cerebral blood flow velocity
CEPP	Cerebral perfusion pressure
CVR	Cerebrovascular resistance

ONSD	Optic nerve sheath diameter
VEP	Visual evoked potential
ODM	Ophthalmo-dynamometry
TCA	Transcranial acoustic
ABP	Arterial blood pressure
VF	Ventricular fibrillation
OHCA	Out-of-hospital cardiac arrest
EMS	Emergency medical service
DBP	Diastolic blood pressure
COPP	Coronary perfusion pressure
EMT	Emergency medical technician
MFDS	Ministry of Food and Drug Safety
HQ-CPR	High-quality CPR
LQ-CPR	Low-quality CPR
KCl	Potassium chloride
KELAS	Korea Excellent Laboratory Animal Supplying Facility
AAALAC	Association for Assessment and Accreditation of Laboratory Animal Care
TV	Tidal volume
RR	Respiratory rate
PaCO ₂	Partial pressure of arterial CO ₂
PaO ₂	Partial pressure of arterial oxygen
RAP	Right atrial pressure
ECG	Electrocardiogram
SpO ₂	Saturation of percutaneous oxygen
AFE	Analog front end
MCU	Micro-processor unit
CMRR	Common mode rejection ratio
SPI	Serial peripheral interface
BSR	Burst suppression ratio
BetaR	Relative beta ratio
DeltaR	Relative delta ratio

SynchFS	Relative synchrony of fast and slow waves
TP	True positive
TN	True negative
FP	False positive
FN	False negative
ROC	Receiver operating characteristic
TPR	True positive rate
FPR	False positive rate
SBP	Systolic blood pressure
IQR	Interquartile range
BLS	Basic life support
ACLS	Advanced cardiovascular life support
IACUC	Institutional Animal Care and Use Committee
BLE	Bluetooth low-energy
ANOVA	Analysis of variance
NCA	Neighborhood component analysis
LR	Logistic regression
KNN	K-nearest neighbors
MLP	Multilayer perceptron
RF	Random forest
SMOTE	Synthetic minority oversampling technique
HR	Heart rate
MRI	Magnetic resonance imaging
CPC	Cerebral performance category
mRS	Modified Rankin scale

Chapter 1. General Introduction

1.1. Electroencephalogram

Electroencephalogram (EEG) is a continuous recording of the brain's spontaneous electrical activity, measured by using electrodes placed on the scalp or the cerebrum cortex [1–3]. Generally, an EEG is recorded noninvasively with multiple surface electrodes attached along the scalp [4, 5]. The locations of the electrodes are usually described by the International 10–20 system [6].

An EEG is generated by the mechanisms of pyramidal neurons in the cerebral cortex [3, 7]. The neurons are electrically polarized while the membrane transports ions through a branch of channels that control signals in and out of the membrane. The most important channel is the sodium-potassium channel, which maintains the basal resting potential of the neuron by pumping three Na^+ ions out of the cell while pumping two K^+ ions into the cell. A resting intracellular potential of -70 mV is created (Figure 1.1 (A)). An action potential causes the signals to move through the neurons, and the Na^+ ions enter the cell through the channel. Depolarization occurs and a positive intracellular potential at approximately 20 mV is created (Figure 1.1 (B)). Immediately after depolarization, the K^+ ions move out of the cells and a negative intracellular potential of approximately -100 mV is created, which is defined as

hyperpolarization (Figure 1.1 (C)). While signals move in and out of the ion channels, neurons communicate with other neurons at their synapses. Excitatory neurotransmitters generate an excitatory postsynaptic potential to promote depolarization and signal propagation to the surrounding neurons. Inhibitory neurotransmitters generate an inhibitory postsynaptic potential to promote hyperpolarization and halt signal propagation. Extracellular potential, which creates a local electric field, during neuronal function is detected by scalp EEG electrodes. The potential of each neuron is too diminutive to be detected by electrodes, but detectable voltage can be created if millions of neurons are aligned perpendicular to the brain surface and depolarized simultaneously [8]. The polarity of the voltage on the electrodes is determined by the depolarization location. Negative voltage is detected when superficial neurons are depolarized (Figure 1.1 (D)), whereas a positive voltage is detected when deep neurons are depolarized (Figure 1.1 (E)). When scalp EEG electrodes are charged, the voltage fluctuation between the two electrodes is amplified to record an EEG [9]. The entire EEG generation mechanism is illustrated in Figure 1.1.

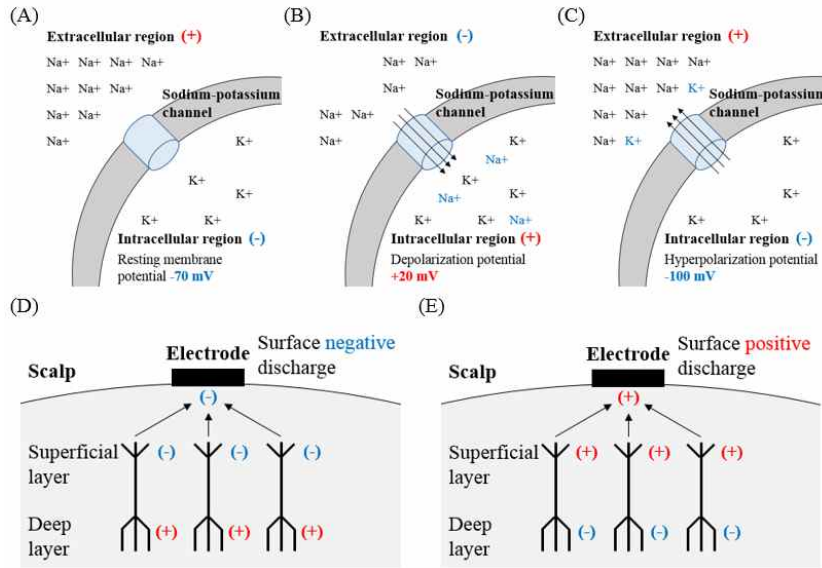


Figure 1.1 Generating mechanism of the EEG: (A) The resting state of neuronal function, (B) Depolarization, (C) Hyperpolarization, (D) Negatively charged electrode, (E) Positively charged electrode.

A certain active electrode is connected to one input of a differential amplifier [10, 11]. Another input of the differential amplifier can differ depending on the montage, i.e. the representation of the EEG channels. The reference electrode is applied in the referential montage. However, another active electrode is applied in the sequential montage. After connecting the electrodes, the differential potentials between the two electrodes are usually amplified, band-pass filtered, and digitized, to be saved and further analyzed. Typically, the sampling rate of the analogue-to-digital converter (ADC) is above 250 Hz. Artifacts that can contaminate the original signal should be removed. Power-line interference with a fundamental frequency of 50 or 60 Hz can be eliminated by a band-reject filter [3, 9]. The basic measurement setup for scalp EEG is illustrated in Figure 1.2.

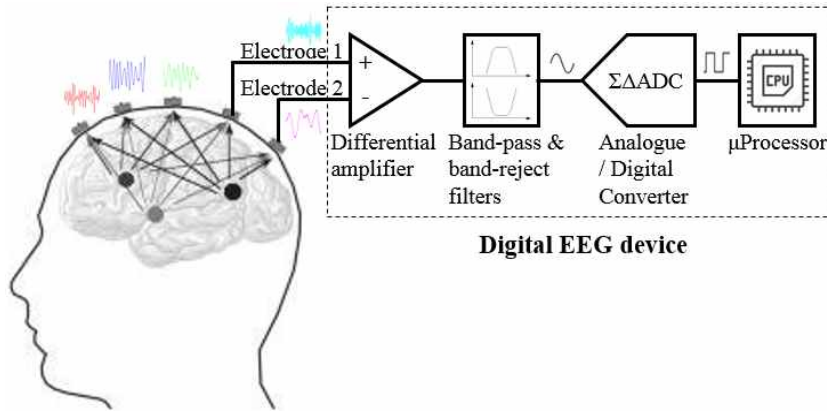


Figure 1.2 Basic measurement setup for scalp EEG.

Conventionally, the EEG signal is analyzed in the time and frequency domain. Continuous suppressed periods or abrupt bursting patterns can pose clinical significances [12–15]. The rhythmic activity of the EEG signal is typically described with frequency bands [16, 17]. A Fourier transform is performed to represent the distribution of the frequency components of the signal. The bandwidth and characteristics of each band are presented in Figure 1.3. Delta waves with low frequencies ranging up to 4 Hz are related to deep sleep or loss of awareness. Theta waves with frequencies ranging from 4 Hz to 8 Hz are easily monitored in the states of drowsiness or meditation in adults. Alpha waves in a frequency range of 8–13 Hz represent relaxed and calm conditions. The alpha waves emerge when the eyes are closed and attenuate with mental activity or when the eyes open. Beta waves with a frequency range of 13–30 Hz can be easily monitored in subjects who are highly anxious or focused with their eyes opened. Gamma waves ranging above 30 Hz are associated with cognitive processes. The nonlinear characteristics of neural

activity can be analyzed to uncover complex dynamics of EEG signals. Several entropy indices have been introduced to reveal the complexity and randomness of the EEG signal [18–21]. Bispectral analysis is a technique for quantifying nonlinear subtle phase coupling [22].

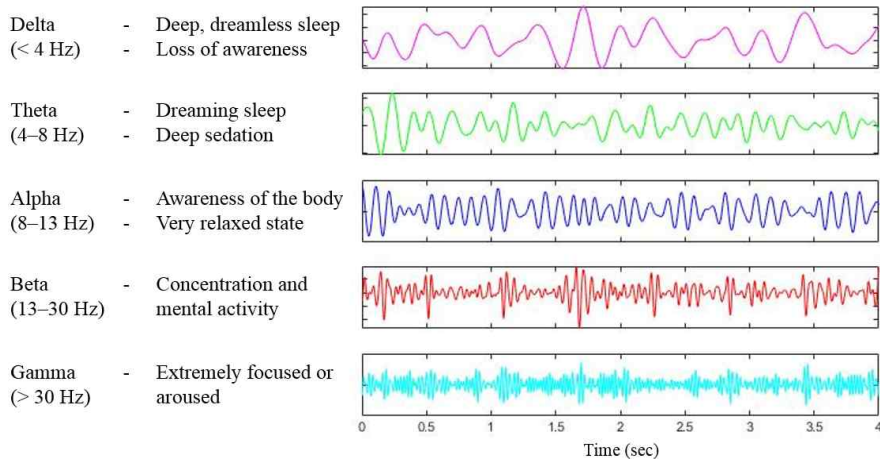


Figure 1.3 Comparison of each frequency band.

1.2. Clinical use of spontaneous EEG

As a diagnostic method for brain activity, EEG has been widely used for a variety of clinical purposes. Most of all, EEG signals are measured for diagnosing epilepsy [23, 24]. Multi-channel EEG signals are measured to detect epileptic activities and to localize the regions from which seizure activities originate. Different types of epileptic seizures can be identified using EEG. Several feature extraction methods have been developed to automatically detect epilepsy stages [25].

During post-resuscitation treatment, EEG bursting patterns, rate, peak, and duration, are investigated to evaluate the return of the neurological function in the resuscitated patients [26]. Early and increased EEG bursting patterns are related to favorable neurological outcomes. Furthermore, EEG activity is routinely monitored to diagnose dementia [27]. An increase in lower frequencies is a noticeable sign of the early stages of dementia. A reduced complexity of the EEG can be another physiological response of the disease.

As a sensitive indicator of the effect of anesthetic administration, EEGs can be analyzed to monitor the depth of anesthesia [22, 28]. The BIS Vista Monitor (Aspect Medical Systems, Norwood, MA, USA) was developed to evaluate patient-specific effects of anesthesia and achieve the desired level of sedation by performing bispectral analysis on the EEG measured from the prefrontal cortex [29]. Sleep-related physiological responses are also monitored with scalp EEG oscillations [30]. With advances in machine learning (ML) methods and wearable sensors, processed EEG signals, such as power spectral density and a structural complexity, can be obtained from a portable EEG device to evaluate the sleep stages [31].

EEG biomarkers, such as entropy indices, bispectral index score (BIS) and epileptic patterns, can be calculated or detected using diverse signal processing techniques and ML methods. They have shown the possibility of monitoring various brain-related disorders or diseases.

1.3. EEG and cerebral hemodynamics

Previous studies have reported the relationship between cerebral blood flow (CBF) and EEG activity during cerebral ischemia. Patients with no neurological deficits underwent carotid endarterectomy under general anesthesia [32, 33]. A distinctive correlation between the levels of regional cerebral blood flow (rCBF) and the EEG activity was found. The EEG activity was not altered with the normal rCBF above 30 ml/100gm/min, and subtle changes were found with the rCBF in the range 18–30 ml/100gm/min. Apparent changes were observed when the rCBF dropped below 18 ml/100gm/min. The amplitude of the EEG decreased at first. Then, the power spectrum was re-distributed toward lower frequencies, and the total spectral power decreased. After the surgery, the rCBF returned to normal conditions, followed by recovery in the EEG activity. These results were supported by previous studies which stated that 30–40% of normal CBF could be the threshold for the recovery of normal brain function and EEG fluttering [34–36]. Similar results were found in cardiac arrest (CA) situations. The EEG activity was lost in a few seconds after the CA occurred [37]. However, the EEG activity returned to the pre-CA state when return of spontaneous circulation (ROSC) was achieved. Recovery time was related to the duration of no- or low-flow and the ischemic episode [38]. The functional relationship between CBF and EEG activity is described in Figure 1.4.

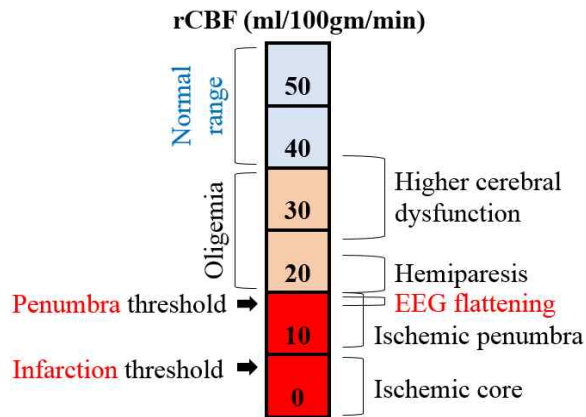


Figure 1.4 Cerebral ischemic thresholds.

The relationship between cerebral circulation and electrical activity is attributable to cerebral oxygenation levels [39, 40]. The relationship between neural activity and oxygenation has been poorly understood; however, the cerebral tissue oxygen metabolism, the rate of oxygen consumption for neural activity, is assumed to be affected by oxygen supply [41]. Cerebral hypoxia can restrain neuronal functions such as transmitting electrical signals to the surrounding neurons and generating action potentials. Previous findings indicate that low rCBF levels below 18 ml/100gm/min lead to an inactive EEG. A study by Losasso *et al.* showed sufficient brain perfusion and oxygen delivery can result in the return of the EEG activity in resuscitated patients after cardiopulmonary resuscitation (CPR) [38]. This result demonstrated the role of well-oxygenated blood flow in the electrical activity of the cerebral cortex, although the minimum oxygenation needed for normal brain function has not been clearly identified.

1.4. EEG use in emergency settings

An emergency EEG was proposed primarily for the diagnosis and management of non-convulsive epileptic seizures [42–44], which can cause impaired consciousness and neurological injury. In such emergency settings, monitoring brain function is critical to prevent irreversible damage to the central nervous system (CNS). As a diagnostic tool for the integrity of CNS neurons, measuring a noninvasive EEG can enable early access to brain cell viability without additional diagnostic modalities, and advance treatments in certain situations [44, 45]. If a reliable noninvasive EEG can be obtained, physicians or EMTs using other diagnostic tools could evaluate and treat the patients more comprehensively.

Typically, a minimum of 16 channels are recommended for EEG monitoring; however, a smaller number of channels can be allowed in special circumstances [46]. For instance, fewer channels can be adopted to capture seizure activity during an emergency procedure [47–49]. The CSM M3 (Cerebral State Monitor M3, Danmeter A/S, Odense, Denmark) [45] and the BIS Vista Monitor provide EEG-based measurements of an anesthetic depth, exploiting only one or two channels.

These devices have been applied in an OOHs. A major obstacle for emergency EEG is the existence of artifacts, which can contaminate the raw EEG signals. Several factors, such as unintended visual or auditory stimulus,

extremely high electrode-skin impedance, and motion artifacts, could cause electroencephalographic alterations. These problems can worsen in CA or CPR situations. However, if secure installation with a low electrode-skin impedance and artifact prevention techniques is feasible, a reliable noninvasive measurement could be obtained. The CSM M3 could provide single-channel out-of-hospital EEG measurements with acceptable rates of artifacts [44]. The successful acquisition of high-quality EEG measurements creates new possibilities for real-time brain function monitoring using small portable EEG devices in emergency settings.

1.5. Noninvasive CPR assessment

CPR is the most effective method for supplying sufficient blood to critical organs in CA patients, and high-quality CPR should be performed to achieve improved survival rates and neurological outcomes [50, 51]. To perform high-quality CPR, several monitoring methods have been suggested as indicators for CPR quality assessment. In the clinical field, certain rates and depth conditions of chest compressions (CCs) are targeted, and CPR feedback devices on CC rates and depth are widely used [52, 53]. However, following certain CC conditions does not always lead to the best performance owing to the different body conditions of patients. This problem has gained increasing interest in the monitoring methods using individual physiological responses [54, 55].

The feasibility of physiology-based CPR assessment methods has been evaluated, and end-tidal carbon dioxide (ETCO₂) has been proposed as a reliable indicator for systemic circulation by the American Heart Association (AHA) [56]. An ETCO₂-directed feedback method improved the chance of ROSC [57, 58]. However, placing endotracheal tube could be demanding and improper installation could generate low values. In addition, it mainly reflects the entire systemic circulation, rather than the cerebral circulation. The burden of CA can be demanding with regard to disability and neurological deficits, owing to prolonged hypoxia, because these factors can influence the survivors' quality of life and their socioeconomic burden [59, 60]. Thus, achieving early neurological recovery by supplying sufficient CBF has been regarded as one of the major goals of CPR [61]. Thus, additional monitoring of the cerebral circulation is highly required.

Recently, several noninvasive monitoring modalities have been applied during CPR. Quantitative infrared pupillometry (QIP), transcranial Doppler ultrasonography (TCD), cerebral oximetry, and electroencephalography have been used for noninvasive CPR quality assessments. The QIP measures pupil size and changes, such as dilation and constriction, with near-infrared light [62]. The pupillary light response (PLR) is a reflex that controls the diameter of the pupil in response to light intensity and is not affected by cognitive functions [63]. Specifically, a higher intensity of light causes pupillary constriction, which allows for reduced light adaptation. The PLR decreases when CBF

decreases [64], such as in CA or CPR situations. Therefore, the QIP can be used to monitor CBF changes during CPR [65]. Patients who experienced a short period of CA had a constricted pupil with a normal PLR during CPR [66], and achieving a positive PLR can be a sign of favorable neurological functions [62]. The continuous appearance of the PLR or a short absence of less than 5 min was related to early survival and favorable neurological outcomes, while no PLR or a longer absence for over 5 min was related to death or unfavorable outcomes [64, 66]. QIP can be useful in assessing cerebral resuscitation because it is not affected by epinephrine and neuromuscular blockade. However, the limitation of this method is that variations in pupil size and response exist owing to aging and the use of drugs (i.e., opioids and sedatives) [67]. TCD has also been applied to patients undergoing CPR. Real-time red cell flow velocity (FV) is measured noninvasively by using ultrasonic waves. TCD can be applied in the CPR setting because the blood FV is reduced to approximately 80% of the pre-CA condition at the beginning of CPR and can be altered according to changes in cerebral vascular resistance [68]. Improved blood FV after more effective CPR efforts can be quantified using the TCD method [69]. However, finding correct vessels could be difficult, and the signal measurements are operator dependent [70]. These problems significantly limit the use of TCD in CPR situations. Cerebral oximetry is the most widely used noninvasive CPR monitoring method. The regional cerebral oxygen saturation (rSO₂) levels, measured by near-infrared spectroscopy (NIRS), are associated with the

occurrence of ROSC and favorable neurological outcomes [71, 72]. A significant difference in rSO₂ levels was identified between resuscitated and deceased patients [73]. The rSO₂ level correlated well with a conventional monitoring parameter for systemic circulation, ETCO₂, allowing ROSC prediction with NIRS values [74]. Achieving higher rSO₂ can improve systemic and cerebral circulation during CPR [73]. However, higher rSO₂ is not always passed on to high-quality cerebral resuscitation. The rSO₂ and EEG showed different changes after prolonged hypoxia-ischemia (HI) [75]. When the mean arterial blood pressure (MAP) was returned to baseline values after HI for 60 min, rSO₂ returned to baseline values quickly; however, the EEG still showed HI-induced suppression activity. Because irreversible damage might occur in the brain owing to prolonged ischemic insults [38], EEG activity should also be monitored. EEG has a great advantage of continuous monitoring of brain neuronal activity over NIRS.

EEG is closely associated with the cerebral circulation and physiologic responses of the brain [76, 77]. The relationship between EEG and cerebral circulation has been investigated over several decades [78]. Because EEG-derived indices, such as BIS, were introduced, EEG has been used to monitor cerebral perfusion during CPR. However, the usefulness of EEG-derived indices during CPR remains controversial [79, 80]. In 2018, Reagan *et al.* reported the first human clinical trial that evaluated cerebral resuscitation by utilizing a portable EEG and NIRS device together [81]. Real-time rSO₂ and

EEG were measured during CPR. Approximately 60% of the EEG data, measured during short pauses for an ECG rhythm check, were interpretable, which demonstrated the feasibility of measuring EEG using a portable device during CPR. Seven distinct EEG patterns were identified with regard to the rSO₂ levels for the first time. This study emphasized the importance of EEG monitoring during CPR because EEG can represent the actual effect of oxygen delivery on brain cell viability. Therefore, new automated methods that quantify the EEG patterns with respect to hemodynamic parameters during CPR could help physicians to better understand the patient's neurological condition and guide proper neuroprotective strategies during CPR. Several noninvasive monitoring methodologies applied during CPR are listed in Table 1.1.

Recent advances in low-cost portable EEG devices have been reported [82, 83]. These devices can improve the applicability of the noninvasive EEG as an indicator of CBF recovery in CA situations. The hypothetical EEG measurement during CPR is illustrated in Figure 1.5.

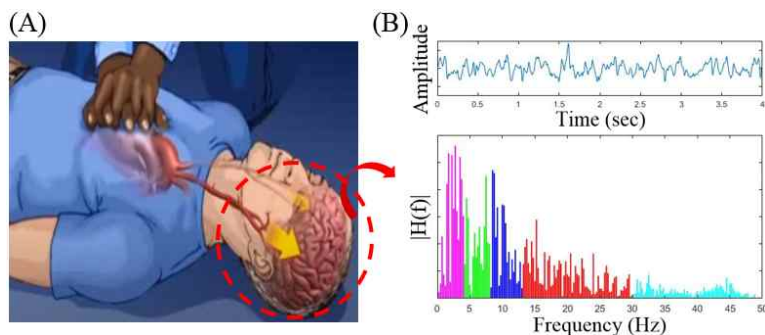


Figure 1.5 Hypothetical EEG measurement and analysis during CPR: (A) Increased blood flow to the brain, (B) Possible EEG analysis in time- and frequency-domain.

Table 1.1 Noninvasive monitoring methodologies applied during CPR.

Methodology	Authors	Year	Research findings
QIP	Larson <i>et al.</i> ,	1995	Portable infrared pupillometry can reveal the presence of midbrain function [65].
	Behrends <i>et al.</i> ,	2012	The presence of PLR during CPR was associated with early survival from CA. The absence of PLR for > 5min during CPR was associated with death or poor neurological outcomes [64].
	Lee <i>et al.</i> ,	2019	Patients with positive PLR during CPR had favorable outcomes [66].
TCD	Lewis <i>et al.</i> ,	1990	Real-time red cell blood flow velocity was measured during CPR. The blood flow velocity was altered because of changes in cerebral vascular resistance and the use of epinephrine [68].
	Blumenstein <i>et al.</i> ,	2010	Improved blood flow velocity after more effective CPR was evaluated [69].
NIRS	Ioroi <i>et al.</i> ,	2002	The rSO ₂ and EEG showed different time profiles after prolonged perinatal asphyxia [75].
	Parnia <i>et al.</i> ,	2014	The ROSC and non-ROSC patients showed a significant difference in rSO ₂ levels [73].
	Xu <i>et al.</i> ,	2015	The amplitudes of rSO ₂ increased during CPR in CA animal models and were higher in the high-quality CPR group than in the low-quality group. They correlated well with ETCO ₂ [74].
	Parnia <i>et al.</i> ,	2016	Higher rSO ₂ during CPR was associated with ROSC and neurologically favorable survival [71].
	Cournoyer <i>et al.</i> ,	2016	Patients who survived to discharge and who had good neurological outcome displayed superior combined initial and mean NIRS values than those of their counterparts [72].
EEG	Ingvar <i>et al.</i> ,	1976	The dominant EEG frequency correlated with the blood flow to the brain [78].
	Charlotte <i>et al.</i> ,	2009	The use of BIS to monitor cerebral function during ACLS was pointless [79].
	Jung <i>et al.</i> ,	2013	As a basic monitoring device during CPR, BIS can help in deciding to continue CPR [80].
	Reagan <i>et al.</i> ,	2018	Portable EEG monitoring during CPR was feasible and can provide information regarding the quality of cerebral resuscitation, in terms of brain functionality. Seven distinct EEG patterns were identified with regard to the different rSO ₂ levels [81].

Abbreviation: QIP, Quantitative infrared pupillometry; TCD, Transcranial Doppler ultrasonography; NIRS, Near-infrared spectroscopy; EEG, Electroencephalogram; PLR, Pupillary light response; CPR, Cardiopulmonary resuscitation; CA, Cardiac arrest; rSO₂, Regional cerebral oxygen saturation; ETCO₂, End-tidal carbon dioxide; BIS, Bispectral index score; ACLS, Advanced cardiovascular life support;

1.6. Noninvasive traumatic brain injury assessment

Traumatic brain injury (TBI) is defined as a disruption of normal brain function [84], and its long-term consequences are a major medical problem. Severe TBI causes immediate cognitive and physical disorders, but symptoms of mild TBI may be felt from several months after injury. Socioeconomic losses, including a financial burdens, might be substantial [85, 86] because TBI requires significant medical costs [87] and reduces the patients' ability to work [88, 89]. These problems have raised the need for accurate prognostication of outcomes following TBI with various neuro-monitoring modalities.

The consequences of TBI fall into two categories: primary injury caused directly by physical impact, and secondary damage resulting from the pathophysiologic responses of primary injury, including hypoperfusion due to cerebral edema and increased intracranial pressure (ICP). Thus, ICP should be monitored continuously in a timely fashion to minimize secondary damage and maintain cerebral perfusion [90–92]. At present, invasive methods containing an insertion of a pressure catheter into the intracranial region have been regarded as the standard. However, there are many associated complications such as nervous system injury, infection, occlusion of the catheter, or bleeding [93–95].

Multiple noninvasive techniques have been suggested to overcome these drawbacks. According to Zhang *et al.*, noninvasive ICP monitoring methods

can be categorized into five groups: fluid dynamics, ophthalmic, otic, electrophysiologic, and others [94]. TCD, near-infrared spectroscopy (NIRS), and cerebral blood flow velocity (CBFV) measure dynamic fluid changes. ICP can be calculated from the TCD measurements, real-time red cell FV, because increased ICP can decrease the blood FV [96]. The TCD could be useful in estimating ICP; however, hand measurements by a skillful technician could generate inter-observer variability [70]. NIRS monitors continuous cerebral blood volume by measuring the concentration of deoxygenated and oxygenated hemoglobin in the blood [97]. Portable NIRS devices can be applied in emergency settings [81]. However, the relationship between cerebral oxygenation levels and ICP has rarely been investigated [98]. CBFV is determined by cerebral perfusion pressure (CEPP) and cerebrovascular resistance (CVR). CEPP is decreased and CVR is increased in case of increased ICP [94]. Based on these relationships, noninvasive ICP monitoring techniques were also developed [96, 99]. These methods have wide applicability in a clinical setting because they do not require any calibration or training. However, ABP measurement at the radial artery and computation process limits the use in emergency settings. The Ophthalmic method can accurately estimate ICP. The optic nerve sheath diameter (ONSD) assessment utilizes the physiologic response that the optic nerve sheath distends owing to increased ICP [100, 101]. A significant correlation between ONSD and ICP was found. In addition, the ONSD assessment could detect increased ICP above 20 mmHg accurately with

an AUC of 0.94 [102]. However, the drawbacks of this method are related to the effect of possible pathologies, such as atrophy and inter-subject variability, including different optic nerve sizes and age [94]. The QIP is also applied to estimate the ICP. Monitoring subtle changes in pupil size effectively diagnose TBI patients [103–105]. TBI patients with an ICP of over 20 mmHg showed reduced constriction compared to healthy people (TBI patients: 20% vs. healthy people: 34%) [106]. However, the QIP measurement can be disturbed by several factors, such as certain medical conditions, medications, and emotional status [107]. Venous ophthalmo-dynamometry (ODM) measures the pressure within the central retinal vein to quantify ICP [108]. An increase in ICP is followed by increased central retinal vein pressure [109, 110]. Portable venous ODM measurement is a validated method for estimating ICP in hospitalized patients. However, the ODM method cannot monitor continuous changes, and a physician skilled in eye examination is necessary [94]. Transcranial acoustic (TCA) signals mixed with head-generated sounds can be measured from the outer ear channel to estimate static and pulsatile ICP [111, 112]. However, the TCA method was mainly validated with low ICP ranges below 15 mmHg. Further research is needed to confirm the functionality of this method for estimating increased ICP. Skull vibration is also related to ICP changes. ICP changes produce a stress field over the skull and determine skull stiffness [113]. The natural frequency responses generated by the skull vibration and stiffness can be measured to estimate the ICP. This method can be developed with a

model for the complex anatomical structure of the human head [113, 114]. Electrophysiologic responses, such as visual evoked potential (VEP), can also be used to estimate ICP [115]. VEP latencies can be delayed owing to increased ICP. However, the existence of inter-subject variability in VEP latencies makes it difficult to differentiate between natural physiological long latencies and the pathophysiologic effects of increased ICP. In addition, continuous visual stimulation might be fatiguing for conscious patients [96, 116]. Spontaneous EEG can be a more convenient method [117, 118]. Previous observational studies examined the correlation between elevated ICP and EEG activity in patients with TBI and found that burst suppression patterns can be an indicator of elevated ICP [119–121]. Spontaneous EEG activity reflects ongoing ICP changes. With stable arterial blood pressure (ABP), an increased ICP could reduce CEPP and CBF. Consequently, ischemic insults and metabolic injury of the brain cells might occur, gradually deactivating cerebral electrical activity. Based on these relationships, EEG activity might have the potential to predict ICP changes [118]. The specific characteristics of the noninvasive ICP monitoring methods are listed in Table 1.2.

Table 1.2 Characteristics of noninvasive ICP monitoring methods.

Methodology		Accuracy (mmHg)	Skill level	Cost of technology	Continuous monitoring	Emergency setting ^①	Properties
Fluid dynamics	TCD	± 10–15	Expert	Moderate	No	Yes	- Finding correct vessels is difficult.
	NIRS	NV	Low	Moderate	No	Yes	- Portable devices available.
	CBFV	± 1.5	Low	Moderate	No	No	- ABP measurement is needed ^② .
Ophthalmic	ONSD assessment	± 5–10	Moderate / High	Moderate / High	No	Yes	- Can be used in emergency department with sonography.
	Pupillometry	NV	Low	Low	No	Yes	- Measurement can be affected by several factors.
	Venous ODM	± 3–5	Expert	Low	No	No	- Repeated examinations can be cumbersome.
Otic	TCA signals	± 5	Moderate	Moderate	Yes	No	-
Electro- physiologic	VEP	NV	Expert	Low	No	No	- Not suitable for many patients with retinal injuries or optic nerve pathologies
	EEG	NV	Low	Low	Yes	Yes	- Portable devices available.
Others	Skull vibrations	NV	Expert	Low	No	No	- Complex mathematical models for human head are needed.

Abbreviation: TCD, Transcranial Doppler ultrasonography; NIRS, Near-infrared spectroscopy; CBFV, Cerebral blood flow velocity; ONSD, Optic nerve sheath diameter; ODM, Ophthalmodynamometry; TCA, Transcranial acoustic; VEP, Visual-evoked potential; EEG, Electroencephalogram; NV, Not validated; ABP, Arterial blood pressure;

^① Hospital-level emergency settings (e.g., an emergency department and intensive care unit)

^② Invasive measurement from the radial artery

1.7. Thesis objectives

The main objectives of this thesis are to investigate the relationships between EEG and physiological parameters such as ETCO₂, carotid blood flow (CaBF), and ICP, and thus evaluate the feasibility of an EEG-based critical care monitoring system in CA and TBI situations. The main reason the CA and TBI situations were considered was because not only the patients' life or death but also the degree of disability depends on the effectiveness of immediate emergency care in these situations [122–125]. Monitoring hemodynamic parameters can lead to better outcomes as hemodynamic data can reveal the consequences of the treatments. However, such monitoring could be difficult in patients with CA and TBI. Furthermore, cell viability of the brain should be obtained early to improve neurological outcomes in these situations; however, real-time brain activity has rarely been monitored to date.

Cerebral circulation showed a positive correlation with systemic circulation during CPR [126], and EEG activity recovered when the cerebral circulation returned to the normal state [38]. Thus, it was assumed that both systemic and cerebral circulation could be evaluated through EEG monitoring. Several studies have attempted to evaluate the quality of CPR using the BIS Vista monitor, and the effectiveness of the BIS machine during CPR has been controversial, mainly because of CPR artifacts [79, 80]. However, in this study, Chapter 2 investigates the relationship between EEG and ETCO₂—an indicator

of systemic circulation during CPR. CPR artifacts on the EEG signal were removed, and an EEG-based brain resuscitation index (EBRI) model was established with a self-developed four-channel EEG device and swine model of ventricular fibrillation (VF). The EBRI model was developed to estimate ETCO₂ to evaluate the recovery of systemic circulation, as an alternative to ETCO₂ measurement.

In Chapter 3, the relationship between cerebral circulation and EEG was investigated using an improved swine model of VF and a single-channel EEG device. CaBF was measured to monitor cerebral circulation. The recovery of cerebral circulation can affect the early recovery of brain function in patients with CA. However, there is no means to monitor cerebral circulation during CPR. Thus, an EEG-based prediction model was developed to estimate the recovery rates of CaBF.

In Chapter 4, the relationship between EEG and ICP in TBI situations is described. After severe head injury, increased ICP might impede cerebral circulation, resulting in attenuated EEG activity. Thus, we assumed that there are differences in EEG functionality between the normal and increased ICP. Several observational studies have reported a relationship between EEG and ICP changes. However, this study quantitatively analyzed EEG changes according to ICP changes in a single animal. A swine model of TBI and an improved single-channel EEG device were utilized to develop the first EEG-based ICP prediction model.

Chapter 2. EEG-based Brain Resuscitation Index for Monitoring Systemic Circulation During CPR

2.1. Introduction

According to a 2017 report by the AHA, over 180000 out-of-hospital cardiac arrest (OHCA) patients are treated annually by emergency medical services (EMS), and the average survival to hospital discharge rate of EMS-treated OHCA is approximately 10% in the United States. [127]. As a core component of the chain of survival, accurate and immediate CPR is critical to improve the survival rates and good neurological recovery of CA patients [59, 128, 129].

To perform high-quality CPR, applying a certain depth and rates of chest compressions (CCs), as directed by CPR guidelines, and monitoring the actual operation are of fundamental importance. A variety of CPR feedback devices have been introduced to assess the depth, speed, and chest recoil of CCs [52, 53]. However, CC-oriented monitoring cannot evaluate the actual recovery of systemic circulation in patients. Therefore, additional methods based on physiological responses are required to evaluate the real effectiveness of CPR [54, 55].

The AHA guidelines suggested three physiologic parameters as indicators of the systemic circulation during CPR— ETCO₂, diastolic arterial pressure

(DBP), and coronary perfusion pressure (COPP) [130]. However, the COPP and DBP, which require central venous cannulation and an insertion of a pressure catheter, are not applicable in real CPR situations. ETCO₂ can be measured through endotracheal intubation [131], and ETCO₂-directed feedback methods can increase the likelihood of ROSC [57, 58]. However, it would be difficult for unskilled emergency medical technicians (EMTs) to install endotracheal tubes, especially in an OOHs, and improper placement might obstruct the airway and show low ETCO₂ [130, 132].

Therefore, in this study, we focused on EEG as a noninvasive surrogate indicator of ETCO₂. EEG is easily measurable and reveals changes in the cerebral circulation. The EEG signals, including spontaneous activity and evoked potential, are monitored to investigate neurological recovery of resuscitated patients [26, 133]. Previous studies measured EEG during CPR and found relationships between EEG activity and cerebral hypoperfusion [37, 38]. We designed an experimental swine model of VF to develop an EEG-based Brain Resuscitation Index (EBRI) to estimate ETCO₂. We hypothesized that an increased cardiac output during CPR leads to an increased systemic circulation. Concurrently, cerebral circulation and oxygenation are also recovered, which can lead to a more improved EEG activity.

2.2. Methods

2.2.1 Ethical statement

The animal test protocol was approved by the Institutional Animal Care and Use Committee of Seoul National University Hospital (IACUC number: 15-0288). All animal care complied with the Laboratory Animal Act of the Korean Ministry of Food and Drug Safety (MFDS).

2.2.2 Study design and setting

A swine model of VF was designed to acquire EEG signals during CPR. After untreated VF for 1 min, 10 cycles of 2-min CPR were delivered manually. The physiological signals, including the frontal EEG, were measured throughout the experiments. Each CPR session consisted of a 50 s long high-quality CPR (HQ-CPR), followed by a 10 s pause, then a 50 s long low-quality CPR (LQ-CPR), and last a 10 s pause. During HQ-CPR, an EMT performed the CCs at a rate of 100 times per minute with a depth of 5 cm. Contrarily, during LQ-CPR, the EMT performed the CCs at a rate of 60 times per minute with a depth of 3 cm. A 10 s hands-off time was used twice to change the CPR mode. During all CPR sessions, an X Series CPR Monitor (Zoll Medical Corporation, Chelmsford, MA, USA) was used to check the actual rates and depth. After all the CPR sessions, 1 mg of epinephrine was injected intravenously and biphasic defibrillation shock of 200 J was applied to restart the

heart. The ROSC was checked after a 2-min HQ-CPR. If the ROSC was not achieved, a second defibrillation and 2-min HQ-CPR were performed, and the ROSC was checked. Defibrillation procedures were attempted up to three times. If the ROSC was achieved, the animals were euthanized with an injection of 20 mg potassium chloride (KCl). The entire test protocol is described in Figure 2.1.

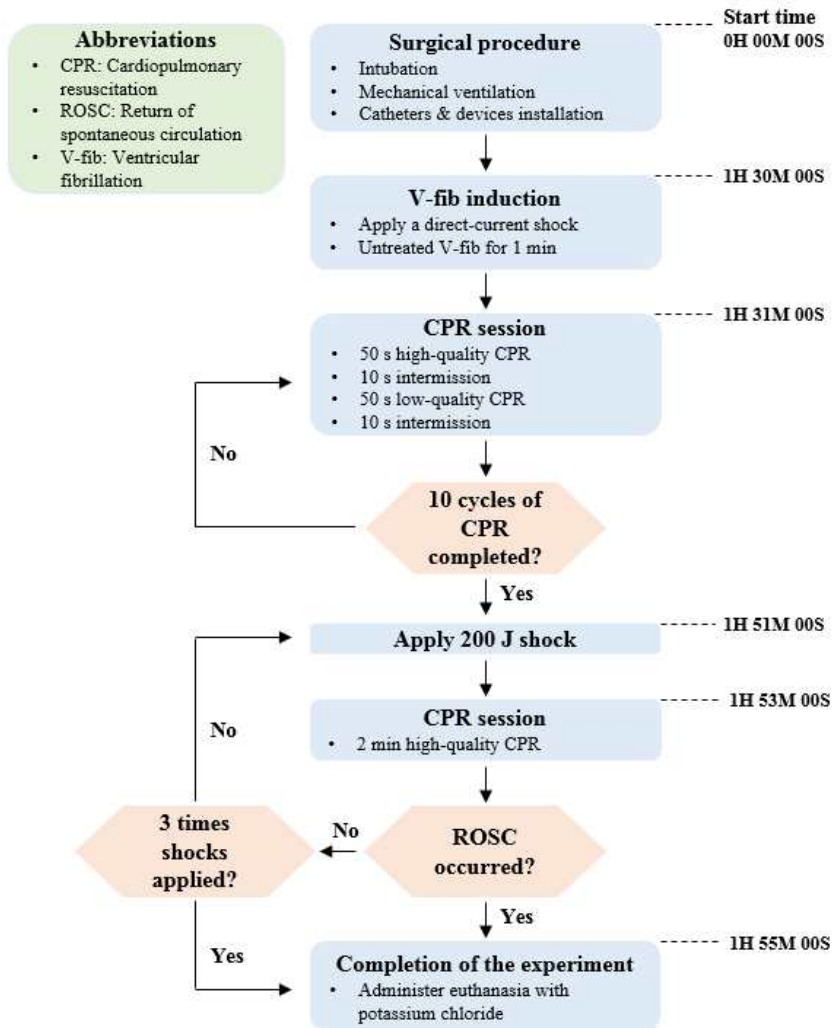


Figure 2.1 The complete test protocol with a timeline.

2.2.3 Experimental animals and housing

Five domestic crossbred female pigs, approximately 3 months of age (44.6 ± 2.7 kg), were studied. The animals were obtained from the supplier of experimental animals (Cronex Co., Ltd., Cheongju, Korea), qualified by the Korean MFDS with a certificate from the Korea Excellent Laboratory Animal Supplying Facility (KELAS). The animals were maintained in an accredited Association for Assessment and Accreditation of Laboratory Animal Care (AAALAC) International (#001169) facility, in accordance with the guide for the care and use of laboratory animals [134]. A certified veterinarian adjudged the animals as healthy, and they were made to fast overnight.

2.2.4 Surgical preparation and hemodynamic measurements

The animals were initially sedated with intra-muscular injections of 5 mg/kg tiletamine hydrochloride and zolazepam hydrochloride (Zoletil, Virbac, Carros, France) and 2 mg/kg xylazine (Rompun, Bayer, Seoul, Korea), followed by inhalation of isoflurane at a dose of 1–1.5%. Monitoring of anesthetic depth of the animals was started with the BIS Vista Monitor. The animals were orally intubated and a Capstar-100 CO₂ analyzer (CWE Inc., Ardmore, PA, USA) was installed. Mechanical ventilation was initiated. A tidal volume (TV) of 12 ml/kg, respiratory rate (RR) of 12 breaths/min, partial pressure of arterial CO₂ (PaCO₂) at approximately 40 mmHg, and partial pressure of arterial oxygen (PaO₂) over 80 mmHg were maintained to continue

the anesthesia. A perivascular probe (MA2PSB, Transonic Systems, Ithaca, NY, USA) and a perivascular flowmeter (T420, Transonic Systems, Ithaca, NY, USA) were installed to detect the CaBF from the surgically dissected internal carotid artery. A Mikro-tip pressure catheter (Millar, Houston, TX, USA) was inserted into the left femoral artery and placed in the descending thoracic aorta to measure the ABP. Another Mikro-tip pressure catheter was inserted into the right atrium to measure the right atrial pressure (RAP). An electrocardiogram (ECG) was taken, and the saturation of percutaneous oxygen (SpO₂) was measured. All signals, except the EEG signals, were gathered and saved using the PowerLab 16/35 hardware with LabChart software (ADInstruments, Dunedin, New Zealand) at a rate of 1 kHz, simultaneously.

A pace-making wire was inserted into the right ventricle via a central vein catheter. The isoflurane was stopped before VF induction to recover the EEG activity. When the EEG started to recover, the animals entered a light sedation status, with a BIS value of approximately 80. A direct-current shock was then applied to induce the VF. Mechanical ventilation was stopped, and the animals were left without assistance for one min. Thereafter, CPR and defibrillation were executed, and manual ventilation using the Ambu Resuscitators (Ambu A/S, Ballerup, Denmark) with 100% oxygen was provided to the animals at a rate of 10 times per minute.

2.2.5 EEG measurement

A battery-powered EEG device with four channels was developed to measure scalp EEG under the referential montage. The device consisted of an analog front end (AFE), which amplified and filtered the raw EEG data; analogue-digital converter (ADC); micro-processor unit (MCU); and Bluetooth communication module. For the design of the input amplifier in the AFE, a large input impedance was considered to reduce the possibility of signal distortion owing to a mismatch of the electrode-skin impedance. Low noise levels, low offset voltage, high common mode rejection ratio (CMRR), and low-power consumption for battery-powered operation were also considered. To meet these requirements, an instrumentation amplifier (INA826, Texas Instruments, Dallas, TX, USA) was used for the input amplifier. The INA826 has a CMRR of over 100 dB, maximum offset voltage of 150 μV , noise level under 0.2 $\mu\text{Vp-p}$, and power consumption of 0.2 mA. For the filter stages in the AFE, second-order Butterworth filters using the Sallen-Key topology were applied as a high-pass filter (cutoff frequency: 0.5 Hz) and low-pass filter (cutoff frequency: 50 Hz). An operational amplifier, TSZ122 (STMicroelectronics Inc., Geneva, Switzerland) was used in the filter stages. The TSZ122 has a CMRR of over 120 dB, maximum offset voltage of 5 μV , noise level under 0.2 $\mu\text{Vp-p}$, and power consumption of 40 μA . In total, the raw EEG signals were band-pass filtered with a frequency range of 0.5–50 Hz and amplified with a gain of 100 V/V in the AFE. The resultant signals were

digitized by the ADC (ADS1299, Texas Instruments, Dallas, TX, USA), specialized for bio-potential measurement. The ADS1299 has a CMRR of 115 dB and an input-referred noise of $0.98 \mu\text{Vp-p}$ at a programmable gain of 24 V/V and a sampling rate of 250 Hz. The digitized data were amplified with a gain of 24 V/V and transmitted to the MCU (ATmega168, Atmel Corporation, San Jose, CA, USA) through serial peripheral interface (SPI) communication. The ATmega168 transmitted the received data to the laptop through a Bluetooth communication module (FB155C, Firmtech, Seongnam, Korea). The data acquisition software based on the LabView2013 platform (National Instruments, Austin, TX, USA) was used to receive and save the EEG data. This device was compliant with the general requirements for the essential performance of electroencephalography, specified in the International Standard IEC 60601-2-26: Accuracy of signal reproduction, input dynamic ranges and differential offset voltage, input noise, frequency response, and CMRR. Figure 2.2 shows the four-channel EEG device and electrode placement. EEG signals were measured with disposable surface electrodes (2223H, 3M Healthcare, Brackell, UK). Reference and ground electrodes were placed on the mastoid, and four active electrodes were placed around the forehead. We took steps to maintain a stable electrode contact. First, the animal's skin was slightly peeled to flatten the forehead region where the EEG device and electrodes were placed. Then, the EEG device and electrodes were secured tightly with medical adhesive tape to prevent displacement during CPR. The technical specifications of the device

are listed in Table 2.1.

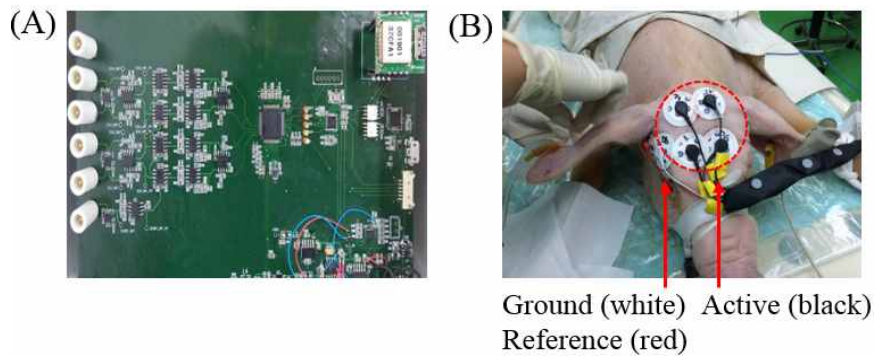


Figure 2.2 Four-channel EEG device: (A) Printed circuit board, (B) Electrodes placement for scalp EEG measurement.

Table 2.1 Technical specifications of the EEG device.

Number of channels	4
Sampling rate	250 Hz
Bandwidth	0.5–50 Hz
Resolution	24-bit
Input range	$\pm 1,000 \mu\text{V}$
Gain control	2,400 V/V
CMRR	$> 80 \text{ dB}$
Noise (peak-to-peak)	$< 3 \mu\text{V}$
Interface	USB, Bluetooth 2.0
Power	Li/Po Battery 3.7V/900mAh

2.2.6 Data analysis

All data were processed using MATLAB R2017b (Mathworks, Natick, MA, USA). The EEG signal and hemodynamic data were synchronized. The EEG signals were processed to extract useful parameters. The entire EEG data were segmented into 4 s long epochs with 3.5 s overlaps with the neighboring epochs. First, CPR artifacts on the EEG signal were removed. Short-time Fourier transform was employed to investigate the frequency responses of the epoch. The frequency bin was 0.25 Hz. Fundamental noise and harmonics, due to CCs, were detected and compensated for by replacing it with the averages of the two neighboring frequency components. If 3.5 Hz is recognized as an artifact frequency, for example, the average amplitude of the 3.25 Hz and 3.75 Hz components was applied as a new 3.5 Hz component. The artifact removal process is described in Figure 2.3.

The resulting signal was re-converted into the time domain to calculate the burst suppression ratio (BSR) [22]. Two frequency-domain parameters, the relative beta ratio (BetaR) [22, 135] and relative delta ratio (DeltaR), were determined from the power spectrum within certain frequency bands [136]. The relative synchrony of fast and slow waves (SynchFS) was determined from the bispectrum domain [22]. If all the calculations for the single epoch were completed, the same process was repeated for the next epoch. In total, four EEG parameters were obtained every half a second. The mean ETCO₂ data were also obtained at the same time intervals. The EEG parameters are listed in Table 2.2.

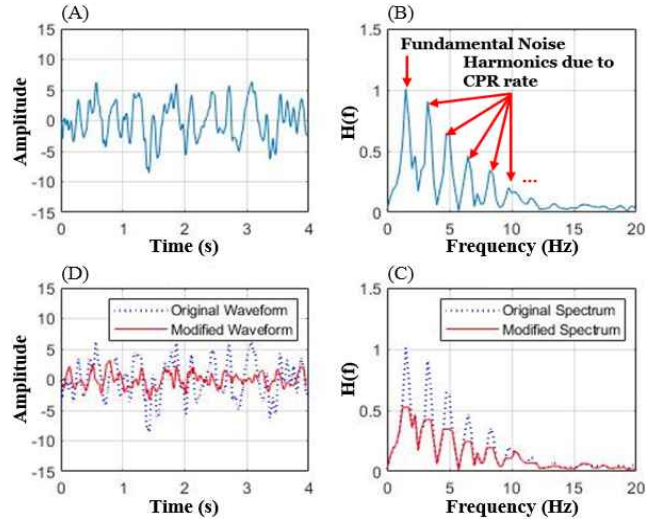


Figure 2.3 Artifact-removal process: (A) The raw EEG signal contaminated by the CPR artifact, (B) Power spectrum of the raw EEG signal, (C) Before and after removing CPR artifacts on the frequency-domain, (D) Before and after removing CPR artifacts on the time-domain.

Table 2.2 Four EEG parameters derived to establish the EBRI model.

Parameters	Definition
BSR	Percentage of continuous periods longer than a half a second during which EEG is suppressed under $\pm 5 \mu\text{V}$ (unit: %)
SynchFS	$\log(B_{0.5-47 \text{ Hz}} / B_{40-47 \text{ Hz}})$
BetaR	$\log(P_{30-47 \text{ Hz}} / P_{11-20 \text{ Hz}})$
DeltaR	$\log(P_{8-20 \text{ Hz}} / P_{1-4 \text{ Hz}})$

Abbreviation: $P_{a-b \text{ Hz}}$, the sum of spectral power from a–b Hz; $B_{a-b \text{ Hz}}$, the sum of bispectral activity from a–b Hz;

2.2.7 EBRI calculation

The EBRI model was established to construct the relationship between the four EEG parameters as an input and the mean ETCO₂ as an output using linear regression methods. Five-fold cross validated regression models were derived

for each animal. For example, to obtain the EBRI model for animal #1, all EEG parameters and ETCO₂ data from the other 4 animals were used to establish the EBRI model. Five different EBRI models were obtained. The final EBRI model was determined using all the data together.

$$EBRI = a + b_1 \times BSR + b_2 \times BetaR + b_3 \times SynchFS + b_4 \times DeltaR \quad (\text{eq.1})$$

2.2.8 Delta-EBRI calculation

To distinguish between an increase- or decrease trend in the estimated ETCO₂, the time differences of the EBRI, defined as delta-EBRI, were calculated. Because we assumed that the EBRI positively correlates with the actual ETCO₂, it should theoretically increase with the increase in actual ETCO₂ values, and decrease in the opposite situation. Therefore, the delta-EBRI values at different time intervals were obtained from the changes in the actual ETCO₂. The time intervals ranged from 0.5 s to 10 s.

The performance of the delta-EBRI was evaluated using the confusion matrix. In the confusion matrix, the two groups were presented: Group 0 with decreased cases and Group 1 with increased cases. Four primary evaluation metrics were determined with the confusion matrix: true positives (TP), true negatives (TN), false positives (FP), and false negatives (FN). The positive and negative indices were considered for Group 0 and Group 1, respectively. TP is the proportion of correctly predicted positive indices, and TN is the proportion of correctly predicted negative indices. FP is the proportion of known negative

cases that was predicted positive, and FN is the proportion of known positive cases that was predicted negative. The accuracy, sensitivity, and specificity were calculated as follows [137]:

$$Accuracy = (TP + TN) / (TP + TN + FP + FN) \quad (\text{eq.2})$$

$$Sensitivity = TP / (TP + FN) \quad (\text{eq.3})$$

$$Specificity = TN / (TN + FP) \quad (\text{eq.4})$$

The second metric was the F1 score, which is calculated from the harmonic mean of the precision ($TP / (TP + FP)$) and recall, also known as the sensitivity (eq.3) [138].

$$F1 \text{ score} = 2 \times (precision \times recall) / (precision + recall) \quad (\text{eq.5})$$

In addition, a receiver operating characteristic (ROC) curve and the area under the curve (AUC) [139] were obtained using the IBM SPSS Statistics 25 software (IBM SPSS Statistics, New York, NY, USA) to evaluate the classification ability. The ROC curve was determined from the combination of the true positive rate (TPR, eq.3) and the false positive rate (FPR, $FP / (FP + TN)$), known as $1 - \text{eq.4}$) at different threshold levels. The AUC is the area under the ROC curve.

2.3. Results

2.3.1 Hemodynamic parameters

Five experiments with 10 repetitions each for the two CPR modes were performed, and all physiologic parameters, including ETCO₂ and EEG signals, were measured. The hemodynamic parameters after the 15th CPR segment in animal #4 were excluded from the analysis because the EEG was missed at that time.

Table 2.3 presents the hemodynamic parameters during the baseline and CPR sessions. All the blood pressure parameters: systolic blood pressure (SBP), DBP, MAP, and COPP, showed higher values in the HQ-CPR sessions than in the LQ-CPR sessions. The ETCO₂ and CaBF were also higher in the HQ-CPR sessions. The BIS values were monitored during the experiments, but they were not considered because the low-frequency CPR artifacts on the EEG were not removed.

Table 2.3 Hemodynamic parameters depending on the CPR modes.

Parameters	Baseline	HQ-CPR	LQ-CPR	<i>p value</i>
	Median (IQR)	Median (IQR)	Median (IQR)	
SBP, mmHg	105 (101, 116)	89 (76, 104)	42 (34, 54)	< 0.01
DBP, mmHg	75 (74, 84)	24 (15, 30)	22 (17, 27)	< 0.01
MAP, mmHg	90 (87, 94)	38 (31, 48)	25 (19, 31)	< 0.01
ETCO2, mmHg	46 (43, 46)	23 (17, 26)	18 (14, 22)	< 0.01
CaBF, ml/min	323 (243, 374)	207 (160, 352)	53 (16, 119)	< 0.01
COPP, mmHg	80 (75, 84)	16 (8, 22)	13 (9, 17)	< 0.01
BIS	81 (78, 84)	-	-	-

Abbreviation: SBP, Systolic blood pressure; DBP, Diastolic blood pressure; MAP, Mean arterial pressure; ETCO2, End-tidal CO2 tension; CaBF, Carotid blood flow; COPP, Coronary perfusion pressure; BIS, Bispectral index score; IQR, Interquartile range;

2.3.2 Changes in EEG parameters

The four EEG parameters, introduced in Table 2.2, were investigated to determine whether the EEG signal can reveal the quality of a CPR session. After removing the artifacts due to CCs, the BSR, BetaR, DeltaR, and SynchFS were obtained at intervals of half a second, and they were compared with the mean ETCO2. Figure 2.4 shows the changes in the EEG parameters in animal #1. Distinct changes were found as the VF and CPR sessions proceeded. Once VF occurred, the EEG activity was lost in 10–15 s with the following increase in BSR. When the HQ-CPR was initiated, the BSR decreased, but increased after the CPR mode was switched to LQ-CPR. Similar patterns continued till the end of the experiment. The overall BIS values increased, indicating that the EEG

activity decreased gradually. Such apparent patterns were found for the other parameters. The degrees of non-linear phase coupling, SynchFS, increased during HQ-CPR and decreased during LQ-CPR. BetaR showed similar changes with regard to the BSR. The DeltaR also showed similar patterns with regard to the BSR. Scatter plots for each parameter and ETCO₂ are illustrated in Figure 2.5.

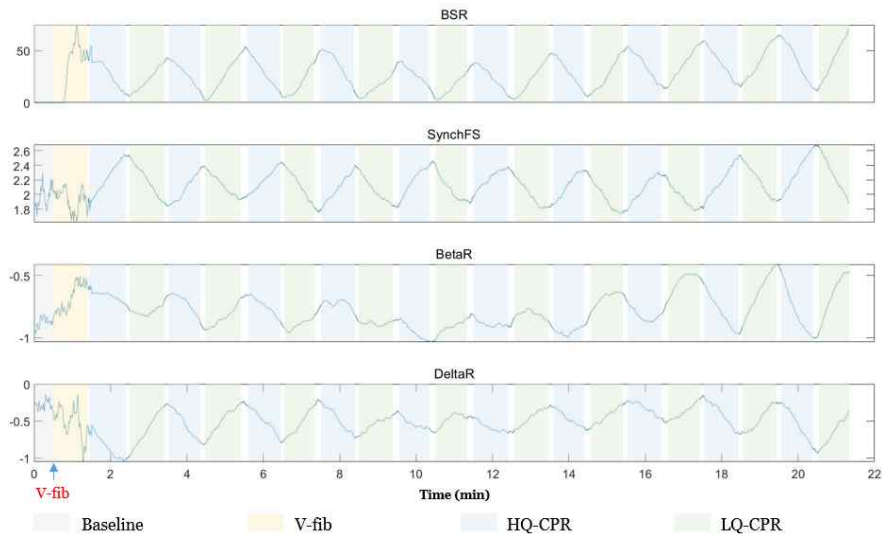


Figure 2.4 Changes in the four EEG parameters throughout the experiments.

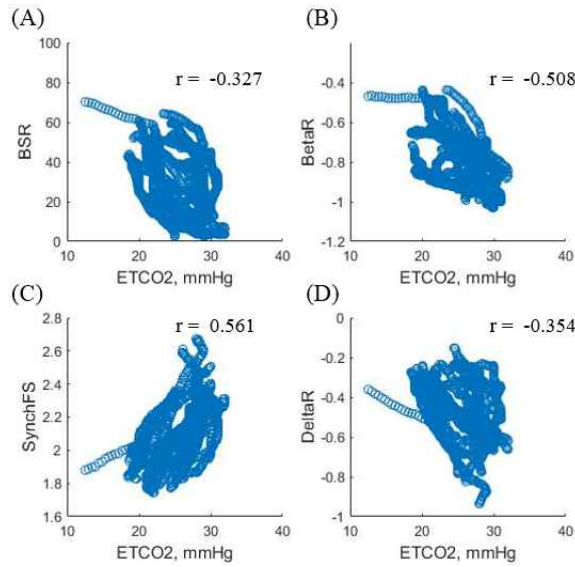


Figure 2.5 Scatter plots between each EEG parameter and ETCO2: (A) BSR, (B) BetaR, (C) SynchFS, (D) DeltaR.

2.3.3 EBRI calculation

The EBRI model was established to formulate the relationship between the four EEG input parameters and the ETCO2, as an output, using the linear regression technique. Five different EBRI models were determined to estimate the ETCO2 of an individual experiment. Figure 2.6 demonstrates the actual ETCO2 and estimated ETCO2 using the EBRI models.

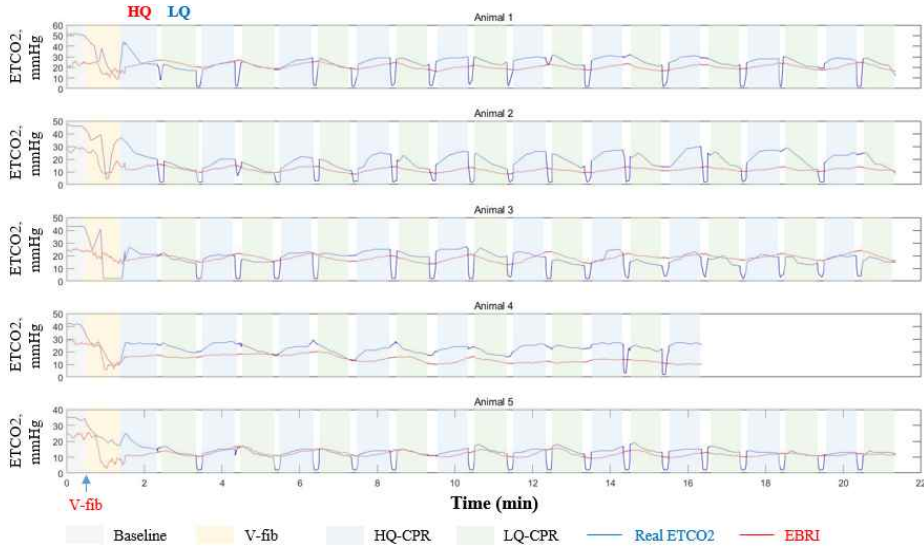


Figure 2.6 Comparison between the actual ETCO2 and estimated ETCO2 with the EBRI model.

The final EBRI model was derived using all experimental data. The y-intercept (a) and coefficients for each parameter (b_1 – b_4) were determined as follows.

$$EBRI = a + b_1 \times BSR + b_2 \times BetaR + b_3 \times SynchFS + b_4 \times DeltaR \quad (eq.6)$$

$$(a = 26.047, b_1 = -0.141, b_2 = 4.481, b_3 = 2.821, b_4 = 5.452)$$

The performance of the EBRI model was evaluated using Pearson's correlation coefficient as a metric of similarity. All CPR sessions, except the first HQ-CPR session, in which the actual ETCO2 increased rapidly at the beginning, were compared. The correlation coefficients between the two signals are presented in Table 2.4. The correlation coefficients were considered for each animal as well as the merged dataset. The correlation coefficients differed

between the experiments. Test 2 showed the highest value of 0.655. Tests 1 and 5 showed correlation coefficients above 0.5. However, poor correlation coefficients less than 0.3 were found in Test 3 and 4. The overall correlation coefficient from the merged dataset was 0.513.

Table 2.4 Correlation coefficients between the actual ETCO₂ and EBRI.

Test	Correlation coefficient
#1	0.520
#2	0.655
#3	0.411
#4	0.464
#5	0.560
Merged data	0.513

2.3.4 Delta-EBRI calculation

The delta-EBRI for different time intervals ranging from 0.5 s to 10 s was obtained with respect to the changes in the actual ETCO₂. The performance was evaluated using the confusion matrix and a ROC curve. The 10 s time interval showed the best performance. The accuracy of the confusion matrix was 0.716, and the AUC was 0.763. Figure 2.7 demonstrates the confusion matrix and the ROC curve, and Table 2.5 summarizes the overall performance metrics.

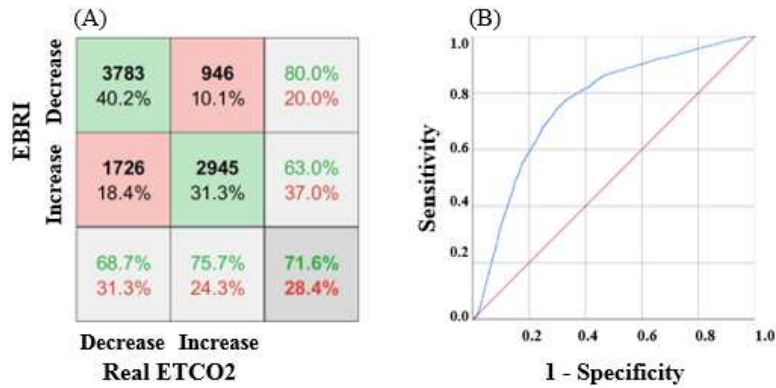


Figure 2.7 Performance of the delta-EBRI with 10 s time interval: (A) Confusion matrix, (B) The ROC curve.

Table 2.5 Performance of the delta-EBRI.

Performance	Value
Accuracy	0.716
Sensitivity	0.687
Specificity	0.757
Precision	0.800
F1 score	0.739
AUC	0.765

Abbreviation: AUC, Area under the curve;

2.4. Discussion

2.4.1 Accomplishment

This swine model of VF was utilized to develop a noninvasive CPR feedback method using the frontal EEG, as an alternative to ETCO2 measurement. To improve the survival rates of CA patients, certain levels of systemic circulation, which is normally assessed with an endotracheal tube and capnography, should be maintained. However, more easily measurable methods

are needed to increase the applicability in emergency settings. In this study, an EBRI model was established to estimate ETCO₂ under the two different CPR modes. The EBRI model correlated with the actual ETCO₂, with a Pearson correlation coefficient of 0.513. The performance of the delta-EBRI, as a classifier between an increase or decrease in ETCO₂, was acceptable with an AUC value of over 0.7. These results suggest that the delta-EBRI, rather than the original EBRI, has a potential as a noninvasive physiologic feedback indicator for systemic circulation assessment during CPR.

Four EEG parameters were considered for establishing the EBRI model. These parameters have been reported to reflect the consciousness level and measure anesthetic depth [140]. First, the BSR, defined as the percentage of continuous periods longer than half a second with an amplitude of less than ± 5 μ V, reflects hypoperfusion caused by an overdose of the anesthetic agents [141, 142]. Furthermore, it can be used as a predictor of neurological recovery of resuscitated patients [26, 133]. A relationship was found between the recovery of cerebral circulation and BSR. The BSR remained almost at zero during pre-VF, but increased rapidly within 10-15 s after VF was induced, at which the cerebral perfusion disturbance occurred [141, 142]. The BSR decreased when CaBF was improved during the HQ-CPR, but increased when CaBF was reduced during LQ-CPR. The overall BSR increased as the CPR sessions were repeated, indicating that the effectiveness of cerebral resuscitation decreased despite the ceaseless CPR efforts. The apparent increase in the SynchFS was

observed under the improved CaBF condition [22]. Additionally, BetaR and DeltaR showed distinct patterns depending on the CPR modes. BetaR, defined as the ratio between the spectral power within 30–47 Hz range and that within 11–20 Hz range, represents the degrees of neural activity with cognitive processing by calculating changes in beta and gamma bands [135]. During HQ-CPR, the BetaR decreased because of improved cerebral circulation that might result in more activated mental activity and increase in the beta band power within the 10–20 Hz range. The DeltaR, defined as the ratio between the spectral power within 1–4 Hz range and that within 8–20 Hz range, was also considered because a sudden decrease in the delta band power is followed by consciousness recovery [136]. DeltaR decreased during HQ-CPR, which means that improved cerebral resuscitation caused a gradual reduction of the delta band power and the appearance of “being awake” EEG patterns. Conversely, during LQ-CPR, the compromised cerebral resuscitation resulted in the opposite changes: increase of the delta band power and isoelectric activity. The changes in the EEG parameters were newly applied to evaluate the real-time CPR quality. ETCO₂ changes coincide with the changes in cardiac output [143], and can be correlated with CBF changes during CPR, with a correlation coefficient of 0.64 [126]. Consequently, the EEG signals affected by CA patient’s cerebral circulation could be closely related to ETCO₂ during CPR, that provided validity for the EBRI modeling process.

The current CPR guidelines recommend measuring ETCO₂ under

endotracheal intubation for assessing systemic circulation [130]. Problems due to improper placement, such as kinking of the endotracheal tube or blocking water vapor, might generate incorrect ETCO₂ measurements [130, 132]. More convenient methods, such as bag-valve mask ventilation, are available, but, there is limited evidence regarding these methods [144]. On the contrary, measuring scalp EEG signals is more convenient than ETCO₂ measurement. A variety of portable low-cost EEG devices can be easily applied to OHCA patients. Once the EEG device is installed, it measures the EEG signals and computes the EBRI automatically without any human intervention. The delta-EBRI derived from the frontal EEG can be a sensitive method for estimating ETCO₂ noninvasively, while providing feedback signals to EMTs.

2.4.2 Limitations

This study had several limitations. First, this experiment was a pilot animal study with a limited number of animals; the EEG activity and cerebral anatomy of juvenile pigs might differ from those of humans. Second, the fixed untreated VF duration was short and caused no damage whereas prolonged no- or low-flow periods could cause irreversible brain damage [38]. As a preliminary study, we applied a short untreated VF to obtain distinctly recovered EEG activity during CPR. However, if the untreated VF becomes longer, minimal or no recovery can be achieved. Further studies with a longer untreated VF are warranted to establish a more practical EBRI model for use in an emergency

setting. Lastly, the duration of each CPR session was short, because the current CPR guidelines recommend basic life support (BLS) for 2 min [145]. Therefore, each CC cycle was composed of 50 s long HQ-CPR and LQ-CPR with twice 10 s hands-off time in between. Owing to such short CCs, no EBRI plateau was found.

2.5. Conclusion

We measured scalp EEG signals during CPR in an experimental swine model of VF and established an EBRI model as a surrogate indicator for systemic circulation assessment during CPR. The EBRI moderately correlated with the actual ETCO₂ and the delta-EBRI showed potential as a real-time physiological classifier to distinguish between the increased or decreased ETCO₂.

Chapter 3. EEG-based Prediction Model of the Recovery of Carotid Blood Flow for Monitoring Cerebral Circulation During CPR

3.1. Introduction

Approximately 395,000 adults experience OHCA each year in the United States [127] and their survival rate is low despite the development of the CPR protocol and various patient monitoring equipment for decades [146, 147]. In an OHCA situation, quick and high-quality CPR is the key to improving both the systemic and cerebral circulation of patients [50, 51]. To enable high-quality CPR, multiple feedback methods based on physiological responses have been introduced and their effectiveness has been evaluated [57, 58]. Monitoring ETCO₂ under endotracheal intubation for systemic circulation assessment is a typical example. These techniques can help EMTs perform individualized optimal CPR, without having to solely adhere to the depth or rate conditions of CCs standardized through CPR guidelines.

The primary goal of CPR is to achieve early ROSC. In addition, achieving favorable neurological recovery has been regarded as another goal because neurological recovery can affect survivors' neurological deficits and their quality of life [59, 60]. However, monitoring neurological activity using

hemodynamic data during CPR is rarely possible. ETCO₂ can monitor systemic circulation effectively, but it is not appropriate to reflect the cerebral circulation or physiological responses of the brain during CPR.

Several methodologies have been suggested to monitor cerebral circulation, such as Transcranial Doppler ultrasonography (TCD). TCD measures the velocity of red blood cells and has the potential to estimate CEPP [148, 149]. However, several drawbacks including its bulky size and the need for a skillful technician to find the arteries and place the probe on the patient's head make TCD techniques unsuitable for an emergency setting. Measuring the CaBF in the ascending internal carotid artery can reflect cerebral circulation effectively; however, the CaBF measurement requires an additional flow meter and a skillful operator, which makes this method less feasible in an emergency setting.

Noninvasive EEG can be regarded as an alternative to overcome these drawbacks. Currently, as a powerful tool for monitoring brain activity, EEG is routinely measured to determine the prognosis of ischemic insults of resuscitated patients [26, 133]. Previous studies have shown the applicability of EEG activity in ongoing CPR situations. EEG activity is known to be sensitive to cerebral circulation during CPR [76, 77]. Once CA occurs, cerebral oxygenation levels decrease significantly, and isoelectric EEG gradually appears [37, 150]. If the cerebral circulation and oxygen delivery are recovered to the normal state after ROSC, the EEG also returns to the pre-CA state [38,

151], as evidenced by the BIS monitoring [152]. In addition, specific EEG patterns have been suggested as feasible indicators for the quality of cerebral circulation and oxygen delivery [81]. However, the direct relationship between CaBF and EEG during CPR has rarely been discussed.

In this study, we designed another experimental swine model of VF, that consisted of four consecutive BLS cycles and advanced cardiovascular life support (ACLS) cycles up to 10 times. Furthermore, we measured hemodynamic data such as CaBF and the frontal EEG using a single-channel EEG device [153]. The relationship between CaBF recovery and noninvasive EEG signals was analyzed. The topmost significant EEG parameters for predicting CaBF recovery were determined, and ML-based prediction models for CaBF recovery were established using the EEG parameters. We hypothesized that CaBF recovery could improve brain cell viability, which can change the EEG activity, even during brief intervals between defibrillation attempts. Conversely, such EEG changes were assumed to be able to predict CaBF recovery.

3.2. Methods

3.2.1 Ethical statement

The animal test protocol was approved by the Institutional Animal Care and Use Committee of Seoul National University Hospital (IACUC number: 17-0106). All animal care complied with the Laboratory Animal Act of the Korean MFDS.

3.2.2 Study design and setting

An animal experiment was designed based on a VF swine model. The LUCAS mechanical CPR machine (LUCAS2 Chest Compression System, Jolife AB, Sweden) was used for mechanical CCs. The CPR machine compressed the chest at a fixed rate of 100 times per minute with a depth of 5 cm. To prevent displacement of the piston, the animals were pinned on the table, and the back plate was positioned underneath the animals as a support for the CPR machine (Figure 3.1 (A)). The exact location of the heart was identified under ultrasonic guidance, and the piston was installed on site. One EMT held the CPR machine to prevent displacement during CPR.

A witnessed OHCA was assumed in this study. The length of untreated VF of 1 min was determined by considering a CA-CALL time, the time of recognition of CA to call for emergency medical services by bystanders [154].

In addition, it was estimated that four consecutive 2-min BLS cycles were performed by the bystanders, with the help of an emergency center by phone, while waiting for the dispatched EMTs to arrive. The EMTs were assumed to arrive at the site when the BLS cycles were completed. The ECG was checked, and the first defibrillation shock was applied. If the ECG rhythm was shockable, a biphasic defibrillation shock of 200 J was applied by the EMTs to restart the heart. Monitoring was initiated when a palpable pulse with organized QRS complexes and the recovery of SBP over 60 mmHg appeared [155]. Sustained ROSC was confirmed if spontaneous circulation continued for 20 min [81]. If a palpable pulse did not appear after the defibrillation, or VF occurred again during the monitoring session, one cycle of 2-min ACLS was immediately performed by EMTs. If the ECG was still shockable, an additional defibrillation shock was applied. However, in the case of pulseless electrical activity or asystole, the defibrillation shock was omitted and the next cycle of ACLS was immediately initiated. If a palpable pulse appeared after the last defibrillation, the monitoring session was initiated. Non-ROSC was confirmed if the sustained ROSC, lasting longer than 20 min, was not achieved after 10 cycles of ACLS. During ACLS sessions, 1 mg epinephrine was administered once every 3 min [156]. After the monitoring session or all 10 ACLS sessions, the animals were euthanized with an injection of 20 mg KCl. EEG, and hemodynamic data were measured continuously during the experiments. The entire test protocol with a timeline is shown in Figure 3.2.

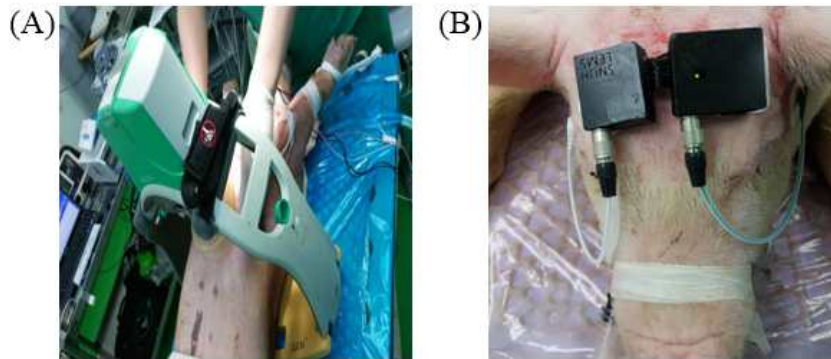


Figure 3.1 Experimental setup: (A) LUCAS CPR machine installed on the chest, (B) A single-channel EEG device installed on the forehead.

3.2.3 Experimental animals and housing

Eight domestic crossbred female pigs, approximately 3 months of age (45.6 ± 2.4 kg), were studied. The animals were obtained from the supplier of experimental animals (Cronex Co., Ltd., Cheongju, Korea), qualified by the Korean MFDS with a certificate of KELAS. The animals were maintained in an accredited Association for AAALAC International (#001169) facility, in accordance with the guide for the care and use of laboratory animals [134]. A certified veterinarian adjudged the animals as healthy, and they were made to fast overnight.

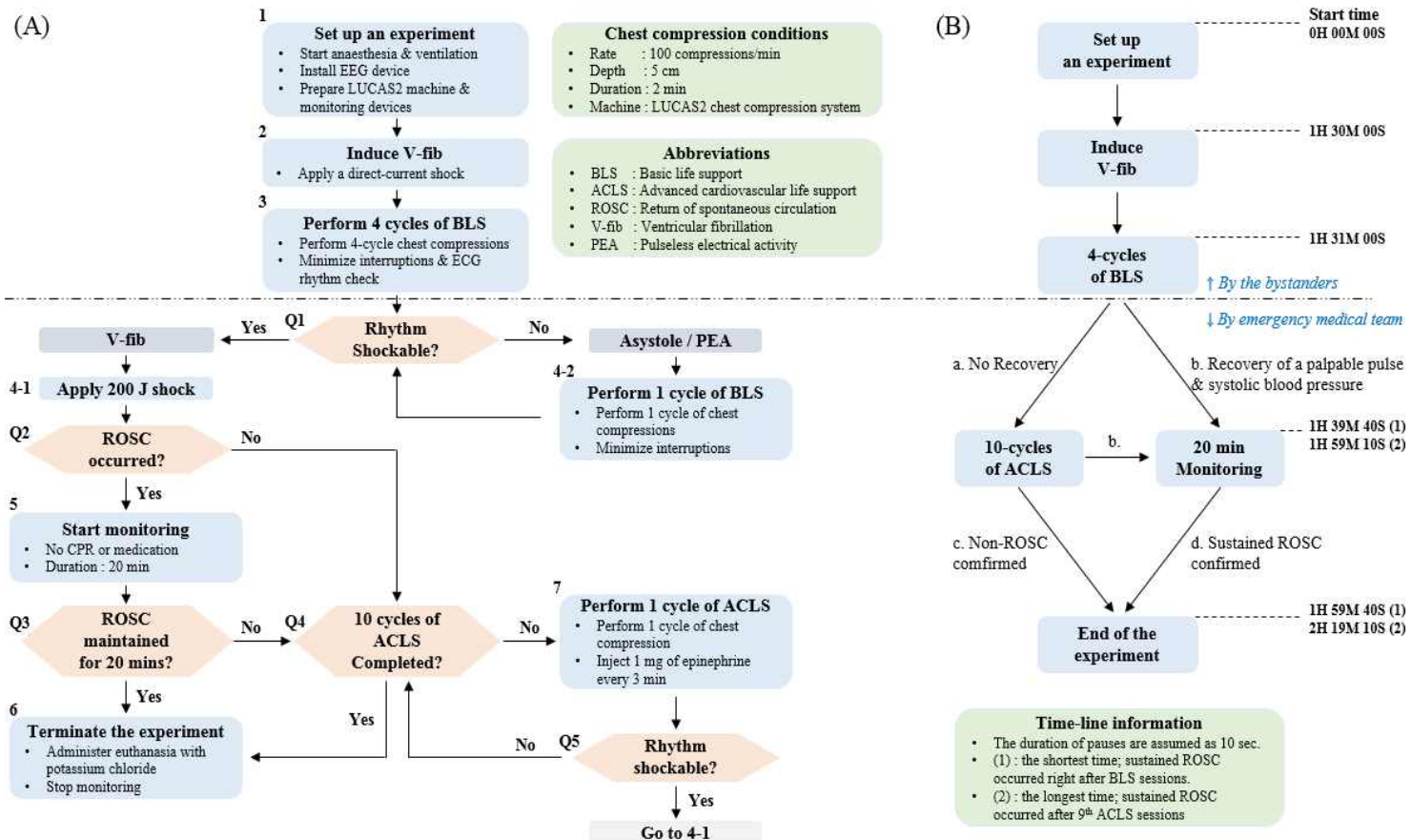


Figure 3.2 The entire test protocol: (A) Flow chart in detail, (B) Simplified flow chart with a timeline.

3.2.4 Surgical preparation and hemodynamic measurements

The animals were initially sedated with intramuscular injections of 5 mg/kg Zoletil and 2 mg/kg Rompun, followed by inhalation of isoflurane at a dose of 1–1.5%. The endotracheal tube was placed in the animals, and a Capstar-100 CO2 analyzer was installed and mechanical ventilation was initiated. A TV of 12 ml/kg, RR of 10 breaths/min, PaCO₂ at approximately 40 mmHg, and PaO₂ over 80 mmHg were maintained to keep the anesthesia.

A MA2PSB perivascular probe combined with a T420 perivascular flowmeter was placed on the internal carotid artery to detect the CaBF. A Mikro-tip pressure was inserted into the left femoral artery and placed in the descending thoracic aorta to measure the ABP. Another Mikro-tip pressure catheter was inserted into the right atrium to measure RAP. An ECG was taken, and the SpO₂ were also measured. All signals, except EEG signals, were gathered and saved using the PowerLab 16/35 hardware with LabChart software at a rate of 1 kHz, simultaneously.

A pace-making wire was inserted into the right ventricle through a central vein catheter. The isoflurane was stopped before VF induction to recover the EEG activity. When the EEG activity started to recover and appeared similar to the recording obtained before the injections, a direct-current shock was applied to induce VF. Mechanical ventilation was stopped, and the animals were left without assistance for 1 min. Thereafter, CPR and defibrillation were executed,

and manual ventilation using the Ambu Resuscitator was initiated to provide positive pressure ventilation to the animal a rate of 10 times per minute.

3.2.5 EEG measurement

An improved single-channel EEG device was prepared for this study. The new EEG device has a configuration similar to that of the previous four-channel device. It was designed to be installed on the forehead. Because the presence of hair can increase the electrode-skin impedance, hair should be avoided for a reliable measurement. In this respect, the large hairless scalp area is appropriate for acquiring high quality signals quickly in emergency settings, and prefrontal EEG activity can represent recovery of consciousness (Figure 3.1 (B)). The single-channel EEG device consisted of the AFE, ADC, MCU, and Bluetooth communication module. The AFE, consisting of the INA826 and TSA122, has a gain of 1,000 V/V and the same passband with a frequency range of 0.5–50 Hz. The two-channel ADC (ADS1292, Texas Instruments, Dallas, TX, USA) was used to digitize the raw EEG signals. The ADS1292 has a CMRR of 120 dB and an input-referred noise of 3.5 μ Vp-p at a programmable gain of 12 V/V and a sampling rate of 250 Hz. The digitized data were amplified with a gain of 12 V/V and transmitted to the MCU (ATmega168) through SPI communication, and the ATmega168 transmitted the received data to the laptop through a Bluetooth low-energy (BLE) module (BOT-CLE310, Chipsen, Seoul,

Korea). Data acquisition software was developed to receive and save the EEG data. This device was compliant with the general requirements for the essential performance of electroencephalography, specified in the International Standard IEC 60601-2-26. The electronic circuit and schematic block diagram of the single-channel EEG device are shown in Figure 3.3. The reference and ground electrodes were placed on either side of the mastoid. Active electrodes, at the bottom of the device, were placed on the forehead. The EEG device and electrodes were secured tightly with medical adhesive tape to prevent displacement during CPR. The technical specifications of the device are listed in Table 3.1.

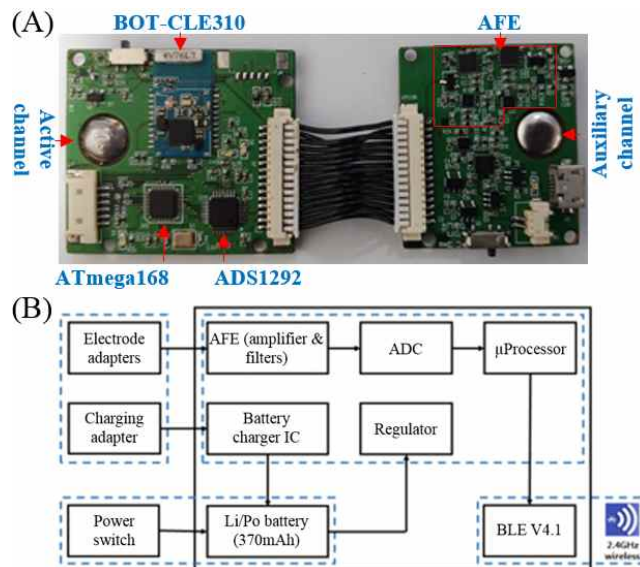


Figure 3.3 A single-channel portable EEG device used in this study: (A) Printed circuit boards, (B) Schematic block diagram.

Table 3.1 Technical specifications of the EEG device.

Number of channels	1
Sampling rate	250 Hz
Bandwidth	0.5–50 Hz
Resolution	24-bit
Input range	$\pm 200 \mu\text{V}$
Gain control	12,000 V/V
CMRR	$> 80 \text{ dB}$
Noise (peak-to-peak)	$< 3 \mu\text{V}$
Interface	Bluetooth low-energy V4.1
Power	Li/Po Battery 3.7V/370mAh

3.2.6 Data processing

All data were processed using the MATLAB R2017b software. Data from approximately 3 s before the defibrillation shocks were selected for analysis. The selected EEG was segmented into three 2 s long sub-epochs with 1.5-s overlaps: 0–2 s, 0.5–2.5 s, and 1–3 s periods. The representative EEG parameters were obtained from the average of three sub-epochs. Segmenting the EEG data and calculating the parameters are similar to the signal processing techniques for the BIS calculation [22]. Time- and frequency domain parameters and entropy indices were determined in this manner. All EEG parameters considered are summarized in Table 3.2.

Table 3.2 EEG parameters considered in this study.

EEG parameters	Definition	Domain
Magnitude	Maximal amplitude during the epoch	Time
SynchFS	$\log(B_{0.5-47 \text{ Hz}} / B_{40-47 \text{ Hz}})$	Frequency
BetaR	$\log(P_{30-47 \text{ Hz}} / P_{11-20 \text{ Hz}})$	Frequency
DeltaR	$\log(P_{8-20 \text{ Hz}} / P_{1-4 \text{ Hz}})$	Frequency
AlphaPR	$P_{8-13 \text{ Hz}} / P_{0.5-47 \text{ Hz}}$	Frequency
BetaPR	$P_{13-30 \text{ Hz}} / P_{0.5-47 \text{ Hz}}$	Frequency
DeltaPR	$P_{0.5-4 \text{ Hz}} / P_{0.5-47 \text{ Hz}}$	Frequency
ThetaPR	$P_{4-8 \text{ Hz}} / P_{0.5-47 \text{ Hz}}$	Frequency
BG_Alpha	$P_{8-47 \text{ Hz}} / P_{0.5-47 \text{ Hz}}$	Frequency
Log energy entropy	$\sum_{k=0}^n \log(p(x_i))^2$	Entropy
Rényi entropy	$\frac{1}{(1 - \alpha)} * \log \sum_{k=0}^n (p(x_i))^\alpha$	Entropy

Abbreviation: $P_{a-b \text{ Hz}}$, the sum of spectral power from a–b Hz; $B_{a-b \text{ Hz}}$, the sum of bispectral activity from a–b Hz; $p(x_i)$, probability distribution function of signal x_i ; α of rényi entropy was 0.5;

3.2.7 Data analysis

First, the recovery rates of the hemodynamic parameters including CaBF were calculated as a relative scale with respect to the pre-VF state. Second, the EEG waveforms were examined according to the test protocol, described in Figure 3.2. The EEG activity was evaluated, along with the recovery rates of CaBF.

Pearson correlation coefficients between the EEG parameters and the recovery rates of CaBF were obtained to evaluate the similarity between the

two datasets. In addition, the recovery rates of CaBF were categorized into four quartile groups: Group 1 (< 25%); Group 2 (25–50%); Group 3 (50–75%); and Group 4 (> 75%). Averages of each EEG parameter among groups were evaluated using one-way analysis of variance (ANOVA). Significance was considered at a level of $p < 0.05$. The ROC curve was used to measure the optimal cut-off values of each EEG parameter; to discriminate between the higher and lower groups of CaBF recovery based on the median value. These tests were performed using the IBM SPSS Statistics 25 software.

3.2.8 Development of machine-learning based prediction model

Based on the relationship between the EEG parameters and the CaBF recovery, ML-based prediction models were established. The recovery rates of CaBF were categorized into two groups according to the median value of around 30%: Group 0 (< 30%); and Group 1 ($\geq 30\%$). The criterion of 30% was chosen because 30–40% of the normal CaBF can be the threshold for the recovery of the brain function and the attenuated EEG activity [35, 36, 157].

The 11 EEG parameters introduced in Table 3.2 and an additional 9 EEG parameters were considered as candidate inputs for the prediction models. The additional 9 EEG parameters are introduced in Table 3.3.

Table 3.3 Additional 9 EEG parameters considered for the prediction models.

EEG parameters	Definition	Domain
BSR	Percentage of continuous periods longer than 0.5 s under $\pm 5 \mu\text{V}$	Time
Ratio05	Percentage of data whose amplitude is under $\pm 5 \mu\text{V}$	Time
DAR	$\log(P_{1-4 \text{ Hz}} / P_{8-13 \text{ Hz}})$	Frequency
DTABR	$\log(P_{1-8 \text{ Hz}} / P_{8-30 \text{ Hz}})$	Frequency
BcSEF	BSR-compensated frequency below which 95% of the total spectral power is occupied	Frequency
ExtraR	$\log(P_{40-47 \text{ Hz}} / P_{0.5-47 \text{ Hz}})$	Frequency
GammaPR	$P_{30-47 \text{ Hz}} / P_{0.5-47 \text{ Hz}}$	Frequency
Shannon entropy	$(-1) * \sum_{k=0}^n (p(x_i) * \log(p(x_i)))$	Entropy
Spectral entropy	Shannon entropy applied to the normalized power spectrum	Entropy

Abbreviation: $P_{a-b \text{ Hz}}$, the sum of spectral power from a–b Hz; $p(x_i)$, probability distribution function of signal x_i ;

The final EEG parameters were selected in two stages. First, the optimal candidate parameters for binary classification were determined through neighborhood component analysis (NCA) [158]. As a supervised learning method, NCA finds a linear transformation of the input data and learns a distance metric. Such distance information classifies multivariate data into a certain class over the data to maximize classification ability. In this study, NCA was applied to select the most significant EEG parameters with their ranking [159]. Then, the EEG parameters that showed significant differences between the two CaBF recovery groups were identified using the Student's t -test.

Significance was considered at a level of $p < 0.05$.

The prediction models were established using three traditional classifiers: logistic regression (LR), support vector machine (SVM), and k-nearest neighbors (KNN), along with one graphical model, multilayer perceptron (MLP), and one ensemble model, random forest (RF), with EEG parameters as inputs and binary CaBF groups as an output. LR is a statistical model that estimates the probability of a certain class between binary groups using a logistic function [160, 161]. SVM is a supervised learning method that classifies multi-class data into a certain class with multi-dimensional hyperplanes [162], and it has been applied to several EEG applications such as seizure detection [163]. KNN is a non-parametric method that classifies the data into a certain class based on similarity measures based on the number of nearest neighbors [164]. KNN-based classification models have been widely used to categorize human emotion from EEG signals [165, 166]. RF is an ensemble learning method that adapts multiple learning methods to achieve better prediction performance. It establishes a multitude of decision trees and classifies the data into a certain class by voting or averaging the outputs of the decision tree forests [167, 168]. MLP is a feedforward artificial neural network with one or multiple layers of perceptron(s), that utilizes a supervised learning algorithm for binary classification, and a backpropagation technique for training [169]. MLP-based models can classify data that are not linearly separable [170, 171]. Probable bias issues due to imbalanced train data were

resolved using the synthetic minority oversampling technique (SMOTE). Classifications based on an imbalanced-class distribution can be biased to the majority class. The problem can be escalated if the size of the majority class considerably exceeds that of the minority classes. SMOTE generates new synthetic data along the lines between randomly selected instances in the minority class and the synthetic data are introduced to training data [172].

The entire development process of the prediction models is shown in Figure 3.4. Their performance was evaluated using the leave-one-out cross-validation method. Out of eight animals, only the data from seven animals were used to establish each classifier, whose performance was evaluated using the remaining data. This process was repeated eight times, and eight cross-validated classifiers were established. The performance of each classifier was averaged over the eight times. Performance measures were expressed using confusion matrices and the ROC curve.

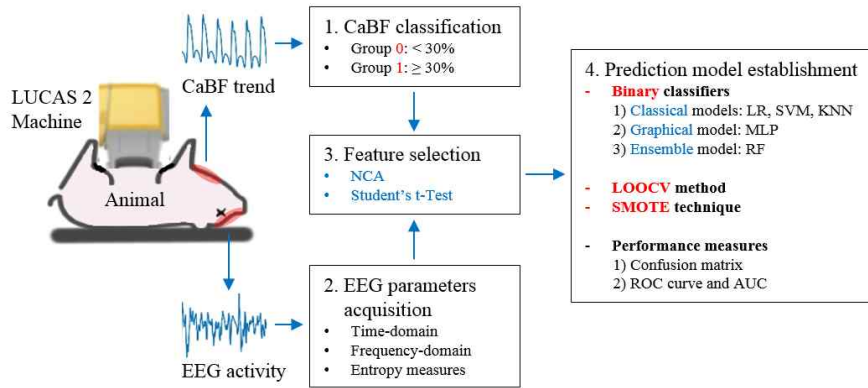


Figure 3.4 The entire development process of the prediction model for the recovery of CaBF.

3.3. Results

3.3.1 Results of CPR process

All eight experiments were performed successfully. During the untreated VF, the MAP decreased rapidly and almost 20% of the baseline MAP was measured as residual pressure. The CaBF dropped to almost 0% of the baseline values. When BLS sessions began, hemodynamic data started to recover. Recovery rates of each hemodynamic parameter over the BLS and ACLS sessions are presented in Table 3.4. Sustained ROSC was confirmed 5 times (Test #1, #3, #4, #6, #7). In total, BLS cycles were performed 32 times and ACLS cycles were performed 48 times.

Table 3.4 Recovery rates of each hemodynamic parameter throughout the experiments.

Test	Parameter	Pre-VF	VF	BLS				ACLS									
				1	2	3	4	1	2	3	4	5	6	7	8	9	10
#1	MAP	100	36.2	66.3	69.9	71.6	69.7	71.9	-	-	-	-	-	-	-	-	-
	COPP	100	15.2	51.4	54.9	56.5	54.7	57.0	-	-	-	-	-	-	-	-	-
	ETCO2	100	47.0	61.6	71.1	76.4	70.7	86.0	-	-	-	-	-	-	-	-	-
	CaBF	100	19.6	52.5	53.5	54.1	32.9	53.7	-	-	-	-	-	-	-	-	-
#2	MAP	100	26.7	41.8	42.4	43.0	40.1	38.7	34.2	29.2	20.2	16.1	14.3	12.7	12.1	12.5	12.5
	COPP	100	26.9	42.0	40.7	42.3	39.1	37.9	32.9	28.9	19.4	15.7	13.4	11.9	14.0	12.9	12.9
	ETCO2	100	46.6	49.4	47.2	48.9	45.7	49.0	46.0	35.6	24.2	13.2	10.5	13.3	12.8	11.4	11.1
	CaBF	100	2.9	37.1	27.0	23.1	18.0	15.1	10.0	8.1	2.5	1.1	0.7	0.1	0.0	0.1	0.1
#3	MAP	100	13.8	43.0	35.7	26.6	25.9	39.0	33.0	29.0	28.4	26.7	23.4	45.3	-	-	-
	COPP	100	11.4	30.6	49.9	67.7	26.6	36.3	31.8	28.6	28.1	26.8	24.3	40.9	-	-	-
	ETCO2	100	48.6	69.1	72.5	71.6	93.4	91.2	87.9	79.7	80.4	83.5	89.5	117.1	-	-	-
	CaBF	100	9.3	38.9	37.1	35.8	36.0	62.5	53.1	47.1	47.2	51.5	49.5	100.5	-	-	-
#4	MAP	100	21.7	64.8	69.4	73.1	75.7	69.3	48.1	-	-	-	-	-	-	-	-
	COPP	100	2.1	49.0	56.0	59.6	56.4	54.3	34.2	-	-	-	-	-	-	-	-
	ETCO2	100	53.8	72.7	86.8	94.4	100.3	86.2	98.6	-	-	-	-	-	-	-	-
	CaBF	100	17.8	59.8	77.0	109.2	113.4	71.5	59.5	-	-	-	-	-	-	-	-

Abbreviation: VF, Ventricular fibrillation; BLS, Basic life support; ACLS, Advanced cardiovascular life support; MAP, Mean arterial pressure; COPP, Coronary perfusion pressure; ETCO2, End-tidal carbon dioxide; CaBF, Carotid blood flow;

Test	Parameter	Pre-VF	VF	BLS				ACLS									
				1	2	3	4	1	2	3	4	5	6	7	8	9	10
#5	MAP	100	25.5	34.4	35.3	34.7	35.4	32.3	28.7	26.1	23.1	18.0	14.1	10.2	7.7	7.3	7.3
	COPP	100	8.5	20.9	20.7	19.1	18.4	17.2	13.9	14.9	10.6	5.7	3.1	-1.3	-1.6	-1.2	-1.2
	ETCO2	100	54.6	72.6	91.0	102.5	124.5	119.6	98.9	93.0	98.3	70.9	72.4	57.4	55.5	46.5	46.5
	CaBF	100	21.6	34.3	18.6	10.4	0.1	4.3	4.7	4.1	3.3	2.1	0.2	-0.6	-0.5	-0.2	-0.2
#6	MAP	100	25.3	27.1	31.3	36.2	39.8	-	-	-	-	-	-	-	-	-	-
	COPP	100	17.0	18.2	21.2	21.2	24.1	-	-	-	-	-	-	-	-	-	-
	ETCO2	100	44.9	90.5	98.8	106.4	115.0	-	-	-	-	-	-	-	-	-	-
	CaBF	100	27.4	30.2	37.4	39.9	37.6	-	-	-	-	-	-	-	-	-	-
#7	MAP	100	29.9	46.3	59.6	57.9	60.0	69.1	69.3	64.9	67.4	64.4	62.3	66.0	64.9	-	-
	COPP	100	25.6	49.6	62.1	56.6	61.1	66.1	69.4	66.4	67.6	68.0	65.6	66.4	66.8	-	-
	ETCO2	100	50.3	64.0	80.4	82.9	90.5	83.4	80.8	75.6	83.2	95.7	101.4	103.7	112.5	-	-
	CaBF	100	7.6	41.7	50.8	45.3	47.0	43.7	41.0	32.9	26.2	33.3	37.7	30.0	34.2	-	-
#8	MAP	100	27.0	54.5	51.8	56.7	54.4	49.1	50.4	48.7	44.8	35.1	29.6	26.3	26.3	25.0	25.0
	COPP	100	16.2	44.8	42.2	46.2	45.1	41.0	34.1	28.9	21.0	18.4	11.8	7.5	9.5	3.0	3.0
	ETCO2	100	52.8	58.3	66.5	95.2	66.5	66.0	79.1	90.2	84.9	90.4	72.3	83.6	100.5	114.9	114.9
	CaBF	100	6.5	28.3	27.8	11.3	29.2	25.2	21.5	15.3	17.7	17.1	16.3	17.0	18.1	20.1	20.1

3.3.2 EEG changes with the recovery of CaBF

The EEG activity between ROSC and non-ROSC cases is compared in Figure 3.5. Before VF, the EEG showed irregular morphology, and its amplitude was above $\pm 20 \mu\text{V}$. After the cerebral oxygenation decreased during the untreated VF, the amplitude decreased within 10–15 s and the isoelectric activity appeared at the end of VF. The activity appeared at the end of VF.

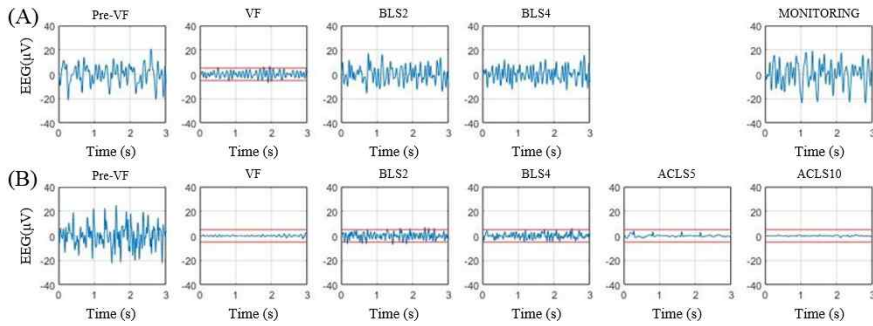


Figure 3.5 Comparison of EEG over time between ROSC and non-ROSC cases. Dashed lines denote the level of $\pm 5 \mu\text{V}$, the limits of the isoelectric state: (A) EEG waveforms of the animal #6, resuscitated after BLS sessions, (B) EEG waveforms of the animal #5, a non-ROSC case.

The recovery of the EEG varied depending on the recovery of the CaBF. For example, in animal #6, the recovery rate reached almost 40% during the last two BLS sessions. At that time, an EEG signal with higher amplitude and increased higher frequency components was observed. It showed that the EEG activity can return to a level similar to the pre-VF values if cerebral resuscitation is successful. In contrast, in animal #5, the recovery rate exceeded 30% during the first LS session, but decreased consistently during the rest of

the CPR sessions. The EEG signal decreased in amplitude and entered the suppression status during the second BLS session. The recovery rates were below 10% and nearly flat patterns due to electrical inactivity appeared. The EEG did not recover until the end of the ACLS sessions.

The Pearson correlation coefficients between the EEG parameters and the recovery rates of CaBF are presented in Table 3.5. Time-domain magnitude and two entropy indices, log energy entropy [18] and Rényi entropy, showed a correlation coefficient of approximately 0.78.

Table 3.5 Pearson correlation coefficients between EEG parameters and the recovery rates of CaBF.

EEG parameters	Correlation coefficient	<i>p value</i>
Magnitude	0.778	< 0.001
SynchFS	0.210	0.228
BetaR	-0.329	0.016
DeltaR	0.196	0.032
AlphaPR	0.189	0.048
BetaPR	0.323	0.001
DeltaPR	0.032	0.797
ThetaPR	-0.354	0.004
BG_Alpha	0.262	0.006
Log energy entropy	0.781	< 0.001
Rényi entropy	0.784	< 0.001

3.3.3 Changes in EEG parameters depending on four CaBF groups

The results of a one-way ANOVA for the three parameters are illustrated in Figure 3.6. For the magnitude, the lowest quartile (Group 1, < 25%) showed significant variations from the other groups, with $p < 0.05$. However, no significant differences were observed among the other three groups. Similar results were observed for the two entropy indices. Table 3.6 demonstrates the results of the post hoc test using the Dunnett T3 method. Differences were obtained by the first group minus the second group.

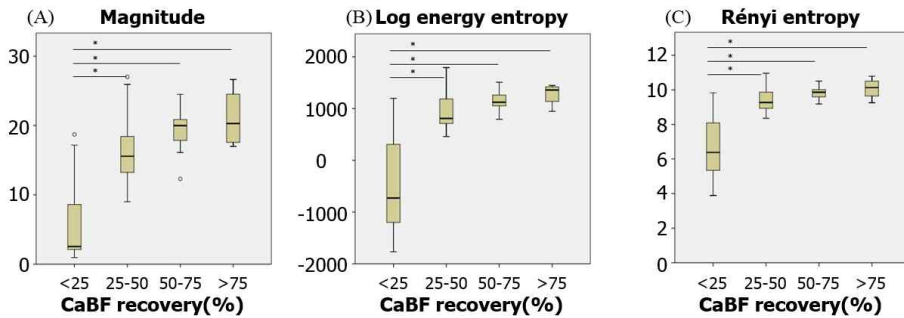


Figure 3.6 Box plots of the means: (A) Magnitude, (B) Log energy entropy, (C) Rényi entropy. Asterisk denotes statistical significance at the $p < 0.001$. Error bars indicate the upper and lower extreme values of the data.

Table 3.6 Multiple comparisons between groups in three EEG parameters.

		Magnitude	Log energy entropy	Rényi entropy
Group		MD / SD	MD / SD	MD / SD
		(<i>p value</i>)	(<i>p value</i>)	(<i>p value</i>)
1	2	-10.39 / 1.24 (< 0.001)	-1375.15 / 164.65 (< 0.001)	-2.69 / 0.319 (< 0.001)
1	3	-13.34 / 1.37 (< 0.001)	-1590.42 / 164.87 (< 0.001)	-3.13 / 0.321 (< 0.001)
1	4	-15.15 / 2.39 (0.012)	-1720.80 / 190.02 (< 0.001)	-3.38 / 0.434 (< 0.001)
2	3	-2.95 / 1.30 (0.169)	-215.27 / 87.24 (0.108)	-0.442 / 0.171 (0.084)
2	4	-4.75 / 2.35 (0.395)	-345.65 / 128.60 (0.180)	-0.695 / 0.338 (0.384)
3	4	-1.80 / 2.41 (0.958)	-130.39 / 128.87 (0.871)	-0.253 / 0.340 (0.957)

Abbreviation: MD, Mean difference; SD, Standard deviation;

3.3.4 EEG parameters depending on two CaBF recovery groups

The ROC curves for the three parameters are illustrated in Figure 3.7. All possible cut-off values are plotted with a combination of the TPR and FPR. The optimal cutoff points are denoted in Figure 3.7. Table 3.7 summarizes the results of ROC curve analysis including AUC, TPR, FPR, and cut-off value. The AUC values of all three parameters were greater than 0.88.

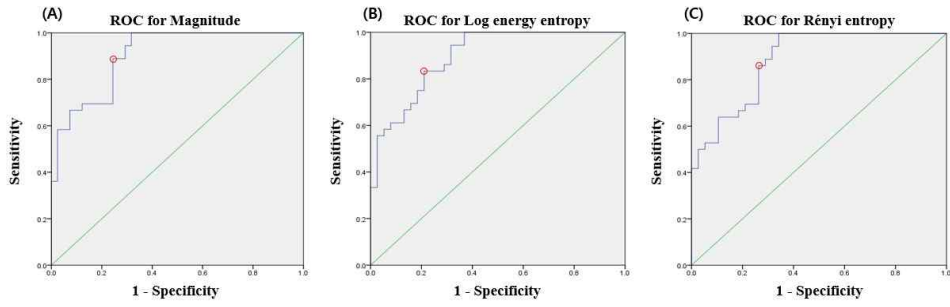


Figure 3.7 ROC curves for three EEG parameters: (A) Magnitude, (B) Log energy entropy, (C) Rényi entropy. Red dots indicate the optimal cut-off values and the diagonal lines indicate random chance.

Table 3.7 Results of the ROC curve analysis for the three EEG parameters.

EEG parameter	AUC	SE	TPR	FPR	Cutoff
Magnitude	0.904	0.033	0.889	0.244	12.802
Log energy entropy	0.896	0.035	0.833	0.211	739.54
Rényi entropy	0.885	0.037	0.861	0.263	8.919

Abbreviation: AUC, Area under the curve; SE, Standard error; TPR, True positive rate; FPR, False positive rate;

3.3.5 EEG parameters for prediction models

Among the 20 EEG parameters introduced in Table 3.2 and Table 3.3, 10 EEG parameters were selected through NCA and the Student's *t*-test. The NCA determined the feature ranking, but EEG parameters with *p* values > 0.05 were excluded after Student's *t*-test, regardless of the ranking. Finally, the top 10 significant parameters were selected. The three parameters, which showed a correlation coefficient of over 0.7 with the recovery rates of CaBF, were included. Table 3.8 summarizes the results of the feature selection process, and Table 3.9 presents the medians, IQRs, and *p* values of each parameter. In addition, EEG parameters from the normal brain and damaged brain were also

compared. The former data were obtained from the five resuscitated animals, and the latter data were obtained from the three deceased animals. Brain damage was assumed to occur under prolonged no- or low-flow longer than 20 min, which corresponded to the 6th ACLS session. The mean differences of each parameter are listed in Table 3.10.

Table 3.8 Results of feature selection process.

EEG parameters	Ranking	<i>p value</i>	Result	Remark
BSR	18	< 0.001	Excluded	Low ranking
Magnitude	11	< 0.001	Selected	-
SynchFS	17	0.264	Excluded	Low ranking
BetaR	4	0.864	Excluded	High <i>P-value</i>
DeltaR	5	< 0.001	Selected	-
DAR	7	< 0.001	Selected	-
DTABR	6	< 0.001	Selected	-
BcSEF	1	< 0.001	Selected	-
ExtraPR	19	0.675	Excluded	Low ranking
AlphaPR	12	0.439	Excluded	Low ranking
BetaPR	16	< 0.001	Excluded	Low ranking
DeltaPR	3	0.014	Selected	-
ThetaPR	15	< 0.001	Excluded	Low ranking
GammaPR	13	0.001	Excluded	Low ranking
Shannon entropy	14	0.607	Excluded	Low ranking
Log energy entropy	10	< 0.001	Selected	-
Spectral entropy	2	0.013	Selected	-
Rényi entropy	8	< 0.001	Selected	-
Ratio05	20	< 0.001	Excluded	Low ranking
BG_Alpha	9	< 0.001	Selected	-

Table 3.9 Final 10 EEG parameters for the prediction models; their median, IQRs, and *p value*.

EEG Parameters	Median (IQR)		<i>p value</i>
	Group 0	Group 1	
Magnitude	4.08 (2.52, 14.28)	18.55 (15.72, 22.29)	< 0.001
DeltaR	0.00 (-0.30, 0.31)	0.25 (-0.08, 0.72)	< 0.001
DAR	0.20 (-0.10, 0.49)	-0.07 (-0.42, 0.36)	< 0.001
DeltaPR	0.28 (0.17, 0.41)	0.20 (0.08, 0.41)	0.014
DTABR	0.18 (-0.10, 0.45)	-0.06 (-0.31, 0.21)	< 0.001
BcSEF	0.00 (0.00, 19.50)	27.0 (22.0, 30.0)	< 0.001
BG_Alpha+	39.90 (26.54, 55.94)	54.53 (39.07, 67.68)	< 0.001
Spectral entropy	0.78 (0.76, 0.80)	0.79 (0.77, 0.81)	0.013
Rényi entropy	6.93 (5.57, 9.06)	9.83 (9.20, 10.11)	< 0.001
Log energy entropy	-241.2 (-1014.8, 729.0)	1122.30 (836.8, 1304.1)	< 0.001

Table 3.10 Comparison of EEG parameters from the normal brain and damaged brain.

EEG Parameters	Normal brain	Damaged brain	<i>p value</i>
Magnitude	22.4 ± 8.4	2.2 ± 1.0	< 0.001
DeltaR	0.78 ± 0.57	-0.66 ± 0.53	< 0.001
DAR	-0.50 ± 0.48	0.92 ± 0.57	< 0.001
DeltaPR	0.11 ± 0.07	0.53 ± 0.22	< 0.001
DTABR	-0.46 ± 0.44	0.75 ± 0.42	< 0.001
BcSEF	29.03 ± 4.0	0.00 ± 0.02	< 0.001
BG_Alpha+	0.70 ± 0.15	0.18 ± 0.12	< 0.001
Spectral entropy	0.81 ± 0.03	0.77 ± 0.05	< 0.001
Rényi entropy	9.92 ± 0.95	5.55 ± 1.06	< 0.001
Log energy entropy	1111 ± 326.3	-1071 ± 488.0	< 0.001

3.3.6 Performances of prediction models

The prediction models, which represent binary classifiers for the recovery of CaBF, were established using different ML algorithms. SMOTE was applied to resolve the class-imbalance problem. New synthetic data were added to the minority class, which made the sample size of each group comparable. Prediction models were established based on the augmented dataset.

The confusion matrices and ROC curves of the prediction models are given in Figure 3.8. The performance of each model was evaluated using six measures, as described in Table 3.10. The accuracy ranged from 0.813 to 0.853, while the sensitivity ranged from 0.689 to 0.807, and the specificity ranged from 0.877 to 0.953. The precision ranged from 0.880 to 0.943, and the F1 score ranged from 0.796 to 0.853. In terms of accuracy, the 3-order polynomial kernel-based

SVM model showed the best performance. In addition, all five classifiers showed high AUC values of over 0.9.

Table 3.11 Performance of prediction models for the recovery of CaBF.

Performance	LR	SVM	KNN	RF	MLP
Accuracy	0.840	0.853	0.813	0.827	0.836
Sensitivity	0.782	0.807	0.689	0.748	0.798
Specificity	0.906	0.906	0.953	0.915	0.877
Precision	0.903	0.906	0.943	0.908	0.880
F1 score	0.838	0.853	0.796	0.820	0.837
AUC	0.933	0.909	0.934	0.915	0.924

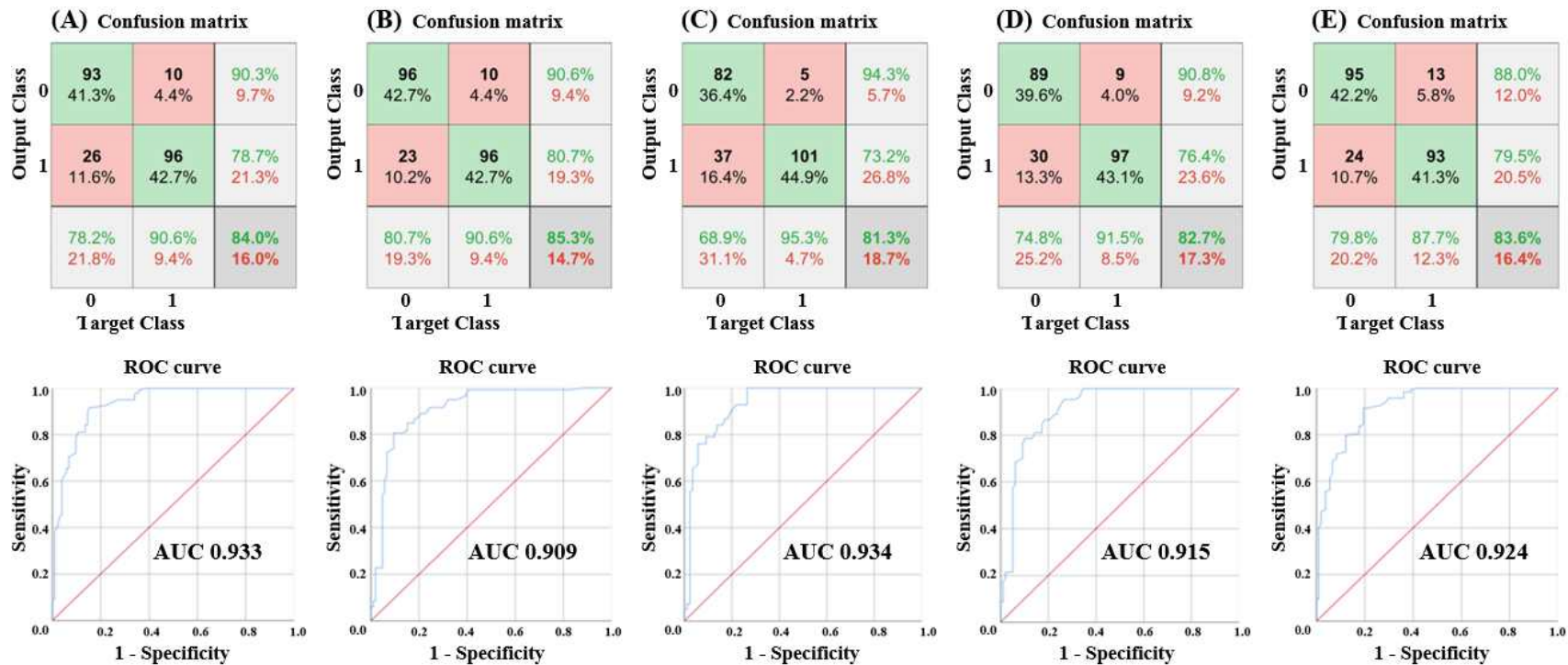


Figure 3.8 The confusion matrices and the ROC curve of the five prediction models: (A) LR, (B) SVM, (C) KNN, (D) RF, (E) MLP.

3.4. Discussion

3.4.1 Accomplishment

The relationships between EEG activity and CaBF were investigated to evaluate the feasibility of noninvasive EEG activity as reliable indicators of cerebral circulation, expressed as CaBF recovery, in the swine model of VF. The current CPR protocol mainly consists of an ECG rhythm check, CCs, defibrillations, and medication [156], while cerebral blood flow is rarely monitored. Newly suggested methods, such as TCD techniques, are not fully applicable for monitoring cerebral hemodynamics during CPR.

Monitoring cerebral circulation during CPR could provide information about neuronal activity and help prevent prolonged ischemic insults and achieve early recovery of normal brain function by delivering improved CPR. EEG has been considered a possible indicator of cerebral circulation because it is heavily affected by the level of cerebral circulation and oxygen delivery [173]. If an easily measurable EEG can reflect the CaBF in an OHCA setting, a feedback method based on noninvasive EEG parameters could guide EMTs to achieve improved CaBF recovery, for example, by guiding the Trendelenburg position [174], that is expected to improve the CaBF and neurological outcomes of CA patients. It is noteworthy that this study used a single-channel EEG signal measured in the frontal region, where the installation of EEG sensors is convenient.

Previous studies have attempted to measure EEG signals during CPR using the BIS monitor and CSM M3 [45]. However, the EEG signal was severely contaminated by artifacts owing to CCs; therefore, unreliable outputs could be generated [79, 175, 176]. Even though short intervals without CCs or defibrillation shocks are prepared, these equipment cannot solely analyze the pauses because of the moving-average function over a certain period of time, such as 30 s [22]. This study focused on the very short pauses between CCs and defibrillation shocks and proved the feasibility of noninvasive EEG signals as an indicator for the recovery of CaBF. The EEG background activity increased and became more complex and irregular with increased CaBF. Concurrently, the higher frequency components including alpha (8–13 Hz) and beta (13–30 Hz) increased, while the lower frequency components including delta (< 4 Hz) and theta (4–8 Hz) decreased. Striking differences were identified with delta-related parameters. The frequency-domain parameters— DeltaR, DAR, DTABR, and DeltaPR— showed relatively high feature rankings and significant differences between the two groups, as presented in Table 3.7. In terms of the quality of cerebral resuscitation, changes in the delta band are important because a decrease in the delta band power coincides with consciousness recovery [136]. These changes in the amplitude and frequency responses affected the functional dynamics of the EEG [177], in terms of complexity, amount of energy, and randomness, which can be observed by the entropy indices. Entropy measures have been applied to EEG signals. Spectral

entropy reflects the rCBF status [178]. Log energy entropy and Rényi entropy have been reported to analyze epileptic events [20, 21]. In this study, log energy entropy and Rényi entropy showed a correlation coefficient above 0.78, with the recovery of CaBF. In addition, all three entropy measures showed a significant difference between the two groups. Thus, these EEG parameters have the potential to reflect spontaneous neuronal activity, and they can be analyzed to evaluate cerebral circulation and oxygen delivery to fulfill the metabolic requirements of brain cells during CPR. The SMV model based on the third-order polynomial kernel function showed the best performance with an accuracy of over 0.813 and an AUC of over 0.909. A polynomial kernel function is a nonlinear kernel function that is used when the class boundaries are non-linear or overlapping [179, 180]. The third-order polynomial kernel function appeared to construct the best class boundary, which resulted in the lowest classification errors within our experimental dataset. If a low CaBF recovery is diagnosed in OHCA patients, EMTs can alter CPR strategies to increase blood flow toward the brain, which makes early recovery of normal brain functions possible.

3.4.2 Limitations

This study had several limitations. First, the experimental model was finalized assuming a witnessed OHCA, wherein a CA-CALL time of 1 min was

presumed, which may differ from actual situations. The changes in the EEG parameters are feasible only with a very short untreated VF. If the duration of untreated VF increases, less prominent or no recovery might occur [38]. Further research should be conducted to investigate the EEG activity under a longer VF period over at least 5 min and establish a more practical prediction model for the recovery of CaBF. Second, this study was performed with a limited number of animals. EEG analysis with larger datasets should be performed to confirm our study. Third, changes in the EEG activity and the performance of the prediction models should be evaluated in real CPR situations. Lastly, the neurological outcomes of the resuscitated animals were not investigated. Sustained ROSC was confirmed with five animals, but they were sacrificed immediately after the monitoring session.

3.5. Conclusion

We measured a single-channel frontal EEG noninvasively during CPR and evaluated the relationships between EEG parameters and the recovery rates of CaBF. Several EEG parameters correlated with CaBF recovery, with a correlation coefficient of approximately 0.78. The prediction models (binary classifiers) with a division criterion of 30% demonstrated competitive performance in discriminating between high- and low-CaBF recovery with an accuracy of over 0.8 and an AUC of over 0.9.

Large sections of this chapter, including figures and tables, have been published previously in *Sensors* [153].

Chapter 4. EEG-based Prediction Model of an Increased Intra-Cranial Pressure for TBI Patients

4.1. Introduction

Traumatic brain injury (TBI) is defined as any traumatically induced disruption of normal brain function [84], and its long-term consequences are a major problem [181]. Approximately 75% of TBI patients experience mild symptoms, such as a short-term loss of consciousness and concentration difficulty, and less than 20% of them suffer from persistent cognitive and physiological disorders, which can develop neurodegenerative diseases such as Alzheimer's disease [182, 183]. TBI is closely associated with daily life. The occurrence of sports-related TBI and the resulting cognitive dysfunction is increasing [184]. In addition, over half of TBI patients struggle with sleeping disorders [185]. Other critical consequences of TBI include high medical costs [87] and lowering a patient's ability to work [88, 89]. Over 5 million Americans have TBI-related disabilities with an annual expense of over 60 billion dollars [181]. These problems have raised the need for accurate prognostication of outcomes following TBI with various neuro-monitoring modalities.

The primary consequences of TBI, directly caused by physical impact, can lead to secondary damage due to the pathophysiologic responses of the primary injury, such as increased ICP and hypoperfusion. To prevent secondary damage

and maintain cerebral perfusion, ICP should be monitored and lowered effectively [90–92]. The use of ICP monitoring is closely related to a low fatality rate [186]. Among several ICP monitoring techniques, invasive methods that involve the insertion of a pressure gauge into the intracranial compartment through burr hole trephination have been regarded as the standard for direct monitoring. However, these methods are vulnerable to several complications, such as nervous system injury and infection, and the procedures are challenging [93–95]. Multiple noninvasive techniques have been developed. TCD techniques are one among them, which measure the cerebral blood flow rate in real time and have shown competitive performance [94–96]. However, noninvasive methods, including TCD techniques, cannot readily replace invasive methods.

Noninvasive EEG can be considered to monitor the ICP because the EEG activity depends on the cerebral circulation [117, 118]. If ICP increases steadily, both the CEPP and CBF decrease, and brain tissue oxygenation also decreases [187]. When the cerebrovascular autoregulation mechanism is lost and ICP reaches the MAP level, the cerebral circulation might halt. Simultaneously, the EEG signal gradually enters the isoelectric state [188]. Prolonged no- or low-flow periods can damage brain function and even result in brain death. Considering the relationships between the EEG activity and ICP, the processed EEG has the potential to reflect the ICP levels [118].

In this study, the relationships between the processed EEG parameters and

ICP levels were investigated in an experimental swine model of TBI. We measured the noninvasive frontal EEG and hemodynamic data while changing the ICP every 6 min and established an EEG-based noninvasive ICP classifier. We hypothesized that the processed parameters derived from the noninvasive EEG signals can distinguish between higher and lower ICP levels.

4.2. Methods

4.2.1 Ethical statement

The animal test protocol was approved by the Institutional Animal Care and Use Committee of Seoul National University Hospital (IACUC number: 19-0097, 20-0115). All animal care complied with the Laboratory Animal Act of the Korean MFDS.

4.2.2 Study design and setting

An animal experiment was designed based on a swine model of TBI to acquire noninvasive EEG and hemodynamic data under diverse ICP levels. A two-way Foley catheter with a diameter of 4.6 mm and a balloon of 30 ml was used to manipulate the ICP. The experiments consisted of the following phases: baseline phase, brain injury phase, secondary interventions with following

monitoring, and a restoration phase. The baseline phase was prepared to acquire frontal EEG and hemodynamic data under normal ICP levels below 20 mmHg for 6 min. During the brain injury phase, the Foley catheter was inflated by injecting saline to increase the ICP. The ICP was raised by 10 mmHg on four occasions: 20–30 mmHg, 30–40 mmHg, 40–50 mmHg, and > 50 mmHg. Then, secondary interventions and monitoring were executed. One of these interventions—hypovolemia, hypoxia, hypothermia, or none—was applied to the animal. To induce hypovolemia, blood was drawn from the internal jugular vein until a MAP < 65 mmHg or a SBP < 90 mmHg was achieved. To induce hypoxia, a fraction of inspired oxygen of 25% and respiratory rate of 6–8 breaths/min were applied until a SpO₂ below 89% was achieved. To induce hypothermia, the body temperature above 38°C was lowered to 33–35°C by operating an esophageal cooling device and a surface cooling device. These changes had to be maintained during the subsequent monitoring for 20 min. If no intervention was applied, the restoration phase was initiated immediately. During the restoration phase, the Foley catheter was deflated by extracting saline to decrease the ICP. The ICP was decreased by 10 mmHg on four occasions: 40–50 mmHg, 30–40 mmHg, 20–30 mmHg, and < 20 mmHg. The baseline and each sub-session in both the injury and restoration phases lasted for 6 min. Thereafter, the animals were euthanized with an injection of KCl (20 mg). If CA occurred during the brain injury or restore phase, the experiment was terminated without resuscitation attempts and the animal was excluded

from the analysis. During the experiments, mechanical ventilation was performed, and a single-channel frontal EEG along with hemodynamic data including ICP was continuously measured in the sphinx position. The entire test scenario is illustrated in Figure 4.1.

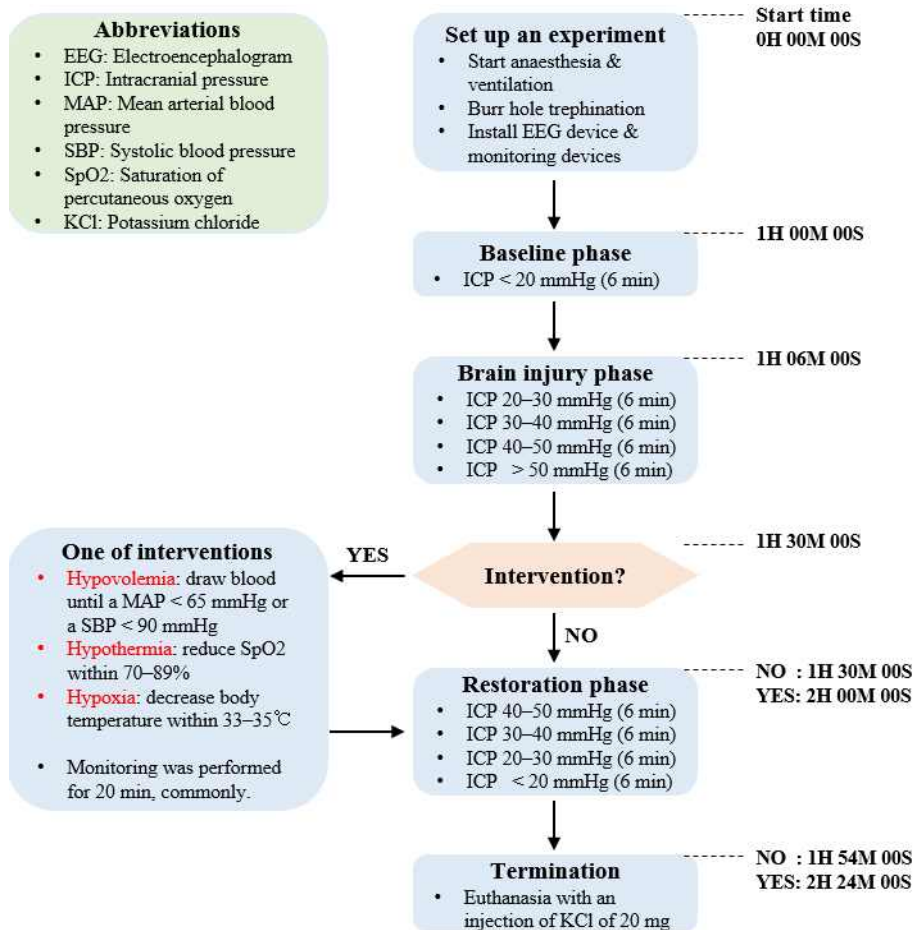


Figure 4.1 The entire test protocol of TBI model with a timeline.

4.2.3 Experimental animals and housing

A total of 30 domestic crossbred female pigs, approximately 3 months of age (41.7 ± 2.3 kg), were studied. The animals were obtained from the supplier

of experimental animals (Cronex Co., Ltd., Cheongju, Korea), qualified by the Korean MFDS with a certificate of KELAS. The animals were maintained in an accredited Association for AAALAC International (#001169) facility, in accordance with the guide for the care and use of laboratory animals [134]. A certified veterinarian adjudged the animals as healthy, and they were made to fast overnight.

4.2.4 Surgical preparation and hemodynamic measurements

The animals were initially sedated with intramuscular injections of 2–4 mg/kg Zoletil and 2 mg/kg Rompun, which was followed by inhalation of isoflurane at a dose at 2–5%. The animals were orally intubated before the initiation of mechanical ventilation. A portable respiratory monitor Capnostream35 (Medtronic, Minneapolis, MN, USA) was installed to monitor the ETCO₂ and SpO₂. To continue the anesthesia, a TV of 10–12 ml/kg, RR of 14–18 breaths/min, PaCO₂ at approximately 40 mmHg, and PaO₂ above 80 mmHg were maintained. Mikro-Tip pressure catheters were inserted into the femoral artery and internal jugular vein to measure ABP and RAP, respectively. The MA2PSB perivascular probe was placed on the internal carotid artery to detect the CaBF, and a T420 perivascular flowmeter was installed. After creating a burr hole on the cranium, a Mikro-Tip pressure catheter was inserted into the parietal lobe to measure the ICP. The appropriate depth of the catheter

was determined by lowering it until a consistent respiratory waveform was observed. An additional burr hole was perforated to insert the Foley balloon catheter into the parietal lobe to elevate the ICP and create the effects of traumatic intracranial hemorrhage (Figure 4.2 (A)). The EEG device was installed to measure the frontal EEG activity (Figure 4.2 (B)). ECG was measured to compute the heart rate (HR). All signals, except the EEG signals, were gathered and saved using the PowerLab 16/35 hardware with LabChart software at a rate of 1 kHz, simultaneously.

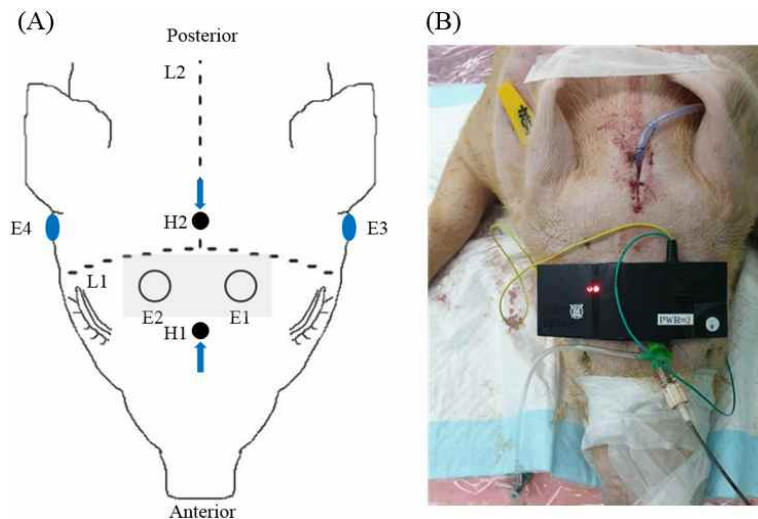


Figure 4.2 Placement of the EEG device and catheters: (A) Schematic of swine head illustrating placement of the EEG device, a pressure catheter for the ICP monitoring, and a Foley catheter: L1, coronal suture; L2, sagittal suture; H1, burr hole for the ICP catheter; H2, burr hole for the Foley catheter; E1, active EEG electrode; E2, auxiliary EEG electrode; E3, reference electrode in the left mastoid; E4, ground electrode in the right mastoid; The gray area indicates the frontal area where the EEG device was placed, (B) Scene of installation of the EEG device and sensors.

4.2.5 EEG measurement

An improved single-channel EEG device was prepared for this study. The new device has the same configuration as the previous single-channel EEG device. Only several connectors and external housing were changed, which did not affect the performance of the device. The external housing was designed assuming the use in emergency situations. To measure EEG in such situations, especially in an OOHS, the EEG device must be compact and light to be wearable. In addition, the setup process must be simple and minimally time-consuming. To meet these requirements, the external housing consists of two rigid parts of the biocompatible polycarbonate and a flexible connecting part of the silicone in between. The flexible part and an adjustable strap hanging on both ends of the device enable good contact between the active electrodes and the scalp, and secure attachment of the device on a rounded forehead. The entire device has dimensions of 110 x 42 x 10 mm and weighs 72 g.

The EEG device adopted the precise resistors with their tolerance of 1%, and capacitors with their tolerance of 10%. The improved electronic circuit of the EEG device and external housing are described in Figure 4.3. The technical specifications of the device are listed in Table 4.1.

This device complied with the general requirements for the essential performance of electroencephalography, specified in the International Standard IEC 60601-2-26, which was tested and validated in an accredited testing laboratory (Korea Compliance Testing Laboratories, Yongin, Korea).

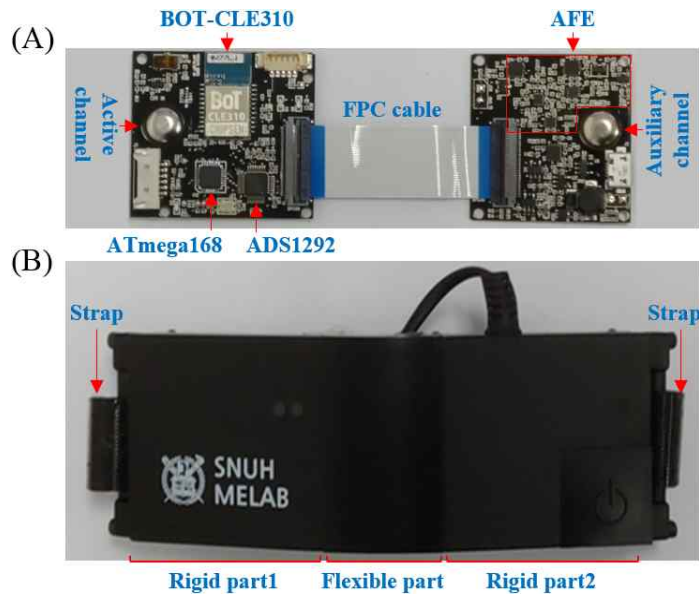


Figure 4.3 An improved single-channel portable EEG device: (A) Printed circuit boards, (B) External housing.

Table 4.1 Technical specifications of the EEG device.

Number of channels	1
Sampling rate	250 Hz
Bandwidth	0.5–50 Hz
Resolution	24-bit
Input range	$\pm 200 \mu\text{V}$
Gain control	12,000 V/V
CMRR	$> 80 \text{ dB}$
Noise (peak-to-peak)	$< 3 \mu\text{V}$
Interface	Bluetooth low-energy V4.1
Power	Li/Po Battery 3.7V/370mAh

4.2.6 Data processing

All data were processed using the MATLAB R2017b software. The EEG and hemodynamic data were synchronized first. The data from the first 1 min of each sub-session in the brain injury and restoration phase were discarded after considering the stabilization after changing the volumes of the Foley catheter. The EEG signal was processed to determine specific parameters. The original EEG was segmented into 2 s long epochs with 1.5 s overlaps with the next epoch. Time- and frequency-domain parameters and entropy indices were obtained every 0.5 s. The averages of hemodynamic data were computed at the same time intervals.

4.2.7 Data analysis

Because of the different interventions, the data only measured during the baseline and brain injury phases were considered in this study. Specifically, EEG parameters and mean values of hemodynamic data, including ICP data were determined in the baseline phase and all four sub-sessions in the brain injury phase. To assess the possibility of the EEG parameters identifying the different ICP levels, a one-way ANOVA was performed with the ICP levels categorized into four groups: Group 1 (< 20 mmHg), Group 2 (20–30 mmHg), Group 3 (30–40 mmHg), and Group 4 (≥ 40 mmHg). A significance level of $p < 0.05$ was applied.

4.2.8 Development of machine-learning based prediction model

Based on the relationship between the EEG parameters and the ICP levels, ML-based prediction models were established. The ICP levels were categorized into two groups: Group 0 (< 25 mmHg), and Group 1 (≥ 25 mmHg). The criterion of 25 mmHg was chosen because ICP values in the 20–30 mmHg range are typically regarded as intracranial hypertension, but the cases with ICP values greater than 25 mmHg require timely treatment [189].

The EEG parameters for the prediction models were determined in two stages. First, the optimal candidate parameters were determined through NCA. Next, the Student's *t*-test was performed to identify EEG parameters that showed significant differences between the two ICP groups. A significance level of $p < 0.05$ was applied. The prediction models were established using three classifiers (LR, SVM, KNN), one graphical model (MLP), and one ensemble model (RF), with the selected EEG parameters as inputs and the binary ICP groups as output. With regard to noninvasive ICP monitoring, HR was also considered as an input. We tested whether the addition of HR improves classification ability.

The first 75–80% of the experiments were used as train data, and the next 20–25% of them were used as test data. If the classes were distributed unevenly and the minority class was rare in the training data, SMOTE was applied to resolve the bias problem by creating a synthetic minority class. When the binary classifiers were established, they were applied to the test data separately. The

performance of each classifier was averaged over the number of test data. Confusion matrices and the ROC curve were obtained to visualize the performance measures.

4.3. Results

4.3.1 Hemodynamic changes during brain injury phase

The EEG activity and all hemodynamic parameters such as HR and ICP were successfully obtained for 24 out of the 30 experiments. Thus, six experiments were excluded from the analysis. Among the multiple hemodynamic data, MAP, ICP, and HR were considered as the primary parameters. Their averages and SDs during the experiments are presented in Table 4.2. The ICP showed normal ranges below 20 mmHg during the baseline phase. The ICP increased as the Foley catheter was inflated during the brain injury phase. Simultaneously, MAP and HR increased as well. The average ICP in each sub-session was lower than the intended values. This was because the ICP increased rapidly at first but gradually decreased owing to the cerebral autoregulation mechanism. Such stabilization periods were considered, and the hemodynamic data measured during the first minute of each sub-session were excluded from the analysis.

Table 4.2 Physiological data during baseline and brain injury phase.

Phase	MAP, mmHg	ICP, mmHg	HR, beats/min
Baseline	81.1 ± 14.2	13.1 ± 5.6	95.3 ± 20.3
Injury 20–30	87.5 ± 17.2	18.7 ± 4.8	99.1 ± 23.7
Injury 30–40	93.4 ± 19.0	24.2 ± 7.1	102.4 ± 24.9
Injury 40–50	97.2 ± 19.5	31.9 ± 9.9	101.7 ± 27.1
Injury > 50	101.5 ± 19.3	38.5 ± 9.7	100.8 ± 31.9

Abbreviation: MAP, Mean arterial pressure; ICP, Intracranial pressure; HR, Heart rate;

4.3.2 EEG changes with an increase of ICP

The ICP levels values were categorized into four groups: Group 1 (< 20 mmHg), Group 2 (20–30 mmHg), Group 3 (30–40 mmHg), and Group 4 (\geq 40 mmHg). The EEG parameters were compared among the groups using a one-way ANOVA. Among the 20 EEG parameters, the results for three parameters (time-domain magnitude, frequency-domain DTABR, and spectral entropy) are described in Figure 4.4 and Table 4.3. For magnitude, Group 1 showed significant differences compared with the other groups, with $p < 0.001$. Differences among the other groups were also significant. For DTABR, Group 1 and Group 2 showed significant differences towards the other groups, with $p < 0.001$. However, Group 3 and Group 4 did not show any significant differences. For spectral entropy, all groups demonstrated significant differences.

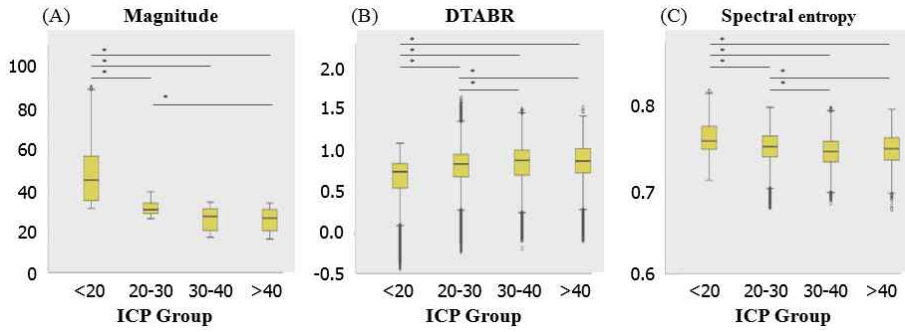


Figure 4.4 Box plots of the means: (A) Magnitude, (B) DTABR, (C) Spectral entropy. Asterisk denotes statistical significance at the $p < 0.001$. Error bars indicate the upper and lower extreme values of the data.

Table 4.3 Multiple comparisons between groups in three EEG parameters.

		Magnitude	DTABR	Spectral entropy
Group		MD / SD (<i>p value</i>)	MD / SD (<i>p value</i>)	MD / SD (<i>p value</i>)
1	2	16.69 / 0.142 (< 0.001)	-0.151 / 0.005 (< 0.001)	0.011 / 0.0002 (< 0.001)
1	3	21.98 / 0.157 (< 0.001)	-0.205 / 0.005 (< 0.001)	0.016 / 0.0003 (< 0.001)
1	4	22.37 / 0.188 (< 0.001)	-0.201 / 0.008 (< 0.001)	0.014 / 0.0005 (< 0.001)
2	3	5.28 / 0.084 (0.001)	-0.054 / 0.005 (< 0.001)	0.005 / 0.003 (< 0.001)
2	4	5.68 / 0.132 (< 0.001)	-0.050 / 0.008 (< 0.001)	0.003 / 0.005 (< 0.001)
3	4	0.397 / 0.149 (0.045)	0.004 / 0.008 (0.997)	-0.002 / 0.005 (0.001)

Abbreviation: MD, Mean difference; SD, Standard deviation;

4.3.3 EEG parameters for prediction models

The EEG parameters were analyzed to establish which ones were suitable for the binary classifier for the two ICP groups: Group 0 (< 25 mmHg), and Group 1 (≥ 25 mmHg). The NCA and Student's t -test were performed to select

the top 10 significant EEG parameters as inputs for the ICP prediction models.

Table 4.4 presents the selected EEG parameters, and their medians, IQRs, and *p values* between the two ICP groups.

Table 4.4 Final 10 EEG parameters for the ICP prediction models; their median, IQRs, and *p value*.

EEG Parameters	Median (IQR)		<i>p value</i>
	Group 0	Group 1	
SynchFS	2.61 (2.42, 2.77)	2.44 (2.34, 2.56)	< 0.001
BetaR	-0.62 (-0.75, -0.49)	-0.60 (-0.70, -0.49)	< 0.001
DTABR	0.70 (0.47, 0.81)	0.90 (0.78, 1.00)	< 0.001
BcSEF	19.41 (16.44, 23.09)	14.85 (12.62, 17.32)	< 0.001
ExtraR	-2.66 (-2.77, -2.56)	-2.85 (-3.01, -2.69)	< 0.001
ThetaPR	0.12 (0.09, 0.16)	0.15 (0.11, 0.19)	< 0.001
GammaPR	0.02 (0.01, 0.03)	0.01 (0.01, 0.02)	< 0.001
Shannon entropy	-19.4 (-169.1, 139.6)	-15.4 (-146.9, 107.4)	< 0.001
Log energy entropy	1957 (1804, 2338)	1866 (1671, 1986)	< 0.001
Rényi entropy	11.36 (11.07, 12.13)	11.16 (10.76, 11.37)	< 0.001

4.3.4 Performances of prediction models

The prediction models (binary classifiers) for the ICP groups, were derived using different ML methods. The potential bias problem was resolved by applying SMOTE. The newly augmented data instances were added to the minority class, and the sample size of each group became comparable.

Figure 4.5 demonstrates the confusion matrices and the ROC curve of the

binary classifiers with the inputs of the EEG parameters alone. The performance of each model is presented in Table 4.5 with six measures. The accuracy ranged from 0.634 to 0.686, while the sensitivity ranged from 0.669 to 0.873, and the specificity ranged from 0.194 to 0.629. The precision ranged from 0.701 to 0.796, and the F1 score ranged from 0.727 to 0.778. The MLP model with 10 hidden neurons and trained with the scaled conjugate gradient algorithm, a supervised learning method for feedforward neural networks [190], showed the highest accuracy of 0.686, and an AUC value of over 0.7.

Figure 4.6 demonstrates the confusion matrices and the ROC curve of the binary classifiers with the inputs of the EEG parameters and the noninvasive HR data. The performance of each model is presented in Table 4.6 with six measures. The accuracy ranged from 0.645 to 0.781, while the sensitivity ranged from 0.722 to 0.863, and the specificity ranged from 0.173 to 0.738. The precision ranged from 0.693 to 0.852, and the F1 score ranged from 0.760 to 0.837. The RF model showed the highest accuracy of 0.781. The RF and MLP models showed an AUC value of over 0.8. The overall classification performance of the models was improved when the HR data were included in the input.

Table 4.5 Performance of prediction models for the ICP groups with the EEG parameters alone.

Performance	LR	SVM	KNN	RF	MLP
Accuracy	0.658	0.647	0.656	0.634	0.686
Sensitivity	0.873	0.740	0.669	0.706	0.740
Specificity	0.194	0.447	0.629	0.479	0.571
Precision	0.701	0.743	0.796	0.745	0.788
F1 score	0.778	0.742	0.727	0.725	0.763
AUC	0.641	0.624	0.692	0.641	0.754

Table 4.6 Performance of prediction models for the ICP groups with the EEG parameters and the HR data.

Performance	LR	SVM	KNN	RF	MLP
Accuracy	0.645	0.713	0.689	0.781	0.760
Sensitivity	0.863	0.834	0.722	0.823	0.771
Specificity	0.173	0.452	0.616	0.690	0.738
Precision	0.693	0.767	0.803	0.852	0.864
F1 score	0.769	0.799	0.760	0.837	0.815
AUC	0.599	0.719	0.722	0.814	0.834

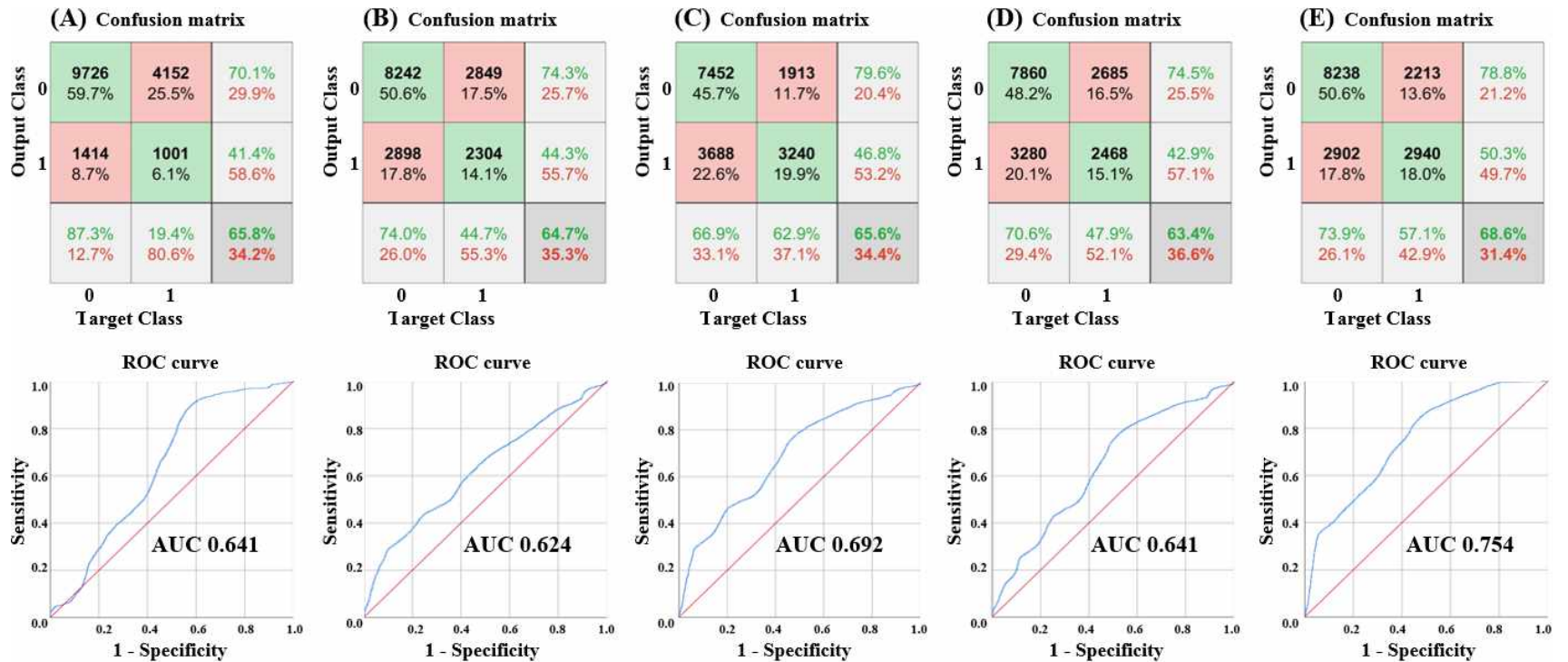


Figure 4.5 Confusion matrices and ROC curves of the five prediction models with the EEG parameters alone as an input: (A) LR, (B) SVM, (C) KNN, (D) RF, (E) MLP.

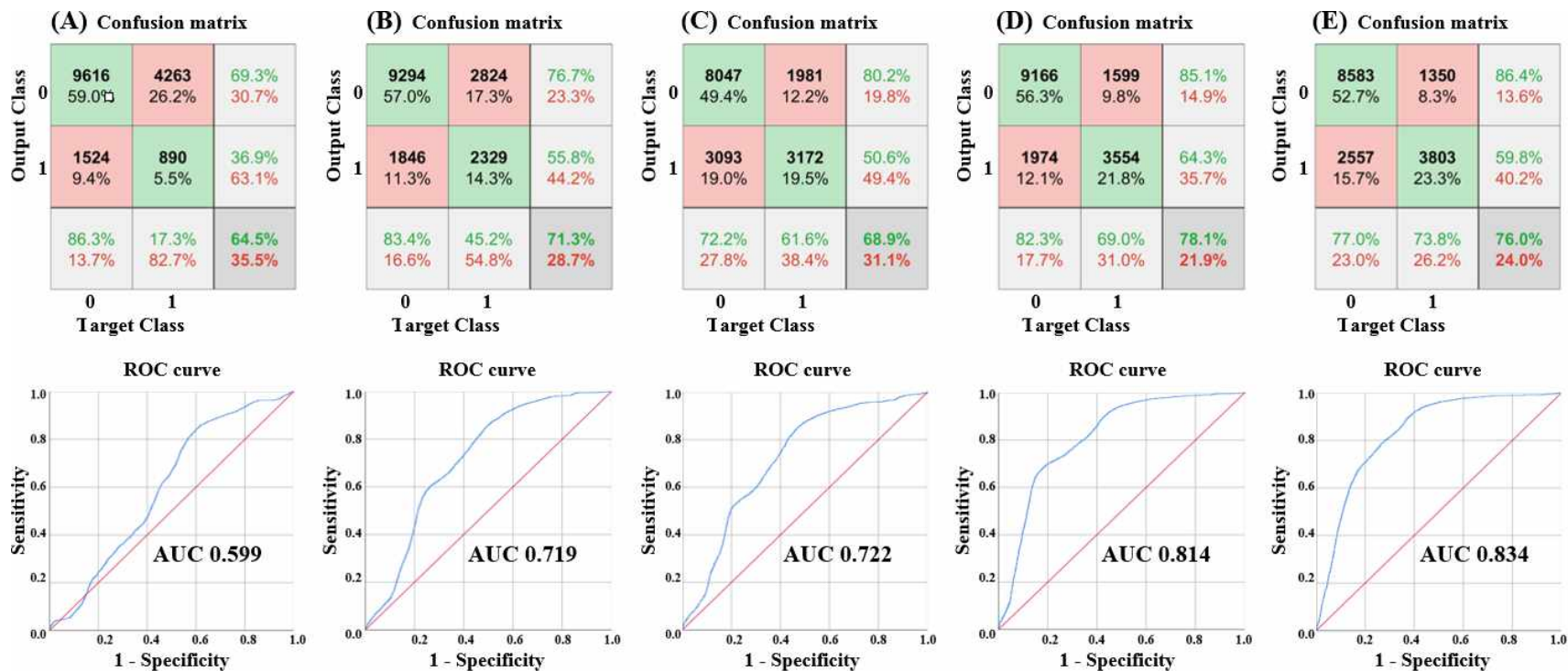


Figure 4.6 Confusion matrices and ROC curves of the five prediction models with the EEG parameters and the HR data as inputs: (A) LR, (B) SVM, (C) KNN, (D) RF, (E) MLP.

4.4. Discussion

4.4.1 Accomplishment

In this study, an EEG-based noninvasive ICP classifier using ML techniques was proposed. The binary classifier was established with the noninvasive EEG parameters and HR data to distinguish higher and lower ICP levels, while the ICP was adjusted with the Foley balloon catheter. Conventionally, bedside invasive ICP monitors, which involve trephination and an insertion of a pressure catheter, are utilized to measure ICP directly. However, despite a high agreement of over 98% with the actual ICP measured with a ventricular catheter [191], the invasive methods could not be adequate for emergency settings. Predicting the ICP in a noninvasive manner can be beneficial because it can be applied in a shorter period of time and complications imposed by invasive methods can be avoided. In particular, an EEG-based ICP classifier may be useful in an OOHS if the EEG can be measured from the injured patient's head. The proposed classifier can be a surrogate indicator of a dangerous ICP level (> 25 mmHg). It is expected to enable earlier treatments for reducing ICP even before admission to the hospital.

An EEG-based ICP classifier is developed with the hypothesis that an elevated ICP can prevent blood flow to the brain and suppress EEG activity. We tested the feasibility of the EEG signal as an indicator for elevated ICP levels. Under the four categories of ICP levels, the EEG parameters showed significant

differences among groups, which strengthens our hypothesis. This study is not the first attempt to investigate the relationship between EEG and ICP. An observational study demonstrated that a strong correlation between the EEG parameters and ICP levels, measured by lumbar puncture, was found in patients with CNS diseases [118]. More frequent burst-suppression patterns were related to increased ICP levels [119–121]. Contrary to previous studies, we performed an experimental intervention study using a TBI model to determine the relationship between EEG and invasive ICP. Several EEG parameters revealed the ongoing ICP changes. In addition, the field application of the noninvasive EEG-based ICP prediction was prepared using ML-based prediction models. Among the five prediction models, the MLP with 10 hidden layers showed the best results. After computing the loss with initial random weights, backpropagation is initiated to train the model by repeatedly sending the loss from the output layer to the hidden layers, and each weight parameter is optimized to minimize the loss. During this process, the MLP model could have more flexible decision boundaries in our experimental dataset.

The overall performance of each prediction model was not comparable to those of the TCD, CBFV, and ONSD methods. For identifying ICP levels over 20 mmHg, the TCD-based estimates have been reported to show a sensitivity of 68.0%, specificity of 84.3% and an AUC of 0.87 [192] while the CBFV-based estimates have been reported to show a sensitivity of 90.0%, specificity of 80.0%, and an AUC of 0.83 [193]. The ONSD-based estimates, combined

with magnetic resonance imaging (MRI), showed a sensitivity of 90.0%, specificity of 92.0%, and an AUC of 0.94 with a cutoff of 5.82 mm. For identifying ICP levels over 25 mmHg, contrarily, the EEG-based prediction model using MLP algorithm showed a sensitivity of 74.0%, specificity of 57.1% and an AUC of 0.754 when the EEG parameters were used alone. However, the use of HR data showed the possibility for further development. When the HR data were also included, the MLP-based model showed a sensitivity of 77.1%, specificity of 73.8% and an AUC of 0.834 while the RF-based model showed a sensitivity of 82.3%, specificity of 69.0% and an AUC of 0.814. These results suggest that the use of other different noninvasive data can improve the prediction models. Furthermore, the EEG-based prediction model showed the AUC values similar to those of the TCD and CBFV methods.

Although an EEG-based noninvasive ICP classifier is at an early stage of development, it has advantages over TCD, CBFV, and ONSD methods. TCD methods require skillful personnel to identify the correct vessels with an ultrasonic probe, and interpret the measurements, which may inevitably cause inter-observer variations [93, 194]. Another limitation is that ABP should be acquired invasively from the radial artery [193]. Similarly, CBFV methods also need to measure ABP to estimate ICP. Vascular access surgery is time-consuming and might inappropriate in such situations that require urgent medical treatments or monitoring. Moreover, continuous monitoring is not possible with these methodologies. However, the proposed EEG-based ICP

classifier measures the frontal EEG activity with a light wearable device (readily applicable to patients), and computes the EEG parameters instantly. This is followed by determining the ICP levels automatically, without any human intervention or additional measurements. Of the various noninvasive ICP monitoring modalities, ONSE methods present the best performance to differentiate between the normal and dangerous ICP. With the help of MRI or ultrasonography, it would be possible to monitor patients with intracranial hypertension in the intensive care unit [195]. However, the EEG-based prediction has advantages of the skill level requirement, cost of technology, continuous monitoring, feasibility in hospital-level emergency settings (e.g., emergency department and intensive care unit), and portability over ONSE.

The Association for the Advancement of Medical Instrumentation standardized the level of accuracy for a noninvasive ICP measurement [96, 196]. According to the guidelines, a difference of 2 mmHg is acceptable when the ICP is below 20 mmHg and differences below 10% are acceptable if the ICP ranges is 20–100 mmHg. To improve the performance, an EEG-based ICP classifier should be able to classify into more number of groups accompanied by further experiments and EEG analysis. Other noninvasive signals can be applied to improve the performance.

4.4.2 Limitations

There are some limitations to this study. First, it is a preliminary study in which many animals have been used in the experimental design. Therefore, it is difficult to generalize the results to real TBI patients without conducting further clinical studies. Data acquisition from human subjects and model improvement should be guaranteed. Second, the use of anesthetic agents and creating two burr holes can affect the EEG activity. Lastly, it was not possible for us to investigate the long-term changes of the EEG owing to the elevated ICP levels.

4.5. Conclusion

We measured the EEG activity noninvasively with varied ICP levels and evaluated the relationships between the EEG parameters and ICP levels. ML-based binary classifiers using the EEG parameters were established to distinguish between higher and lower ICP levels. The lower ICP levels were defined as < 25 mmHg, while higher ICP levels were defined as ≥ 25 mmHg. The prediction model could be an acceptable classifier with the EEG parameters as input. Furthermore, the performance was improved when another noninvasive parameter, HR, was also applied, resulting in an AUC of 0.834.

Chapter 5. Summary and Future works

5.1 Thesis summary and contributions

The primary objective of this dissertation is to develop an EEG-based noninvasive monitoring technique for critical care in emergency settings. Brain cells communicate with each other by generating electrical signals, even when they are sleeping. An EEG is a recording of the electrical activity generated by neuronal function, which is usually detected using electrodes attached to the scalp. EEG activity is closely related to brain disorders and cerebral hemodynamics. As a useful tool for monitoring brain activity, EEG has been widely used to diagnose brain-related disorders and several EEG-derived indices have been used in clinical practice. This study attempts to develop noninvasive diagnostic tools for physiologic parameters monitoring in CA and TBI situations, with easily obtainable EEG signals.

In the first study, an EEG-based Brain Resuscitation Index (EBRI) was proposed to estimate ETCO₂ to assess systemic circulation during CPR. Several EEG parameters, which are used to determine the depth of the anesthesia, were analyzed according to the different CPR modes. During higher quality CPR, the primary hemodynamic parameters, including MAP and CaBF, and the secondary parameter, ETCO₂, increased. The opposite changes were found during lower-quality CPR. The linearly regressed EBRI correlated

positively with the actual ETCO₂, and the delta-EBRI showed potential as a real-time indicator for notifying the increased or decreased ETCO₂. Particularly, the delta-EBRI can be used to evaluate the recovery of systemic circulation during CPR.

In the second study, the relationship between the EEG parameters and CaBF recovery were investigated. Previous studies have demonstrated that prolonged no- or low-flow can develop ischemic insults and deteriorate the EEG activity and presented seven distinct EEG patterns with regard to the different levels of rSO₂ [81]. Several EEG parameters that were measured during the brief-period intervals showed a high correlation with the CaBF recovery. The EEG-based binary classifiers were established to distinguish the higher and lower CaBF groups. The prediction models showed excellent performance, with an accuracy of over 0.8 and an AUC of over 0.9. These models are expected to monitor the recovery of the cerebral resuscitation, which is rarely possible with ETCO₂ monitoring.

In the third study, an EEG-based prediction model was established to estimate the elevated ICP levels. Because ICP values greater than 20–25 mmHg can cause neurological disorders and sustained ICP values of over 40 mmHg can result in brain death, accurate ICP monitoring is required for TBI patients. The proposed binary ICP classifiers using the noninvasive EEG and HR data could differentiate between the normal and dangerous ICP levels, with an accuracy of 0.78 and an AUC of over 0.8. Their performance cannot be

comparable to that of invasive methods, which are regarded as the standard for direct ICP monitoring. However, the EEG-based noninvasive monitoring techniques show performance similar to other noninvasive methodologies, such as TCD, CBFV, and have the potential to indicate the dangerous ICP levels, even in an OOHS, for which the invasive methods cannot be applied.

Four EEG parameters were used to predict the CaBF and ICP levels, which could directly affect brain activity: DTABR, BcSEF, Log energy entropy, and Rényi entropy. DTABR and BcSEF are closely related to the shift in the spectral profile. When the EEG activity was more recovered with a higher CaBF recovery or lower ICP levels, the power spectrum shifted toward higher frequencies, leading to higher BcSEF and lower DTABR. The opposite changes were observed when the EEG became deactivated or entered isoelectric status with lower CaBF recovery or higher ICP levels. The increased complexity and randomness of the EEG coincided with the spectral shift toward higher frequencies. These changes were revealed in the Log energy entropy and Rényi entropy. Overall, these four EEG parameters have the potential to reflect changes in CaBF and ICP. Furthermore, the importance of delta-related parameters should also be highly investigated to monitor cerebral physiologic data. Especially, four delta-related parameters showed significant differences between high- and low-CaBF recovery with relatively high NCA feature rankings. Because changes in delta band power are related to consciousness recovery [136], the delta-related parameters can be used effectively in

evaluating the return of the normal EEG activity during CPR.

These studies were performed to monitor physiologic data, which are primarily considered in CA and TBI situations, using a noninvasive EEG. Different EEG features and prediction models were achieved for specific purposes. However, all the studies demonstrate that a noninvasive EEG can yield clinically important predictive outcomes, which can be utilized with a combination of other diagnostic methods.

5.2 Future direction

This dissertation analyzes the relationships between the EEG activity and physiological parameters for immediate ETCO₂, CaBF, and ICP levels to establish noninvasive prediction models. In CA and TBI situations, the effectiveness of treatments and recovery of patients are typically evaluated by measuring physiological responses such as hemodynamic profiles. The EEG, which reveals brain cell viability, has been suggested as a surrogate indicator of physiological data. In this study, the processed EEG signals were analyzed with ETCO₂, CaBF, and ICP, and the performance of an EEG-based prediction model was also evaluated using these physiological data. However, in terms of brain functionality, EEG analysis relating to these physiological data may not be completely appropriate. By contrast, EEG should be solely investigated to

assess the neurological status of patients. In the long term, EEG could be utilized both immediately after injury and during inpatient treatments, without having to rely on other methodologies. If a reliable EEG is obtainable in an OOHS, it could guide optimal resuscitation efforts or ICP-lowering treatments. For example, favorable EEG changes could help EMTs advance further treatment. Otherwise, they might decide on early hospital transfers. During hospitalization, EEG can be monitored with evaluation scoring systems, such as the cerebral performance category (CPC) [197, 198] and modified Rankin scale (mRS) [199, 200].

In CA situations, the CPC is considered the standard evaluation method of resuscitated patients. The CPC scores on a 5-point scale are determined after reviewing medical records and physical examinations [201]. However, the CPC would be inadequate for evaluating different levels of brain injury [202]. Thus, the mRS on a 7-point scale can be applied because it is more focused on brain injury and neurological outcomes. To achieve an earlier recovery of brain function and produce better prognostication of resuscitated patients, these evaluation indices in conjunction with the EEG parameters should be investigated. In case of an OHCA, CA characteristics (e.g., the type and location of patient, time interval from emergency call to arrival of EMTs, initial heart rhythm, no-flow period, and witnessed status) can be considered together. Current guidelines recommend delaying neurological examinations and prognostication for at least 72 h after ROSC. Thus, new methods for earlier

neurological assessment could be advantageous. If the influence of the improved EEG signals during CPR on achieving favorable outcomes (CPC score 1–2 and mRS score 0–3) could be disclosed, the CA patients' neurological and functional outcomes could be estimated. Besides, an EEG-based resuscitation scoring system could be established eventually, and prolonged failure to obtain improved EEG signals during CPR may be included in the decision-making process for termination of resuscitation or other treatments. The CPC and mRS can also be utilized with EEG signals to assess neurological status during TBI. These evaluation indices evaluate the levels of consciousness and effectiveness of treatments for TBI patients. Quantitative EEG in severe brain injury situations should be analyzed during the entire course of treatment. Then, the relationships among EEG, ICP, and standard evaluation indices could be identified. The capability of a noninvasive EEG to monitor ICP could be improved and an EEG-based noninvasive ICP evaluation method could also be improved, which can guide more effective treatment strategies, without having to use other ICP monitoring methodologies.

The EEG acquisition system should also be improved in terms of artifact prevention techniques. The consistent placement of electrodes with low contact impedance is an essential prerequisite for reliable emergency EEG measurement. Mechanical flexibility and rigid attachment should be guaranteed for this purpose. Configurations of the electrodes also require improvement. EEG can be measured continuously for several hours with conductive wet

electrodes because the conductive gel on the electrodes dehydrates, and the electrodes need to be replaced regularly. Therefore, novel dry electrodes that can allow long-term high-fidelity EEG recordings without conductive gel or skin preparation should be utilized. When using dry electrodes, increased electrode-skin impedance might attenuate the raw EEG signals. Typically, stratum corneum, the outmost layer of skin with a dry dielectric property, can disturb electrical behavior in the skin-electrode interface [203]. Because the thickness of stratum corneum can increase the electrode-skin impedance, sharp tip microneedle structure, which penetrates the stratum corneum, could ensure the fixation of electrodes while reducing the electrode-skin impedance significantly [204]. Novel signal processing techniques for removing artifacts are also required. A recently developed CPR artifact removal technology, See-Thru CPR (Zoll Medical Corporation, Chelmsford, MA, USA), eliminates compression artifacts on the ECG signal to visualize the underlying heart rhythm while minimizing the compression pauses [205]. Such signal processing techniques can be applied to achieve artifact-free EEG signals.

With the future advances mentioned above, the feasibility of EEG-based prediction should be further investigated. Thus, several limitations in animal experiments should be resolved to establish more practical prediction models. In a swine model of VF, various untreated VF durations and CPR conditions should be considered. In a swine model of TBI, the effects of multiple interventions, including hypovolemia, hypothermia, and hypoxia, which TBI

patients might experience, should be reflected in the EEG-based noninvasive ICP prediction models. Moreover, clinical trials are required to verify and generalize results from animal experiments to the real patients.

Bibliography

- [1] E. Niedermeyer and F. L. da Silva, *Electroencephalography: basic principles, clinical applications, and related fields*. Lippincott Williams & Wilkins, 2005.
- [2] "Electroencephalography (EEG)," in *Wiley Encyclopedia of Biomedical Engineering*.
- [3] P. Olejniczak, "Neurophysiologic Basis of EEG," *Journal of Clinical Neurophysiology*, vol. 23, no. 3, 2006.
- [4] K. Jerbi *et al.*, "Task-related gamma-band dynamics from an intracerebral perspective: Review and implications for surface EEG and MEG," *Human Brain Mapping*, vol. 30, no. 6, pp. 1758-1771, 2009.
- [5] S. Musall, V. von Pfössl, A. Rauch, N. K. Logothetis, and K. Whittingstall, "Effects of Neural Synchrony on Surface EEG," *Cerebral Cortex*, vol. 24, no. 4, pp. 1045-1053, 2012.
- [6] R. W. Homan, J. Herman, and P. Purdy, "Cerebral location of international 10–20 system electrode placement," *Electroencephalography and Clinical Neurophysiology*, vol. 66, no. 4, pp. 376-382, 1987/04/01/ 1987.
- [7] S. Herculano-Houzel, "The human brain in numbers: a linearly scaled-up primate brain," (in eng), *Front Hum Neurosci*, vol. 3, pp. 31-31, 2009.
- [8] P. L. Nunez and R. Srinivasan, *Electric fields of the brain: the neurophysics of EEG*. Oxford University Press, USA, 2006.
- [9] W. O. Tatum IV, *Handbook of EEG interpretation*. Demos Medical Publishing, 2014.
- [10] R. N. Harner, "A Recommendation for Standard EEG Montages," *American Journal of EEG Technology*, vol. 17, no. 2, pp. 105-114, 1977/06/01 1977.
- [11] C. E. Henry, "Relative Merits of Different Montages for Optimal Display of EEG Patterns," *American Journal of EEG Technology*, vol. 17, no. 1, pp. 21-51, 1977/03/01 1977.

- [12] N. A. Nussmeler, C. Arlund, and S. Slogoff, "Neuropsychiatric Complications after Cardiopulmonary Bypass Cerebral Protection by a Barbiturate," *Anesthesiology: The Journal of the American Society of Anesthesiologists*, vol. 64, no. 2, pp. 165-170, 1986.
- [13] J. Bruhn, T. W. Bouillon, and S. L. Shafer, "Bispectral index (BIS) and burst suppression: revealing a part of the BIS algorithm," *Journal of clinical monitoring and computing*, vol. 16, no. 8, pp. 593-596, 2000.
- [14] J. Hofmeijer, M. C. Tjepkema-Cloostermans, and M. J. van Putten, "Burst-suppression with identical bursts: a distinct EEG pattern with poor outcome in postanoxic coma," *Clinical neurophysiology*, vol. 125, no. 5, pp. 947-954, 2014.
- [15] B. Schack, H. Witte, M. Helbig, C. Schelenz, and M. Specht, "Time-variant non-linear phase-coupling analysis of EEG burst patterns in sedated patients during electroencephalic burst suppression period," *Clinical neurophysiology*, vol. 112, no. 8, pp. 1388-1399, 2001.
- [16] H. Adeli, S. Ghosh-Dastidar, and N. Dadmehr, "A wavelet-chaos methodology for analysis of EEGs and EEG subbands to detect seizure and epilepsy," *IEEE Transactions on Biomedical Engineering*, vol. 54, no. 2, pp. 205-211, 2007.
- [17] T. Ergenoglu, T. Demiralp, Z. Bayraktaroglu, M. Ergen, H. Beydagi, and Y. Uresin, "Alpha rhythm of the EEG modulates visual detection performance in humans," *Cognitive Brain Research*, vol. 20, no. 3, pp. 376-383, 2004.
- [18] S. Raghu, N. Sriraam, and G. P. Kumar, "Classification of epileptic seizures using wavelet packet log energy and norm entropies with recurrent Elman neural network classifier," *Cognitive neurodynamics*, vol. 11, no. 1, pp. 51-66, 2017.
- [19] U. R. Acharya, H. Fujita, V. K. Sudarshan, S. Bhat, and J. E. Koh, "Application of entropies for automated diagnosis of epilepsy using EEG signals: A review," *Knowledge-based systems*, vol. 88, pp. 85-96, 2015.
- [20] A. B. Das and M. I. H. Bhuiyan, "Discrimination and classification of focal and non-focal EEG signals using entropy-based features in the

- EMD-DWT domain," *Biomedical Signal Processing and Control*, vol. 29, pp. 11-21, 2016/08/01/ 2016.
- [21] Y. Yin, K. Sun, and S. He, "Multiscale permutation Rényi entropy and its application for EEG signals," *PLoS One*, vol. 13, no. 9, p. e0202558, 2018.
 - [22] I. J. Rampil, "A primer for EEG signal processing in anesthesia," *Anesthesiology: The Journal of the American Society of Anesthesiologists*, vol. 89, no. 4, pp. 980-1002, 1998.
 - [23] U. R. Acharya, S. V. Sree, G. Swapna, R. J. Martis, and J. S. Suri, "Automated EEG analysis of epilepsy: a review," *Knowledge-Based Systems*, vol. 45, pp. 147-165, 2013.
 - [24] S. Smith, "EEG in the diagnosis, classification, and management of patients with epilepsy," *Journal of Neurology, Neurosurgery & Psychiatry*, vol. 76, no. suppl 2, pp. ii2-ii7, 2005.
 - [25] U. R. Acharya, S. Vinitha Sree, G. Swapna, R. J. Martis, and J. S. Suri, "Automated EEG analysis of epilepsy: A review," *Knowledge-Based Systems*, vol. 45, pp. 147-165, 2013/06/01/ 2013.
 - [26] R. G. Geocadin *et al.*, "Neurological recovery by EEG bursting after resuscitation from cardiac arrest in rats," *Resuscitation*, vol. 55, no. 2, pp. 193-200, 2002.
 - [27] E. Neto, E. A. Allen, H. Aurlien, H. Nordby, and T. Eichele, "EEG spectral features discriminate between Alzheimer's and vascular dementia," *Frontiers in neurology*, vol. 6, p. 25, 2015.
 - [28] X.-S. Zhang, R. J. Roy, and E. W. Jensen, "EEG complexity as a measure of depth of anesthesia for patients," *IEEE transactions on biomedical engineering*, vol. 48, no. 12, pp. 1424-1433, 2001.
 - [29] T. Musialowicz, P. Lahtinen, O. Pitkänen, J. Kurola, and I. Parviainen, "Comparison of Spectral Entropy and BIS VISTA™ monitor during general anesthesia for cardiac surgery," *Journal of Clinical Monitoring and Computing*, vol. 25, no. 2, p. 95, 2011/04/22 2011.
 - [30] D. J. Nieuwenhuijs, "Processed EEG in natural sleep," *Best Practice & Research Clinical Anaesthesiology*, vol. 20, no. 1, pp. 49-56, 2006.
 - [31] T. Nakamura, V. Goverdovsky, M. J. Morrell, and D. P. Mandic,

- "Automatic sleep monitoring using ear-EEG," *IEEE journal of translational engineering in health and medicine*, vol. 5, pp. 1-8, 2017.
- [32] F. W. SHARBROUGH, J. M. MESSICK, and T. M. SUNDT, "Correlation of Continuous Electroencephalograms With Cerebral Blood Flow Measurements During Carotid Endarterectomy," *Stroke*, vol. 4, no. 4, pp. 674-683, 1973.
- [33] W. Trojaborg and G. Boysen, "Relation between EEG, regional cerebral blood flow and internal carotid artery pressure during carotid endarterectomy," *Electroencephalography and Clinical Neurophysiology*, vol. 34, no. 1, pp. 61-69, 1973/01/01/ 1973.
- [34] J. Overgaard, C. Mosdal, and W. A. Tweed, "Cerebral circulation after head injury," *J Neurosurg*, vol. 55, pp. 63-74, 1981.
- [35] T. Dalkara, E. Morikawa, N. Panahian, and M. Moskowitz, "Blood flow-dependent functional recovery in a rat model of focal cerebral ischemia," *American Journal of Physiology-Heart and Circulatory Physiology*, vol. 267, no. 2, pp. H678-H683, 1994.
- [36] R. S. Marshall, "The functional relevance of cerebral hemodynamics: why blood flow matters to the injured and recovering brain," *Current Opinion in Neurology*, vol. 17, no. 6, pp. 705-709, 2004.
- [37] R. Pana, L. Hornby, S. Shemie, S. Dhanani, and J. Teitelbaum, "Time to loss of brain function and activity during circulatory arrest," *Journal of Critical Care*, vol. 34, pp. 77-83, 2016.
- [38] T. J. Losasso, D. A. Muzzi, F. B. Meyer, and F. W. Sharbrough, "Electroencephalographic Monitoring of Cerebral Function During Asystole and Successful Cardiopulmonary Resuscitation," *Anesthesia & Analgesia*, vol. 75, no. 6, pp. 1021-1024, 1992.
- [39] M. E. Watts, R. Pocock, and C. Claudianos, "Brain Energy and Oxygen Metabolism: Emerging Role in Normal Function and Disease," (in eng), *Front Mol Neurosci*, vol. 11, pp. 216-216, 2018.
- [40] E. L. Rolett, A. Azzawi, K. J. Liu, M. N. Yongbi, H. M. Swartz, and J. F. Dunn, "Critical oxygen tension in rat brain: a combined ³¹P-NMR and EPR oximetry study," *American Journal of Physiology-Regulatory, Integrative and Comparative Physiology*, vol. 279, no. 1, pp. R9-R16,

2000.

- [41] A. N. Shetty *et al.*, "Cerebral oxygen metabolism during and after therapeutic hypothermia in neonatal hypoxic–ischemic encephalopathy: a feasibility study using magnetic resonance imaging," *Pediatric Radiology*, vol. 49, no. 2, pp. 224-233, 2019/02/01 2019.
- [42] S. G. Abdel Baki, A. Omurtag, A. A. Fenton, and S. Zehtabchi, "The new wave: time to bring EEG to the emergency department," *International Journal of Emergency Medicine*, vol. 4, no. 1, p. 36, 2011/06/24 2011.
- [43] R. Jaitly, J. A. Sgro, A. R. Towne, D. Ko, and R. J. DeLorenzo, "Prognostic value of EEG monitoring after status epilepticus: a prospective adult study," *Journal of Clinical Neurophysiology*, vol. 14, no. 4, pp. 326-334, 1997.
- [44] R. Nitzschke, J. Müller, S. Maisch, and G. N. Schmidt, "Single-channel electroencephalography of epileptic seizures in the out-of-hospital setting: an observational study," *Emergency Medicine Journal*, vol. 29, no. 7, pp. 536-543, 2012.
- [45] R. Anderson and J. Jakobsson, "Cerebral state monitor, a new small handheld EEG monitor for determining depth of anaesthesia: a clinical comparison with the bispectral index during day-surgery," *European journal of anaesthesiology*, vol. 23, no. 3, pp. 208-212, 2006.
- [46] A. C. N. Society, "Guideline 1: Minimum technical requirements for performing clinical electroencephalography," *Journal of clinical neurophysiology: official publication of the American Electroencephalographic Society*, vol. 23, no. 2, p. 86, 2006.
- [47] B. J. Kolls and A. M. Husain, "Assessment of hairline EEG as a screening tool for nonconvulsive status epilepticus," *Epilepsia*, vol. 48, no. 5, pp. 959-965, 2007.
- [48] B. Schultz, R. Bender, A. Schultz, and I. PICHLMAYR, "ELECTROENCEPHALOGRAPHIC MONITORING IN THE ICU-REDUCTION OF THE NUMBER OF RECORDED CHANNELS," *BIOMEDIZINISCHE TECHNIK*, vol. 37, no. 9, pp. 194-199, 1992.
- [49] G. L. Stidham, S. K. Nugent, and M. C. Rogers, "Monitoring cerebral

- electrical function in the ICU," *Critical care medicine*, vol. 8, no. 9, pp. 519-523, 1980.
- [50] R. O. Cummins, J. P. Ornato, W. H. Thies, and P. E. Pepe, "Improving survival from sudden cardiac arrest: the "chain of survival" concept. A statement for health professionals from the Advanced Cardiac Life Support Subcommittee and the Emergency Cardiac Care Committee, American Heart Association," *Circulation*, vol. 83, no. 5, pp. 1832-1847, 1991.
 - [51] T. Iwami *et al.*, "Continuous Improvements in "Chain of Survival" Increased Survival After Out-of-Hospital Cardiac Arrests," *Circulation*, vol. 119, no. 5, pp. 728-734, 2009.
 - [52] A. Cheng *et al.*, "Improving cardiopulmonary resuscitation with a CPR feedback device and refresher simulations (CPR CARES Study): a randomized clinical trial," *JAMA pediatrics*, vol. 169, no. 2, pp. 137-144, 2015.
 - [53] S. Kirkbright, J. Finn, H. Tohira, A. Bremner, I. Jacobs, and A. Celenza, "Audiovisual feedback device use by health care professionals during CPR: a systematic review and meta-analysis of randomised and non-randomised trials," *Resuscitation*, vol. 85, no. 4, pp. 460-471, 2014.
 - [54] B. Weston, J. Jasti, E. Lerner, A. Szabo, T. Aufderheide, and M. Colella, "Does an individualized feedback mechanism improve quality of out-of-hospital CPR?," *Resuscitation*, vol. 113, pp. 96-100, 2017.
 - [55] S. H. Friess *et al.*, "Hemodynamic directed CPR improves cerebral perfusion pressure and brain tissue oxygenation," *Resuscitation*, vol. 85, no. 9, pp. 1298-1303, 2014.
 - [56] E. Committee, "Task Forces of the American Heart. 2005 American Heart Association guidelines for cardiopulmonary resuscitation and emergency cardiovascular care," *Circulation*, vol. 112, no. 24 Suppl, 2005.
 - [57] S. M. Hartmann, R. W. Farris, J. L. Di Gennaro, and J. S. Roberts, "Systematic review and meta-analysis of end-tidal carbon dioxide values associated with return of spontaneous circulation during cardiopulmonary resuscitation," *Journal of intensive care medicine*,

- vol. 30, no. 7, pp. 426-435, 2015.
- [58] J. L. Hamrick, J. T. Hamrick, J. K. Lee, B. H. Lee, R. C. Koehler, and D. H. Shaffner, "Efficacy of chest compressions directed by end-tidal CO2 feedback in a pediatric resuscitation model of basic life support," *Journal of the American Heart Association*, vol. 3, no. 2, p. e000450, 2014.
 - [59] V. R. Moulaert, J. A. Verbunt, C. M. van Heugten, and D. T. Wade, "Cognitive impairments in survivors of out-of-hospital cardiac arrest: a systematic review," *Resuscitation*, vol. 80, no. 3, pp. 297-305, 2009.
 - [60] J. Torgersen *et al.*, "Cognitive dysfunction and health-related quality of life after a cardiac arrest and therapeutic hypothermia," *Acta Anaesthesiologica Scandinavica*, vol. 54, no. 6, pp. 721-728, 2010.
 - [61] G. Debaty *et al.*, "Tilting for perfusion: head-up position during cardiopulmonary resuscitation improves brain flow in a porcine model of cardiac arrest," *Resuscitation*, vol. 87, pp. 38-43, 2015.
 - [62] M. D. Larson and M. Behrends, "Portable infrared pupillometry: a review," *Anesthesia & Analgesia*, vol. 120, no. 6, pp. 1242-1253, 2015.
 - [63] S. Mathôt, L. Van der Linden, J. Grainger, and F. Vitu, "The pupillary light response reveals the focus of covert visual attention," *PloS one*, vol. 8, no. 10, p. e78168, 2013.
 - [64] M. Behrends, C. U. Niemann, and M. D. Larson, "Infrared pupillometry to detect the light reflex during cardiopulmonary resuscitation: a case series," *Resuscitation*, vol. 83, no. 10, pp. 1223-1228, 2012.
 - [65] M. D. Larson and I. Muhiudeen, "Pupillometric analysis of the absent light reflex," *Archives of neurology*, vol. 52, no. 4, pp. 369-372, 1995.
 - [66] H. J. Lee *et al.*, "A feasibility study for the continuous measurement of pupillary response using the pupillography during CPR in out-of-hospital cardiac arrest patients," *Resuscitation*, vol. 135, pp. 80-87, 2019.
 - [67] J. P. Diamond, "The Pupil. Anatomy, Physiology and Clinical Applications," *British Journal of Ophthalmology*, vol. 85, no. 1, p. 121, 2001.

- [68] L. M. Lewis, C. R. Gomez, B. E. Ruoff, S. M. Gomez, I. S. Hall, and B. Gasirowski, "Transcranial Doppler determination of cerebral perfusion in patients undergoing CPR: methodology and preliminary findings," *Annals of emergency medicine*, vol. 19, no. 10, pp. 1148-1151, 1990.
- [69] J. Blumenstein *et al.*, "Cerebral flow pattern monitoring by transcranial Doppler during cardiopulmonary resuscitation," *Anaesthesia and intensive care*, vol. 38, no. 2, pp. 376-380, 2010.
- [70] P. H. Raboel, J. Bartek, M. Andresen, B. M. Bellander, and B. Romner, "Intracranial Pressure Monitoring: Invasive versus Non-Invasive Methods—A Review," *Critical Care Research and Practice*, vol. 2012.
- [71] S. Parnia *et al.*, "Cerebral oximetry during cardiac arrest: a multicenter study of neurologic outcomes and survival," *Critical care medicine*, vol. 44, no. 9, pp. 1663-1674, 2016.
- [72] A. Cournoyer, M. Iseppon, J. M. Chauny, A. Denault, S. Cossette, and É. Notebaert, "Near-infrared Spectroscopy Monitoring During Cardiac Arrest: A Systematic Review and Meta-analysis," *Academic Emergency Medicine*, vol. 23, no. 8, pp. 851-862, 2016.
- [73] S. Parnia *et al.*, "A feasibility study of cerebral oximetry during in-hospital mechanical and manual cardiopulmonary resuscitation," *Critical care medicine*, vol. 42, no. 4, pp. 930-933, 2014.
- [74] J. Xu *et al.*, "Pulse oximetry: a non-invasive, novel marker for the quality of chest compressions in porcine models of cardiac arrest," *PloS one*, vol. 10, no. 10, p. e0139707, 2015.
- [75] T. Ioroi, C. Peeters-Scholte, I. Post, C. Leusink, F. Groenendaal, and F. van Bel, "Changes in cerebral haemodynamics, regional oxygen saturation and amplitude-integrated continuous EEG during hypoxia-ischaemia and reperfusion in newborn piglets," *Experimental brain research*, vol. 144, no. 2, pp. 172-177, 2002.
- [76] J. Moss and M. Rockoff, "EEG monitoring during cardiac arrest and resuscitation," *Jama*, vol. 244, no. 24, pp. 2750-2751, 1980.
- [77] M. R. England, "The changes in bispectral index during a hypovolemic cardiac arrest," *Anesthesiology: The Journal of the American Society*

- of Anesthesiologists*, vol. 91, no. 6, pp. 1947-1947, 1999.
- [78] D. H. Ingvar, B. Sjölund, and A. Ardö, "Correlation between dominant EEG frequency, cerebral oxygen uptake and blood flow," *Electroencephalography and Clinical Neurophysiology*, vol. 41, no. 3, pp. 268-276, 1976.
 - [79] C. Chollet-Xémard *et al.*, "Bispectral index monitoring is useless during cardiac arrest patients' resuscitation," *Resuscitation*, vol. 80, no. 2, pp. 213-216, 2009.
 - [80] J. Y. Jung, Y. Kim, and J.-E. Kim, "Usefulness of the bispectral index during cardiopulmonary resuscitation-A case report," *Korean Journal of Anesthesiology*, vol. 64, no. 1, p. 69, 2013.
 - [81] E. M. Reagan *et al.*, "Monitoring the relationship between changes in cerebral oxygenation and electroencephalography patterns during cardiopulmonary resuscitation: a feasibility study," *Critical Care Medicine*, vol. 46, no. 5, pp. 757-763, 2018.
 - [82] C. Berka *et al.*, "Real-time analysis of EEG indexes of alertness, cognition, and memory acquired with a wireless EEG headset," *International Journal of Human-Computer Interaction*, vol. 17, no. 2, pp. 151-170, 2004.
 - [83] S. Yoshimoto *et al.*, "Wireless EEG patch sensor on forehead using on-demand stretchable electrode sheet and electrode-tissue impedance scanner," *2016 38th Annual International Conference of the IEEE Engineering in Medicine and Biology Society (EMBC)*, pp. 6286-6289, 2016.
 - [84] J. Head, "Definition of mild traumatic brain injury," *J Head Trauma Rehabil*, vol. 8, no. 3, pp. 86-87, 1993.
 - [85] N. P. Ryan *et al.*, "Longitudinal outcome and recovery of social problems after pediatric traumatic brain injury (TBI): contribution of brain insult and family environment," *International journal of developmental neuroscience*, vol. 49, pp. 23-30, 2016.
 - [86] N. A. Kayani, S. Homan, S. Yun, and B. P. Zhu, "Health and economic burden of traumatic brain injury: Missouri, 2001–2005," *Public health reports*, vol. 124, no. 4, pp. 551-560, 2009.

- [87] H. Van Deynse *et al.*, "The incremental cost of traumatic brain injury during the first year after a road traffic accident," *Brain injury*, vol. 33, no. 9, pp. 1234-1244, 2019.
- [88] T. Tsaousides, A. Warshowsky, T. A. Ashman, J. B. Cantor, L. Spielman, and W. A. Gordon, "The relationship between employment-related self-efficacy and quality of life following traumatic brain injury," *Rehabilitation psychology*, vol. 54, no. 3, p. 299, 2009.
- [89] J. P. Cuthbert, C. Harrison-Felix, J. D. Corrigan, J. M. Bell, J. K. Haarbauer-Krupa, and A. C. Miller, "Unemployment in the United States after traumatic brain injury for working-age individuals: prevalence and associated factors 2 years postinjury," *The Journal of head trauma rehabilitation*, vol. 30, no. 3, p. 160, 2015.
- [90] N. Carney *et al.*, "Guidelines for the management of severe traumatic brain injury," *Neurosurgery*, vol. 80, no. 1, pp. 6-15, 2017.
- [91] A. I. Maas, M. Dearden, F. Servadei, N. Stocchetti, and A. Unterberg, "Current recommendations for neurotrauma," *Current opinion in critical care*, vol. 6, no. 4, pp. 281-292, 2000.
- [92] A. Bhatia and A. K. Gupta, "Neuromonitoring in the intensive care unit. I. Intracranial pressure and cerebral blood flow monitoring," *Intensive care medicine*, vol. 33, no. 7, pp. 1263-1271, 2007.
- [93] P. Raboel, J. Bartek, M. Andresen, B. Bellander, and B. Romner, "Intracranial pressure monitoring: invasive versus non-invasive methods—a review," *Critical care research and practice*, vol. 2012, 2012.
- [94] X. Zhang *et al.*, "Invasive and noninvasive means of measuring intracranial pressure: a review," *Physiological measurement*, vol. 38, no. 8, p. R143, 2017.
- [95] D. S. Nag, S. Sahu, A. Swain, and S. Kant, "Intracranial pressure monitoring: Gold standard and recent innovations," *World journal of clinical cases*, vol. 7, no. 13, p. 1535, 2019.
- [96] D. Popovic, M. Khoo, and S. Lee, "Noninvasive monitoring of intracranial pressure," *Recent patents on biomedical engineering*, vol. 2, no. 3, pp. 165-179, 2009.

- [97] "Noninvasive Monitoring of Cerebrovascular Reactivity with Near Infrared Spectroscopy in Head-Injured Patients," *Journal of Neurotrauma*, vol. 27, no. 11, pp. 1951-1958, 2010.
- [98] "Near-Infrared Spectroscopy in the Monitoring of Adult Traumatic Brain Injury: A Review," *Journal of Neurotrauma*, vol. 32, no. 13, pp. 933-941, 2015.
- [99] B. Schmidt *et al.*, "Adaptive noninvasive assessment of intracranial pressure and cerebral autoregulation," *Stroke*, vol. 34, no. 1, pp. 84-89, 2003.
- [100] T. Soldatos, D. Karakitsos, K. Chatzimichail, M. Papathanasiou, A. Gouliamos, and A. Karabinis, "Optic nerve sonography in the diagnostic evaluation of adult brain injury," *Critical Care*, vol. 12, no. 3, p. R67, 2008/05/13 2008.
- [101] V. Rajajee, M. Vanaman, J. J. Fletcher, and T. L. Jacobs, "Optic Nerve Ultrasound for the Detection of Raised Intracranial Pressure," *Neurocritical Care*, vol. 15, no. 3, pp. 506-515, 2011/12/01 2011.
- [102] T. Geeraerts *et al.*, "Use of T2-weighted magnetic resonance imaging of the optic nerve sheath to detect raised intracranial pressure," *Critical Care*, vol. 12, no. 5, p. R114, 2008/09/11 2008.
- [103] R. Du, M. Meeker, P. Bacchetti, M. D. Larson, M. C. Holland, and G. T. Manley, "Evaluation of the Portable Infrared Pupillometer," *Neurosurgery*, vol. 57, no. 1, pp. 198-203, 2005.
- [104] M. Meeker *et al.*, "Pupil Examination: Validity and Clinical Utility of an Automated Pupillometer," *Journal of Neuroscience Nursing*, vol. 37, no. 1, pp. 34-40, 2005.
- [105] J. B. Rosenberg, A. L. Shiloh, R. H. Savel, and L. A. Eisen, "Non-invasive Methods of Estimating Intracranial Pressure," *Neurocritical Care*, vol. 15, no. 3, pp. 599-608, 2011/12/01 2011.
- [106] B. B. Bruce, "Noninvasive Assessment of Cerebrospinal Fluid Pressure," *Journal of Neuro-Ophthalmology*, vol. 34, no. 3, pp. 288-294, 2014.
- [107] K. N. Fountas, E. Z. Kapsalaki, T. G. Machinis, A. N. Boev, J. S. Robinson, and E. C. Troup, "Clinical implications of quantitative

- infrared pupillometry in neurosurgical patients," *Neurocritical Care*, vol. 5, no. 1, pp. 55-60, 2006/08/01 2006.
- [108] J. B. Jonas, K. Pfeil, A. Chatzikonstantinou, and F. Rensch, "Ophthalmodynamometric measurement of central retinal vein pressure as surrogate of intracranial pressure in idiopathic intracranial hypertension," *Graefe's Archive for Clinical and Experimental Ophthalmology*, vol. 246, no. 7, pp. 1059-1060, 2008/07/01 2008.
- [109] R. Firsching, M. Schütze, M. Motschmann, and W. Behrens-Baumann, "Venous ophthalmodynamometry: a noninvasive method for assessment of intracranial pressure," (in English), *Journal of Neurosurgery*, vol. 93, no. 1, p. 33, 01 Jan. 2000 2000.
- [110] M. Motschmann *et al.*, "Ophthalmodynamometry: a reliable method for measuring intracranial pressure," *Strabismus*, vol. 9, no. 1, pp. 13-16, 2001/01/01 2001.
- [111] P. K. Eide, "A new method for processing of continuous intracranial pressure signals," *Medical Engineering & Physics*, vol. 28, no. 6, pp. 579-587, 2006/07/01/ 2006
- [112] A. Levinsky, S. Papyan, G. Weinberg, T. Stadheim, and P. K. Eide, "Non-invasive estimation of static and pulsatile intracranial pressure from transcranial acoustic signals," *Medical Engineering & Physics*, vol. 38, no. 5, pp. 477-484, 2016/05/01/ 2016
- [113] Z. Li and Y. Luo, "Finite element study of correlation between intracranial pressure and external vibration responses of human head," *Adv. Theor. Appl. Mech*, vol. 3, no. 3, pp. 139-149, 2010.
- [114] X. Yue and L. Wang, "Deformation of skull bone as intracranial pressure changing," *African Journal of Biotechnology*, vol. 8, no. 5, 2009.
- [115] X. Wu and Z. Ji, "Non-invasive detection for intracranial high pressure with FVEP picked-up by independent component analysis," *Sheng wu yi xue gong cheng xue za zhi= Journal of biomedical engineering= Shengwu yixue gongchengxue zazhi*, vol. 24, no. 5, pp. 1015-1018, 2007.
- [116] C. Wiegand and P. Richards, "Measurement of intracranial pressure in

- children: a critical review of current methods," *Developmental Medicine & Child Neurology*, vol. 49, no. 12, pp. 935-941, 2007.
- [117] C. Munari and F. Calbucci, "Correlations between intracranial pressure and EEG during coma and sleep," *Electroencephalography and clinical neurophysiology*, vol. 51, no. 2, pp. 170-176, 1981.
 - [118] H. Chen, J. Wang, S. Mao, W. Dong, and H. Yang, "A new method of intracranial pressure monitoring by EEG power spectrum analysis," *Canadian journal of neurological sciences*, vol. 39, no. 4, pp. 483-487, 2012.
 - [119] M. Connolly, P. Vespa, N. Pouratian, N. R. Gonzalez, and X. Hu, "Characterization of the relationship between intracranial pressure and electroencephalographic monitoring in burst-suppressed patients," *Neurocritical care*, vol. 22, no. 2, pp. 212-220, 2015.
 - [120] C. Perez *et al.*, "Dynamic interaction between EEG and ICP: a pilot study based on wavelet coherence (P6. 064)," ed: AAN Enterprises, 2017.
 - [121] A. Sanz-García *et al.*, "Identifying causal relationships between EEG activity and intracranial pressure changes in neurocritical care patients," *Journal of Neural Engineering*, vol. 15, no. 6, p. 066029, 2018.
 - [122] L. Wik, P. A. Steen, and N. G. Bircher, "Quality of bystander cardiopulmonary resuscitation influences outcome after prehospital cardiac arrest," *Resuscitation*, vol. 28, no. 3, pp. 195-203, 1994.
 - [123] M. E. H. Ong, G. D. Perkins, and A. Cariou, "Out-of-hospital cardiac arrest: prehospital management," *The Lancet*, vol. 391, no. 10124, pp. 980-988, 2018.
 - [124] J. Ghajar, "Traumatic brain injury," *The Lancet*, vol. 356, no. 9233, pp. 923-929, 2000.
 - [125] B. L. Edlow *et al.*, "Early detection of consciousness in patients with acute severe traumatic brain injury," *Brain*, vol. 140, no. 9, pp. 2399-2414, 2017.
 - [126] L. M. Lewis, J. Stothert, J. Standeven, B. Chandel, M. Kurtz, and J. Fortney, "Correlation of end-tidal CO₂ to cerebral perfusion during

- CPR," *Annals of emergency medicine*, vol. 21, no. 9, pp. 1131-1134, 1992.
- [127] E. J. Benjamin *et al.*, "Heart disease and stroke statistics—2017 update," 2017.
 - [128] K. G. Monsieurs *et al.*, "European resuscitation council guidelines for resuscitation 2015: section 1. Executive summary," *Resuscitation*, vol. 95, pp. 1-80, 2015.
 - [129] S. G. Beesems, K. M. Wittebrood, R. J. de Haan, and R. W. Koster, "Cognitive function and quality of life after successful resuscitation from cardiac arrest," *Resuscitation*, vol. 85, no. 9, pp. 1269-1274, 2014.
 - [130] M. S. Link *et al.*, "Part 7: adult advanced cardiovascular life support: 2015 American Heart Association guidelines update for cardiopulmonary resuscitation and emergency cardiovascular care," *Circulation*, vol. 132, no. 18_suppl_2, pp. S444-S464, 2015.
 - [131] "Editorial Board," *Circulation*, vol. 132, no. 16_suppl_1, pp. S1-S1, 2015.
 - [132] B. S. Kodali and R. D. Urman, "Capnography during cardiopulmonary resuscitation: current evidence and future directions," *Journal of emergencies, trauma, and shock*, vol. 7, no. 4, p. 332, 2014.
 - [133] G. Feng, G. Jiang, Z. Li, and X. Wang, "Prognostic value of electroencephalography (EEG) for brain injury after cardiopulmonary resuscitation," *Neurological Sciences*, vol. 37, no. 6, pp. 843-849, 2016.
 - [134] N. R. Council, *Guide for the care and use of laboratory animals*. National Academies Press, 2010.
 - [135] B. R. Sheth, S. Sandkühler, and J. Bhattacharya, "Posterior beta and anterior gamma oscillations predict cognitive insight," *Journal of Cognitive Neuroscience*, vol. 21, no. 7, pp. 1269-1279, 2009.
 - [136] C. W. Long, N. K. Shah, C. Loughlin, J. Spydell, and R. F. Bedford, "A comparison of EEG determinants of near-awakening from isoflurane and fentanyl anesthesia. Spectral edge, median power frequency, and delta ratio," *Anesthesia and analgesia*, vol. 69, no. 2, pp. 169-173, 1989.
 - [137] S. Visa, B. Ramsay, A. L. Ralescu, and E. Van Der Knaap, "Confusion Matrix-based Feature Selection," *MAICS*, vol. 710, pp. 120-127, 2011.

- [138] C. Goutte and E. Gaussier, "A probabilistic interpretation of precision, recall and F-score, with implication for evaluation," in *European conference on information retrieval*, 2005: Springer, pp. 345-359.
- [139] J. Fan, S. Upadhye, and A. Worster, "Understanding receiver operating characteristic (ROC) curves," *Canadian Journal of Emergency Medicine*, vol. 8, no. 1, pp. 19-20, 2006.
- [140] J. C. Sigl and N. G. Chamoun, "An introduction to bispectral analysis for the electroencephalogram," *Journal of clinical monitoring*, vol. 10, no. 6, pp. 392-404, 1994.
- [141] M. Momeni and A. Gaudin, "Intraoperative cerebral hypoperfusion and electroencephalogram suppression resulting in neurological complications after cardiac surgery: the need for an in depth investigation," *Acta Anaesthesiologica Belgica*, vol. 67, no. 2, pp. 73-79, 2016.
- [142] Y. Morimoto, Y. Monden, K. Ohtake, T. Sakabe, and S. Hagihira, "The detection of cerebral hypoperfusion with bispectral index monitoring during general anesthesia," *Anesthesia & Analgesia*, vol. 100, no. 1, pp. 158-161, 2005.
- [143] C. V. Gudipati, M. Weil, J. Bisera, H. G. Deshmukh, and E. Rackow, "Expired carbon dioxide: a noninvasive monitor of cardiopulmonary resuscitation," *Circulation*, vol. 77, no. 1, pp. 234-239, 1988.
- [144] F. J. Cereceda-Sánchez and J. Molina-Mula, "Systematic Review of Capnography with Mask Ventilation during Cardiopulmonary Resuscitation Maneuvers," *Journal of clinical medicine*, vol. 8, no. 3, p. 358, 2019.
- [145] M. E. Kleinman *et al.*, "Part 5: adult basic life support and cardiopulmonary resuscitation quality: 2015 American Heart Association guidelines update for cardiopulmonary resuscitation and emergency cardiovascular care," *Circulation*, vol. 132, no. 18_suppl_2, pp. S414-S435, 2015.
- [146] K. N. Sawyer *et al.*, "Sudden Cardiac Arrest Survivorship: A Scientific Statement From the American Heart Association," *Circulation*, vol. 141, no. 12, pp. e654-e685, 2020.

- [147] M. R. Daya *et al.*, "Out-of-hospital cardiac arrest survival improving over time: results from the Resuscitation Outcomes Consortium (ROC)," *Resuscitation*, vol. 91, pp. 108-115, 2015.
- [148] R. Aaslid, T. Lundar, K. Lindegaard, and H. Nornes, "Estimation of cerebral perfusion pressure from arterial blood pressure and transcranial Doppler recordings," in *Intracranial pressure VI*: Springer, 1986, pp. 226-229.
- [149] M. Czosnyka, B. F. Matta, P. Smielewski, P. J. Kirkpatrick, and J. D. Pickard, "Cerebral perfusion pressure in head-injured patients: a noninvasive assessment using transcranial Doppler ultrasonography," *Journal of neurosurgery*, vol. 88, no. 5, pp. 802-808, 1998.
- [150] J. W. De Vries, P. F. Bakker, G. H. Visser, J. C. Diephuis, and A. C. van Huffelen, "Changes in cerebral oxygen uptake and cerebral electrical activity during defibrillation threshold testing," *Anesthesia & Analgesia*, vol. 87, no. 1, pp. 16-20, 1998.
- [151] B. Schäuble, D. W. Klass, and B. F. Westmoreland, "Resuscitation artifacts during electroencephalography," *American journal of electroneurodiagnostic technology*, vol. 42, no. 1, pp. 16-21, 2002.
- [152] N. Azim and C. Wang, "The use of bispectral index during a cardiopulmonary arrest: a potential predictor of cerebral perfusion," *Anaesthesia*, vol. 59, no. 6, pp. 610-612, 2004.
- [153] H. Kim, K. H. Kim, K. J. Hong, Y. Ku, S. D. Shin, and H. C. Kim, "Frontal EEG Changes with the Recovery of Carotid Blood Flow in a Cardiac Arrest Swine Model," *Sensors*, vol. 20, no. 11, p. 3052, 2020.
- [154] A. Mullie, P. Lewi, R. Van Hoeyweghen, and C. R. S. Group, "Pre-CPR conditions and the final outcome of CPR," *Resuscitation*, vol. 17, pp. S11-S21, 1989.
- [155] L. Wei, T. Yu, P. Gao, W. Quan, and Y. Li, "Detection of Spontaneous Pulse Using Acceleration Signals Acquired From CPR Feedback Sensor in Porcine Model of Cardiac Arrest," *Circulation*, vol. 134, no. suppl_1, pp. A12827-A12827, 2016.
- [156] M. A. Peberdy *et al.*, "Part 9: post-cardiac arrest care: 2010 American Heart Association guidelines for cardiopulmonary resuscitation and

- emergency cardiovascular care," *Circulation*, vol. 122, no. 18_suppl_3, pp. S768-S786, 2010.
- [157] J. Overgaard, C. Mosdal, and W. A. Tweed, "Cerebral circulation after head injury: Part 3: Does reduced regional cerebral blood flow determine recovery of brain function after blunt head injury?," *Journal of neurosurgery*, vol. 55, no. 1, pp. 63-74, 1981.
 - [158] J. Goldberger, G. E. Hinton, S. Roweis, and R. R. Salakhutdinov, "Neighbourhood components analysis," *Advances in neural information processing systems*, vol. 17, pp. 513-520, 2004.
 - [159] S. Raghu and N. Sriraam, "Classification of focal and non-focal EEG signals using neighborhood component analysis and machine learning algorithms," *Expert Systems with Applications*, vol. 113, pp. 18-32, 2018.
 - [160] A. Subasi and E. Ercelebi, "Classification of EEG signals using neural network and logistic regression," *Computer methods and programs in biomedicine*, vol. 78, no. 2, pp. 87-99, 2005.
 - [161] R. Tomioka, K. Aihara, and K.-R. Müller, "Logistic regression for single trial EEG classification," *Advances in neural information processing systems*, vol. 19, pp. 1377-1384, 2006.
 - [162] H. Bhavsar and M. H. Panchal, "A review on support vector machine for data classification," *International Journal of Advanced Research in Computer Engineering & Technology*, vol. 1, no. 10, 2012.
 - [163] B. Richhariya and M. Tanveer, "EEG signal classification using universum support vector machine," *Expert Systems with Applications*, vol. 106, pp. 169-182, 2018.
 - [164] L. E. Peterson, "K-nearest neighbor," *Scholarpedia*, vol. 4, no. 2, p. 1883, 2009.
 - [165] N. Sulaiman, M. N. Taib, S. Lias, Z. H. Murat, S. A. M. Aris, and N. H. A. Hamid, "EEG-based stress features using spectral centroids technique and k-nearest neighbor classifier," in *2011 UkSim 13th International Conference on Computer Modelling and Simulation*, 2011: IEEE, pp. 69-74.
 - [166] T. Lan, A. Adami, D. Erdogmus, and M. Pavel, "Estimating cognitive

- state using EEG signals," in *2005 13th European Signal Processing Conference*, 2005: IEEE, pp. 1-4.
- [167] L. Fraiwan, K. Lweesy, N. Khasawneh, H. Wenz, and H. Dickhaus, "Automated sleep stage identification system based on time–frequency analysis of a single EEG channel and random forest classifier," *Computer methods and programs in biomedicine*, vol. 108, no. 1, pp. 10-19, 2012.
 - [168] D. R. Edla, K. Mangalorekar, G. Dhavalikar, and S. Dodia, "Classification of EEG data for human mental state analysis using Random Forest Classifier," *Procedia computer science*, vol. 132, pp. 1523-1532, 2018.
 - [169] D. E. Rumelhart, G. E. Hinton, and R. J. Williams, "Learning representations by back-propagating errors," *nature*, vol. 323, no. 6088, pp. 533-536, 1986.
 - [170] G. Cybenko, "Approximation by superpositions of a sigmoidal function," *Mathematics of control, signals and systems*, vol. 2, no. 4, pp. 303-314, 1989.
 - [171] H.-S. Choi, B. Lee, and S. Yoon, "Biometric authentication using noisy electrocardiograms acquired by mobile sensors," *IEEE Access*, vol. 4, pp. 1266-1273, 2016.
 - [172] N. V. Chawla, K. W. Bowyer, L. O. Hall, and W. P. Kegelmeyer, "SMOTE: synthetic minority over-sampling technique," *Journal of artificial intelligence research*, vol. 16, pp. 321-357, 2002.
 - [173] B. Foreman and J. Claassen, "Quantitative EEG for the detection of brain ischemia," *Critical Care*, vol. 16, no. 2, p. 216, 2012/03/20 2012.
 - [174] F. Zadini, E. Newton, A. A. Abdi, J. Lenker, G. Zadini, and S. O. Henderson, "Use of the trendelenburg position in the porcine model improves carotid flow during cardiopulmonary resuscitation," *Western Journal of Emergency Medicine*, vol. 9, no. 4, p. 206, 2008.
 - [175] D. M. Fatovich, I. G. Jacobs, A. Celenza, and M. J. Paech, "An observational study of bispectral index monitoring for out of hospital cardiac arrest," *Resuscitation*, vol. 69, no. 2, pp. 207-212, 2006.
 - [176] R. Nitzschke and G. N. Schmidt, "Electroencephalography during Out-

- of-hospital Cardiopulmonary Resuscitation," *The Journal of Emergency Medicine*, vol. 43, no. 4, pp. 659-662, 2012/10/01/ 2012.
- [177] Z. Liang *et al.*, "EEG entropy measures in anesthesia," (in English), *Frontiers in Computational Neuroscience*, Original Research vol. 9, no. 16, 2015-February-18 2015.
- [178] A. Maksimow *et al.*, "Correlation of EEG spectral entropy with regional cerebral blood flow during sevoflurane and propofol anaesthesia*," *Anaesthesia*, vol. 60, no. 9, pp. 862-869, 2005.
- [179] Y.-W. Chang, C.-J. Hsieh, K.-W. Chang, M. Ringgaard, and C.-J. Lin, "Training and testing low-degree polynomial data mappings via linear SVM," *Journal of Machine Learning Research*, vol. 11, no. 4, 2010.
- [180] D.-X. Zhou and K. Jetter, "Approximation with polynomial kernels and SVM classifiers," *Advances in Computational Mathematics*, vol. 25, no. 1-3, pp. 323-344, 2006.
- [181] M. Faul, L. Xu, M. Wald, and V. Coronado, "Traumatic brain injury in the United States: emergency department visits, hospitalizations and deaths 2002–2006. US Department of Health and Human Services Centers for Disease Control and Prevention, 2010," ed, 2013.
- [182] V. E. Johnson, W. Stewart, and D. H. Smith, "Traumatic brain injury and amyloid- β pathology: a link to Alzheimer's disease?," *Nature Reviews Neuroscience*, vol. 11, no. 5, pp. 361-370, 2010.
- [183] "Traumatic Brain Injury: A Major Medical Problem That Could Be Treated Using Transcranial, Red/Near-Infrared LED Photobiomodulation," *Photomedicine and Laser Surgery*, vol. 33, no. 9, pp. 443-446, 2015.
- [184] A. E. Lincoln, S. V. Caswell, J. L. Almquist, R. E. Dunn, J. B. Norris, and R. Y. Hinton, "Trends in concussion incidence in high school sports: a prospective 11-year study," *The American journal of sports medicine*, vol. 39, no. 5, pp. 958-963, 2011.
- [185] J. Mathias and P. Alvaro, "Prevalence of sleep disturbances, disorders, and problems following traumatic brain injury: a meta-analysis," *Sleep medicine*, vol. 13, no. 7, pp. 898-905, 2012.
- [186] A. Farahvar, L. M. Gerber, Y.-L. Chiu, N. Carney, R. Härtl, and J.

- Ghajar, "Increased mortality in patients with severe traumatic brain injury treated without intracranial pressure monitoring," (in English), vol. 117, no. 4, p. 729, 2012.
- [187] K. Jangra and K. Jain, "Cerebral Oxygenation," *Yearbook of Anesthesiology-8*, p. 70, 2019.
 - [188] R. Myers, J. Stockard, and L. Saidman, "Monitoring of cerebral perfusion during anesthesia by time-compressed Fourier analysis of the electroencephalogram," *Stroke*, vol. 8, no. 3, pp. 331-337, 1977.
 - [189] L. Rangel-Castillo, S. Gopinath, and C. S. Robertson, "Management of intracranial hypertension," *Neurologic clinics*, vol. 26, no. 2, pp. 521-541, 2008.
 - [190] M. F. Møller, "A scaled conjugate gradient algorithm for fast supervised learning," *Neural Networks*, vol. 6, no. 4, pp. 525-533, 1993/01/01/ 1993.
 - [191] T. Berlin, C. Murray-Krezan, and H. Yonas, "Comparison of parenchymal and ventricular intracranial pressure readings utilizing a novel multi-parameter intracranial access system," *Springerplus*, vol. 4, no. 1, p. 10, 2015.
 - [192] A. Ragauskas *et al.*, "Improved diagnostic value of a TCD-based non-invasive ICP measurement method compared with the sonographic ONSD method for detecting elevated intracranial pressure," *Neurological Research*, vol. 36, no. 7, pp. 607-614, 2014/07/01 2014.
 - [193] F. M. Kashif, G. C. Verghese, V. Novak, M. Czosnyka, and T. Heldt, "Model-based noninvasive estimation of intracranial pressure from cerebral blood flow velocity and arterial pressure," *Science translational medicine*, vol. 4, no. 129, pp. 129ra44-129ra44, 2012.
 - [194] Q. Shen, J. Stuart, B. Venkatesh, J. Wallace, and J. Lipman, "Inter observer variability of the transcranial Doppler ultrasound technique: impact of lack of practice on the accuracy of measurement," *Journal of clinical monitoring and computing*, vol. 15, no. 3-4, pp. 179-184, 1999.
 - [195] C. Robba *et al.*, "Ultrasound non-invasive measurement of intracranial pressure in neurointensive care: a prospective observational study," *PLoS medicine*, vol. 14, no. 7, p. e1002356, 2017.

- [196] K. B. Evensen and P. K. Eide, "Measuring intracranial pressure by invasive, less invasive or non-invasive means: limitations and avenues for improvement," *Fluids and Barriers of the CNS*, vol. 17, pp. 1-33, 2020.
- [197] I. G. Stiell *et al.*, "Comparison of the Cerebral Performance Category score and the Health Utilities Index for survivors of cardiac arrest," *Annals of emergency medicine*, vol. 53, no. 2, pp. 241-248. e1, 2009.
- [198] R. Phelps, F. Dumas, C. Maynard, J. Silver, and T. Rea, "Cerebral performance category and long-term prognosis following out-of-hospital cardiac arrest," *Critical care medicine*, vol. 41, no. 5, pp. 1252-1257, 2013.
- [199] T. J. Quinn, J. Dawson, M. Walters, and K. R. Lees, "Reliability of the modified Rankin Scale: a systematic review," *Stroke*, vol. 40, no. 10, pp. 3393-3395, 2009.
- [200] J. L. Banks and C. A. Marotta, "Outcomes validity and reliability of the modified Rankin scale: implications for stroke clinical trials: a literature review and synthesis," *Stroke*, vol. 38, no. 3, pp. 1091-1096, 2007.
- [201] E. L. Kiehl *et al.*, "C-GRA pH: A Validated Scoring System for Early Stratification of Neurologic Outcome After Out-of-Hospital Cardiac Arrest Treated With Targeted Temperature Management," *Journal of the American Heart Association*, vol. 6, no. 5, p. e003821, 2017.
- [202] K. D. Raina, C. Callaway, J. C. Rittenberger, and M. B. Holm, "Neurological and functional status following cardiac arrest: method and tool utility," *Resuscitation*, vol. 79, no. 2, pp. 249-256, 2008.
- [203] C.-T. Lin *et al.*, "Noninvasive neural prostheses using mobile and wireless EEG," *Proceedings of the IEEE*, vol. 96, no. 7, pp. 1167-1183, 2008.
- [204] T. Kawana, Y. Yoshida, Y. Kudo, C. Iwatani, and N. Miki, "Design and Characterization of an EEG-Hat for Reliable EEG Measurements," *Micromachines*, vol. 11, no. 7, p. 635, 2020.
- [205] K. Appold, "Resuscitation technology aims to offer more benefits: current advances in resuscitation technology are improving safety,

outcomes, and cost-effectiveness in a range of clinical settings," *RT for Decision Makers in Respiratory Care*, vol. 27, no. 6, pp. 12-15, 2014.

초 록

뇌파는 대뇌피질이나 두피의 전극을 통해서 뇌의 전기적 신호를 기록한 것을 의미한다. 뇌 기능 관찰을 위한 진단도구로써 뇌파는 뇌전증이나 치매 진단 등의 목적으로 활용되고 있다. 본 논문에서는 비침습적 뇌파를 이용하여 응급환자의 주요 생리학적 지표를 모니터링하는 기술을 개발하였다.

처음 두 연구에서 심폐소생술의 효과를 평가하기 위한 심정지 돼지실험모델을 고안하였다. 현재의 심폐소생술 지침은 체순환 평가를 위해 기도삽관을 통한 호기말 이산화탄소 분압의 측정을 권고한다. 하지만, 정확한 기도삽관이 특히 병원 밖 상황에서 어려울 수 있다. 따라서, 간편히 측정할 수 있고 소생 환자의 신경학적 예후를 진단하는데 사용되는 뇌파를 이용한 예측 기술이 심폐소생술 품질평가지표의 대안으로 제안되었다. 첫 번째 실험에서는 고품질과 저품질 기본심폐소생술을 10회 반복하면서 측정된 뇌파를 분석하였다. 심폐소생술의 품질에 따른 뇌파의 변화를 이용하여 체순환 평가를 위한 EEG-based Brain Resuscitation Index (EBRI) 모델을 도출하였다. EBRI 모델에서 획득한 호기말 이산화탄소 분압 예측치는 실제 값과 양의 상관관계를 보이며, 병원 밖 상황에서의 활용 가능성을 보였다. 두

번째 실험에서는 두 가지 심폐소생술(기본심폐소생술, 전문심폐소생술)이 수행되었다. 제세동 직전에 수집된 뇌파는 심폐소생술 도중 경동맥혈류의 회복률과 함께 분석되었다. 심폐소생술 도중 경동맥혈류의 회복률을 반영하는 뇌파 변수를 규명한 후, 이를 이용하여 높은 회복률(30% 이상)과 낮은 회복률(30% 미만)을 구분하는 기계학습 기반 이진분류모델을 도출하였다. 서포트 벡터 머신 기반의 예측모델이 0.853의 정확도와 0.909의 곡선하면적을 보이며 가장 우수한 성능을 보였다. 이러한 예측모델은 심정지 환자의 뇌 소생을 향상시켜 빠른 뇌 기능 회복을 가능하게 할 것으로 기대된다.

세 번째 연구에서 비침습적 뇌파를 이용하여 두개내압을 예측하는 모델을 개발하기 위한 외상성 뇌손상 돼지실험모델이 고안되었다. 외상성 뇌손상은 물리적 충격에 의해 정상적인 뇌 기능이 중단된 상태를 의미하며, 이 때의 두개내압 상승과 관류저하가 뇌파에 영향을 끼칠 수 있다. 따라서, 우리는 뇌파 기반 두개내압 예측모델을 개발하였다. 폴리카테터로 실험동물의 두개내압을 변경하면서 뇌파를 획득하였다. 두개내압의 정상구간(25 mmHg 미만)과 위험구간(25 mmHg 이상)을 유의미하게 구분하는 뇌파 변수를 규명한 후 기계학습 기반 이진분류모델을 도출하였다. 다층 퍼셉트론 기반의 예측모델이 0.686의 정확도와 0.754의 곡선하면적을 보이며 가장 우수한 성능을 보였다. 또다른 비침습

데이터인 심박수 정보와 함께 사용하였을 때 정확도와 곡선하면적은 각각 0.760과 0.834로 향상되었다. 제안된 예측모델은 응급상황에서 비침습적으로 두개내압을 관찰하여 정상 수준의 두개내압을 유지하는데 도움을 줄 것으로 기대된다.

본 논문은 응급환자의 주요 생리학적 지표를 비침습적 뇌파를 이용하여 관찰하는 예측모델을 제안하고 성능을 검증하였다. 본 연구에서는 뇌파를 이용하여 즉각적인 호기말 이산화탄소 분압, 경동맥혈류, 두개내압을 추정하기 위한 예측모델을 수립하였다. 하지만, 뇌파 데이터는 장기간의 신경학적, 기능적 회복과 함께 평가되어야 한다. 본 논문에서 개발한 예측모델의 성능과 적용 가능성은 향후 다양한 임상연구를 통해 cerebral performance category와 modified Rankin scale 등의 신경학적 평가지표와 함께 분석, 개선되어야 할 것이다.

주요어: 응급상황, 뇌파, 심폐소생술, 외상성 뇌손상, 생리학적 지표, 예측모델

학 번: 2015-30263